Title
Investigating Early Retinal Remodeling and Secondary Cone Degeneration in Retinitis Pigmentosa

Author
Ellis, Erika

Publication Date
2022

Peer reviewed|Thesis/dissertation

UNIVERSITY OF CALIFORNIA

Los Angeles

Investigating Early Retinal Remodeling and Secondary Cone Degeneration in Retinitis Pigmentosa

A dissertation submitted in partial satisfaction of the requirements for the degree

Doctor of Philosophy in Molecular, Cellular, and Integrative Physiology

by

Erika Marie Ellis

2022

ABSTRACT OF THE DISSERTATION

Investigating Early Retinal Remodeling and Secondary Cone Degeneration in Retinitis Pigmentosa

by

Erika Marie Ellis

Doctor of Philosophy in Molecular, Cellular, and Integrative Physiology

University of California, Los Angeles, 2022

Professor Alapakkam P. Sampath, Chair

In retinitis pigmentosa (RP), primary rod degeneration leads to the secondary degeneration of cones, resulting in loss of normal retinal input. Retinal function is further disrupted by downstream retinal remodeling. The mechanisms underlying these degenerative processes are currently incompletely understood. In my thesis research, I use whole-cell electrophysiology recordings from retinal slices to investigate changes in retinal physiology during retinal degeneration.

In the first section of my thesis, I investigate the changes in the rod-to-rod bipolar cell synapse during the early stages of degeneration in the CNGB1 KO mouse model. Previous studies show that rod bipolar cells lack light-evoked responses prior to the loss of light responses in rods, despite intact rod-to-rod bipolar cell synapses. Using a weak mGluR6 antagonist, CPPG, I show that although rod bipolar cells lose light-evoked responses they retain the molecular machinery required to support mGluR6-driven responses. These results

indicate that the breakdown in synaptic transmission between rods and rod bipolar cells is most likely due to presynaptic dysfunction with impaired glutamate release from rods.

In the second section of my thesis I characterized changes in cone membrane physiology during secondary cone degeneration by performing whole-cell patch clamp recordings from degenerating cones in rd10 mice. I show that, despite significant morphological changes, including the loss of the outer segment and cone pedicle, cones maintain relatively normal membrane physiology. What's more, cones continue to produce small light-evoked responses even at late stages of degeneration, and these responses are transmitted on to second-order neurons. These findings are encouraging for future research aimed at reactivating dormant cones to restore vision to patients with RP.

In the final section of my thesis I explore the evolutionary origins of one of the vertebrate retina's most unique features: the use of the metabotropic glutamate receptor in the ON bipolar cell pathway. My results indicate that the division of light information into ON and OFF pathways at the first synaptic connection and the mediation of the ON pathway through a metabotropic glutamate receptor evolved over 500 million years ago and is a fundamental feature of the vertebrate retina.

The dissertation of Erika Marie Ellis is approved.

Gordon L. Fain

Thomas J. O'Dell

Roxana Radu

Gabriel H. Travis

Alapakkam P. Sampath, Committee Chair

University of California, Los Angeles

2022

This dissertation is dedicated to my beloved Mother, Shelley Ellis, who taught me to make my own path in life and to always chase my dreams.

TABLE OF CONTENTS

LIST OF FIGURES

LIST OF ABBREVIATIONS AND SYMBOLS

ATP	Adenosine 5’-triphosphate
BK	Voltage-gated potassium channels
Ca^{2+}	Calcium
cGMP	Guanosine 3′,5′-cyclic monophosphate
Cl^-	Chloride
CNG	Cyclic nucleotide gated channel
CNGα	α-subunit of the cyclic nucleotide gated channel
CNGβ1 KO	Mouse model of RP with a knockout of the CNG channel β1-subunit
CPPG	(RS)-α-cyclopropyl-4-phosphonophenylyglycine; a weak group II/III metabotropic glutamate receptor antagonist
Cs^+	Cesium; blocks HCN channels
DILT	L-cis-diltiazem; blocks CNG channels
DL-AP4	DL-2-Amino-4-phosphonobutyric acid; a strong metabotropic glutamate receptor agonist
ERG	Electroretinography
EZ	Ellipsoid zone; OCT layer corresponding to photoreceptor outer segments
GDP	Guanosine diphosphate
GLUT-1	Glucose transporter 1
GMP	Guanosine monophosphate
GTP	Guanosine triphosphate
HCN1	Hyperpolarization-activated cyclic nucleotide-gated channel
$I_{1/2}$	Intensity of the half-maximal response
i_{Ca}	Synaptic voltage-gated Ca^{2+} channel conductance

i_{CNG}	Cyclic nucleotide gated channel conductance
i_h	Hyperpolarization-activated cyclic nucleotide-gated channel conductance
i_{kx}	Voltage-gated potassium channel conductance
ISR	Isradipine; blocks L-type voltage-gated Ca^{2+} channels
K^+	Potassium
K-Asp	Potassium-Aspartate
mGluR6	Metabotropic glutamate receptor
Na^+	Sodium
NFA	Niflumic acid; blocks Ca^+-activated Cl^- channels
OCT	Optical coherence tomography
ONL	Outer nuclear layer
P	Postnatal day
PDE	Phosphodiesterase
rd1	Mouse model of RP with a nonsense mutation in rod-specific *PDE6-β*
rd10	Mouse model of RP with a missense mutation in rod-specific PDE6-β
RdCVF	Rod-derived cone viability factor
Rh	Photoreceptor photopigment
Rh∗	Activated photoreceptor photopigment
R_{max}	Maximal response
RNA	Ribonucleic acid
RP	Retinitis pigmentosa
TEA	Tetraethylammonium; blocks sustained voltage-gated K^+ channels
TRPM1	Transient receptor potential cation channel subfamily M member 1
WT	Wild type mouse lines, includes 129s and C57 mouse lines

ACKNOWLEDGEMENTS

There are neither words nor time enough to sufficiently acknowledge all of the people whose efforts and support made this work possible.

I will start by thanking my advisors: Dr. Alapakkam P Sampath and Dr. Gordon Fain. Gordon's enthusiasm and genuine love of scientific exploration is truly inspirational. I will always be grateful to Sam for his kindness that reaches well outside of the lab. It has been an honor to be a part of this family, and I am grateful to have the support and mentorship of such incredible people.

I would like to thank everyone in the Sampath/Fain Lab: Dr. Rikard Frederiksen, for helping me trouble shoot every problem and sharing my excitement for every success; Dr. Khris Griffis, our coding and statistics master; Dr. Ala Morshendian, for keeping me grounded; Dr. Paul Bonezzi, for providing me with fresh motivation to make it over that final stretch; Kate, for keeping lab and life interesting; Dr. Nori Ingram, for teaching me how to patch cones and, more importantly, that anything on a rig can be fixed with rainbow duct tape, spit, and prayer to the science gods.

I would like to thank the other members of my committee: Dr. Thomas O'Dell, Dr. Roxana Radu, and Dr. Gabriel Travis for their patience and invaluable feedback. I would also thank my clinical mentor Dr. Michael Gorin who exemplifies the physician I aspire to become.

My path into this program has been anything but straight or easy but it has been a fantastic adventure. Looking back there are a few people who were pivotal to my trajectory: Dr. Frank Powel who taught me that if your research isn't fun then you're doing it wrong; Melanie Daub who changed my life with a single small email; Dr. Gabe Murphy who introduced me to the magical world of electrophysiology and led me to discover my love for vision science and ophthalmology; Dr. Chris Heichel who helped me believe in myself during a time when it would have been easy to give up; Dr. Sanjoy Bhattacharya who took a chance by accepting me into the inaugural class of his incredible MVSIO program; Dr. Richard Lee who showed me it is possible to do everything and to do it all at once.

I would also like to acknowledge a few amazing ladies who have laughed and cried with me through all the most important moments: Beth Stubblefield, Julia Bachman, and Rachel Zarndt. I am so fortunate to have you all in my life.

Above all, none of my achievements would be possible without the unwavering love and support of my family; My father John, for his faith that all my education will eventually lead to a job, or at the very least a meaningful and fulfilling life; my brother Greg, therapist and master editor, who truly deserves at least partial credit for this work; and my mother Shelley who would have been so proud of who I am becoming.

VITA

EDUCATION AND RESIDENCY TRAINING

EyeSTAR Ophthalmology Residency Program 2019-Present
U. of California Los Angeles - Stein Eye Institute, Los Angeles, CA

Translational Year Internship 2018-2019
HCA, Oak Hill Hospital, Spring Hill, FL

Master of Science in Vision Science and Investigative Ophthalmology 2016-2018
U. of Miami - Bascom Palmer Eye Institute, Miami, FL

Doctor of Medicine 2010-2016
U. of California San Diego School of Medicine, San Diego, CA

Bachelor of Science in Biomedical Engineering, with a Minor in Mathematics 2005-2010
U. of Arkansas, Fayetteville, AR

PUBLICATIONS

Ellis, EM, R Frederiksen, A Morshedian, GL Fain, AP Sampath. Separate ON and OFF pathways in vertebrate vision first arose during the Cambrian. *Current Biology* 2020. 30(11):633-634.

Ellis, EM, JE Lee, L Saunders, WW Haw, DB Granet, and CW Heichel. Complication rates of resident-performed cataract surgery: impact of early introduction of cataract surgery training. *JCRS*. 2018; 44(9):1109-1115.

Ellis, EM, M Kinori, N Hodgson, SL Robbins, and DB Granet. Pulled-in-two syndrome risk factors, management, and outcomes: a multi-center survey. *JAAPOS*. 2016; 20(5):387-391.

Ellis, EM, G Gauvain, B Sivyer, and GJ Murphy. Shared and distinct retinal input to the mouse superior colliculus and dorsal lateral geniculate nucleus. *J Neurophysiology*. 2016; 116(2):602-10.

Basaran, KE, M Villongco, B Ho, **EM Ellis**, R Zarndt, J Antonova, SR Hopkins, and FL Powell. Ibuprofen blunts ventilatory acclimatization to sustained hypoxia in humans. *PLoS ONE*. 2016; 11(1): e0146087.

Jin, S, **EM Ellis**, JV Veetil, H Yao, and K Ye. Visualization of HIV protease inhibition using a novel Förster resonance energy transfer molecular probe. *Biotechnol. Prog*. 2011; 27(4):1107-1114.

SELECT PRESENTATIONS

Stein Eye Research Retreat	Oral Presentation	2022
MCIP Student Seminar Series	Oral Presentation	2022
ARVO Annual Meeting	Oral Presentation	2020-22
AUPO Annual Meeting	Oral Presentation	2017
HHMI Scientific Meeting of Medical Fellows	Oral Presentation	2015
Janelia Research Campus Junior Scientist Seminar Series	Oral Presentation	2015
SFN Annual Meeting	Poster Presentation	2014
Environmental Biology Annual Meeting	Poster Presentation	2012
ACS Annual Meeting	Oral Presentation	2010

SELECT HONORS AND AWARDS

Stein Eye Research Retreat, 2nd Place Award for Trainee Presentations	2022
Robert B. Barlow, Jr. Travel Grant, ARVO	2020
NIH TL1 Training Grant, UCSD School of Medicine	2016
HHMI Research Fellowship, UCSD School of Medicine	2013-2014
summa cum laude, U. of Arkansas	2010
First Ranked Senior Scholar, U. of Arkansas	2010
U. of Arkansas Chancellor's Scholarship, U. of Arkansas	2005-2010
Honors College Undergraduate Research Grant, U. of Arkansas	2009
Ann Powell Wood Award for Study Abroad, U. of Arkansas	2008
Libby Finch Study Abroad Scholarship, U. of Arkansas	2007

OTHER PROFESSIONAL AND ACADEMIC ACTIVITIES

Association for Research in Vision and Ophthalmology, *Member*	2013-Present
American Medical Association, *Member*	2010-Present
Tau Beta Pi, The Engineering Honors Society, *Member*	2009-Present
Alpha Epsilon Delta, National Health Preprofessional Honor Society, *Member*	2007-Present
U. of Miami DOCS Community Health Fairs, *Volunteer*	2016-2018
Graduate Teaching Assistantship, U of Miami	2016-2018
Darwin Eye Project, *Volunteer*	2017
Journal of Neurophysiology Podcast, *Featured Author*	2016
UC San Diego Student-Run Free Clinic, *Volunteer*	2010-2016
Howard Hughes Medical Institute Medical Fellows Program, *Regional Co-Chair*	2014-2015
Janelia Association of Research Scientists, *Member*	2013-2015
Lasker/IRRF Initiative on Restoring Vision to the Blind, *Participant*	2014
Northwest Arkansas Prosthetic Limb Drive, *Organizer*	2010
U. of Arkansas Ballroom and Swing Dance Club, *Co-founder and President*	2005-2010
Community Development in Belize, *Student Representative and Project Leader*	2008

CHAPTER 1:

An Introduction to the Retina and Retinitis Pigmentosa

Why Study Vision

Sensory systems create an internal representation of the world that enables us to appropriately interact with our surroundings. As humans, we rely primarily on vision to form our perception of the world. Vision plays a central role in almost every aspect our lives: it allows for object identification used to pick out your clothes in the morning or find food at the grocery store, for navigation enabling you to walk through a crowded room or drive to work, for communication through the reading of signs and labels, and for socialization through the recognition of facial expressions and body language. In addition to image-forming functions, visual input also has critical non-image-forming functions, including balance, coordination, and control of circadian rhythms[1]. Biologically, the importance of vision throughout our evolutionary development is reflected in the amount of space our brain devotes to vision: over 30% of the cortex is involved in the processing of visual information in more than 30 different visual areas[2]. Beyond its functional role in our lives, vision creates a vibrant experience of the world. The importance of vision is apparent in the societal value we place on visual aesthetic as seen in our art, architecture, fashion, movies, and other cultural creations. Given the immense role that vision plays in our daily lives, it is easy to understand the value of studying both normal visual information processing and pathological disruption of vision in retinal diseases.

Brief Overview of the Structure of the Retina

Vision begins in the retina. As described over 100 years ago through the exquisite illustrations of Ramon y Cajal (see Fig 1.1)[3], visual information is processed as it flows from photoreceptors through bipolar cells to the retinal ganglion cells. Along this path, additional processing occurs through the lateral connections of horizontal cells and amacrine cells. The circuits established by these five major neuronal cell types allow the retina to extract specific types of visual information—

such as color, size, speed, and the direction of motion of a stimulus—before forwarding this information to various brain regions for more complex processing.

The initial and most critical step in vision is the detection of light. This task falls to the highly specialized photoreceptor cells that convert light stimuli into an electrical signal. The vertebrate retina contains two major types of photoreceptors: rods that mediate low light or scotopic vision, and cones that mediate bright light or photopic vision. This duplex retinal structure enables the retina to function over an extensive range of environments, encoding information across almost 10 log units of light intensities (see Fig 1.2)[4,5]. The rest of the visual system depends on the ability of photoreceptors to reliably detect light, and defects in photoreceptor function result in significant visual impairment.

The differences in sensitivity and other response properties between cones and rods primarily arise from the expression of different isoforms of phototransduction proteins (see Fig 1.3). Evolutionary studies looking at the origin of photopigments demonstrate that cone photoreceptors are much older than rods[6–8]. Rods likely evolved from cones in our earliest vertebrate ancestors through molecular and structural adaptations that optimized sensitivity[9,10]. Rods are so sensitive they can produce a response to the absorption of a single photon of light[11,12]. This specialization comes at cost, as there is a tradeoff between sensitivity and temporal/spatial resolution. To maximize sensitivity, rods have a longer integration period resulting in slower responses that decrease temporal resolution. Additionally, rod signals converge, and many rods synapse onto a single bipolar cell. The pooling of rod signals increases sensitivity of the retina but decreases spatial resolution.

Cones are specialized for bright light conditions. Cones have significantly faster responses, enabling a higher temporal resolution for better motion detection. Unlike rod circuits, cone circuits prioritize spatial resolution over sensitivity, and cone circuits tend to diverge, with a single cone often synapsing onto many different bipolar cells[13]. The exception is the human fovea

where spatial resolution is the highest, and where each cone connects with only two bipolar cells, passing information onto only two ganglion cells[14]. Cones also have multiple types of opsins with different spectral sensitivities, allowing for detection of color information. Anatomically, cones are shorter than rods with disks formed from invaginations of the cell membrane, while rods have fully encapsulated intracellular disks with longer outer segments to increase the probability of light absorption.

Photoreceptors are highly specialized and have many unique characteristics when compared to other neurons. In the dark, photoreceptors maintain a depolarized resting membrane potential at around -40 mV, compared to conventional neurons that typically rest at approximately -70 mV. As a result of the depolarized resting membrane potential, photoreceptors have continuous synaptic neurotransmitter release in the dark. Light stimulation leads to hyperpolarization of the cell membrane and produces a decrease in neurotransmitter release[12]. Additionally, while many neurons in the brain send digital signals with the all-or-none signaling of action potentials, photoreceptors have an analog signaling system where graded changes in membrane potential result in graded changes in the release of neurotransmitter[15].

While rods and cones have key anatomical and molecular differences, the basic mechanism of phototransduction is the same, as illustrated in Figure 1.4[16]. In the dark, cGMP levels in the cell are elevated and cyclic nucleotide-gated channels (CNG channels) in the outer segment remain open, allowing for a large influx of Na^+ that generates the dark current. The dark current maintains a depolarized resting membrane potential and produces continuous release of glutamate from the photoreceptor synapse. Absorption of light causes photoisomerization of the visual pigment and activation of the opsin. Activated opsin catalyzes the exchange of GDP for GTP on the α subunit of the G-protein transducin. The α-transducin-GTP complex dissociates from the βγ subunit and binds to phosphodiesterase (PDE), activating PDE which hydrolyzes cGMP to GMP. The resulting decrease in cGMP leads to closure of CNG channels, reducing the

dark current and hyperpolarizing the cell membrane. At the synapse, the membrane hyperpolarization causes closure of voltage-gated Ca^{2+} channels, ultimately producing a reduction in synaptic glutamate release. In this way, light signals are converted into electrical signals through phototransduction and passed on to the rest of the visual system through the photoreceptor-bipolar cell synapse [17].

Cone Membrane Physiology and Energy Requirements

Phototransduction converts light stimuli into membrane voltage changes through the closure of CNG channels. Other important membrane conductances act to shape the light-evoked photoresponse and to facilitate the transmission of light signals to bipolar cells through the control of neurotransmitter release[18,19]. Figure 1.5 shows the major membrane ion channels in the cone.

The primary ion channel of the outer segment is the CNG channel. The CNG channel is a non-selective cation channel. As discussed above, CNG channels remain open in the dark to produce the dark current that maintains the depolarized resting potential, and they close with light exposure to produce the hyperpolarizing photoresponse. The outer segment also contains a Na^+/Ca^{2+}-K^+ exchanger to remove Ca^{2+} that enters through the CNG channel. Controlling outer-segment Ca^{2+} concentration is important, as Ca^{2+} driven feedback regulates many components of phototransduction, such as guanylate-cyclase cGMP production and cGMP binding affinity of the CNG channel[20–22]. These feedback mechanisms play an important role in light adaptation[23].

The inner segment contains several important voltage-gated channels, including the hyperpolarization-activated cyclic nucleotide-gated channel (HCN1) and voltage-gated K^+ channels. As the name suggests, the HCN1 channel is activated by membrane hyperpolarization to generate the i_h current, and it deactivates with depolarization. With light driven hyperpolarization of the cell, HCN1 is activated, resulting in an inward current that depolarizes the cell, speeding the recovery from the light response[24,25]. The sustained voltage-gated K^+ channel is responsible

for the i_{kx} current. I_{kx} is a hyperpolarizing current that is active at depolarized membrane potentials and helps to stabilize the resting membrane potential[26,27]. Ca^+-activated K^+ BK channels and Ca^+-activated Cl^- channels also act to stabilize the resting membrane potential[28,29].

Voltage-gated Ca^{2+} channels in the cone pedicle control the synaptic release of glutamate[25]. These channels are open at depolarized membrane potentials and close with light-evoked hyperpolarization. They are tightly coupled with the synaptic ribbon, so that changes in Ca^{2+} influx quickly translate into changes in Ca^{2+}-dependent synaptic vesicle exocytosis[30].

Maintaining the ion gradients needed to generate these membrane currents is the most energetically demanding process in a photoreceptor (see Fig. 1.6)[31,32]. In order to maintain the outer segment dark current, the Na^+ that enters through open CNG channels must be removed. This is achieved with an ATP-dependent Na^+/K^+ pump. An ATP-driven pump is also required to remove the influx of Ca^{2+} through synaptic voltage-gated Ca^{2+} channels. In rods, maintaining the dark current is the dominant ATP expenditure (Fig 1.6A). Cones, on the other hand, have a much larger synapse with multiple synaptic ribbons, and the voltage-gate Ca^{2+} conductance dominates cone ATP consumption (Fig. 1.6B).

Retinitis Pigmentosa

In inherited retinal dystrophies, genetic mutations of photoreceptor-specific genes cause the dysfunction or death of photoreceptors, and the retina loses the ability to detect visual information. The most common inherited retinal dystrophy is retinitis pigmentosa (RP)[33,34], which is characterized by primary rod photoreceptor death followed by secondary cone photoreceptor death resulting in vision loss and eventual blindness. RP was first described in the modern medical literature by A.C. van Trigt in 1853[35], and the name ‘retinitis pigmentosa’ was coined a few years later by the Dutch ophthalmologist FC Donders[36], who mistakenly thought it to be an inflammatory-driven disease. However, descriptions of familial visual impairment likely to be RP

can be found dating back to ancient Egyptian times. RP has a prevalence of approximately 1 in 4000 people, affecting approximately 2 million people worldwide[33]. RP is highly genetically heterogeneous, and over 3000 causative mutations have been identified in more than 60 genes (see Fig 1.7)[34,37,38] . There is also significant genetic overlap between RP and other inherited retinal dystrophies, where different mutations in a given gene can lead to different forms of retinal dystrophies with distinct clinical phenotypes.

Due to the heterogeneous nature of the disease, the presentation and progression of RP varies greatly. In general, RP presents in early adolescents with signs of rod dysfunction, including impaired night vision or nyctalopia, loss of peripheral vision, and abnormal dark adaptation[39,40]. Rod degeneration in RP begins in the mid-periphery of the retina and then progresses, extending both outward to the far-periphery and inward toward the central retina. As the disease progresses, cone photoreceptors also degenerate, and patients begin to lose their central vision.

Obtaining a thorough family history is a key part of the diagnosis of RP. RP can follow autosomal recessive, autosomal dominant, or X-linked patterns of inheritance[34,38]. Examination of the retina can reveal intraretinal pigment deposits, arteriolar attenuation, and a waxy pallor of the optic disc, as seen in the fundus photo in Figure 1.8A[41]. In addition to family history and a retinal exam, RP can be diagnosed with retinal imaging and electroretinography (ERG). Optical coherence tomography (OCT) imaging allows examination of the retinal layers. In RP patients, OCT imaging shows perifoveal loss of photoreceptors, with a centrally preserved island of photoreceptors in the fovea (Fig 1.8B)[41]. Fundus autofluorescence shows a hyperautofluorescent ring, corresponding to the area of active degeneration around the edges of the preserved central retina (Fig 1.8C)[41]. In the early stages of RP, ERG studies show abnormal rod function with grossly normal cone function (see Fig 1.9)[34]. Early ERG changes can be detected prior to the development of visual symptoms. As RP progresses, rod function continues to decline, and cone function eventually also becomes impaired. In advanced stages of RP, the rod and cone ERG

responses are undetectable. The diagnosis of RP can be confirmed with genetic testing, although testing is not necessary; for approximately 30% of cases, the genetic mutation cannot at present be identified[34].

Currently there are no treatments to slow or stop the progression of RP. Strategies for developing potential treatments tend to fall into one of three broad approaches: 1) correction of the underlying genetic defect, 2) neuroprotective therapy to slow degeneration, or 3) restoration of light sensitivity in late stages of degeneration[42].

Significant advances are being made in the development of gene therapies. The FDA recently approved the first in vivo gene therapy which treats Leber congenital amaurosis[43], a different form of inherited retinal dystrophy. Gene therapy techniques include the use of Crisper/Cas9 systems[44–46], gene replacement therapy[47–49], and RNA therapeutics[50,51] to correct the causative genetic defect and theoretically cure the disease. A major obstacle in gene therapy for RP is the diversity of genetic mutations underlying the disease. For the most part, each gene therapy has to be tailored to a specific genetic defect. With the large number of causative mutations, any specific mutation can be quite rare, and each developed gene therapy will only be applicable to a small subset of RP patients. Additionally, gene therapy must be used at the early stages of RP before significant vision loss. Treating patients at later stages of degeneration after significant photoreceptor death will have little benefit. Despite these obstacles, gene therapies are being developed for some of the more common RP mutations, and there are a number of clinical trials currently underway[52].

Neuroprotective therapies do not address the causative genetic mutation, but aim to slow photoreceptor loss in other ways. A major benefit of neuroprotective treatments is that they are more broadly applicable to different forms of RP. Examples of neuroprotective therapies include treatment with neurotrophic factors[53,54], antioxidant therapies[55,56], and anti-apoptotic drugs. Treatment with neurotrophic factors is challenging due to the short half-life of these agents. To

overcome this obstacle, gene therapy can be used to mediate continuous expression of these factors[57]. Targeting microglial cells to activate their neuroprotective functions has been shown to promote photoreceptor survival in RP[58–60]. Additionally, genetic manipulation of specific metabolic pathways can also be used to promote photoreceptor survival. Several studies have shown that upregulating the mTOR pathway in cones increases aerobic glycolysis and anabolic pathways and delays cone degeneration [61]. Other studies have identified key enzymes of aerobic glycolysis or oxidative phosphorylation that could be possible targets for metabolic reprogramming[62–66]. Like gene therapy, neuroprotective treatment is most beneficial at early stages of retinal degeneration.

For patients in the late stages of RP who already have significant or even complete vision loss, treatments are being developed to restore photosensitivity to the retina. Retinal prosthetics have successfully restored light perception to patients with advanced RP. These devices consist of an electrical chip implanted onto the retina to provide direct electrical stimulation to retinal cells. Retinal prosthetics are limited by their low spatial resolution and inability to stimulate individual targeted cells. As a result, patients require significant training to interpret the visual signals their brains receive.

Optogenetics and small molecule therapies aim to produce more precise photostimulation to better mimic normal visual input. In optogenetic therapy, light-sensitive ion channels are introduced into specific retinal cell types. In addition to allowing for cell-specific light stimulation, depolarizing and hyperpolarizing optogenetic channels could be combined in order to mimic normal retinal ON and OFF pathways. Optogenetics is a promising technique, and the first optogenetic therapy for RP is currently in phase 2 clinical trials.

The best way to harness complete visual processing power of the retina, and restore the most physiologically normal vision, would be to restore light sensitivity at the level of the photoreceptor. One way to restore the function of photoreceptors is to replace them with a photoreceptor transplant[67]. Recent work suggests that transplanted photoreceptors are capable

of integrating into the existing retinal circuitry[68]. Another approach is to target surviving dormant cones, which have been shown to persist in the retina into the late stages of RP. Restoring light sensitivity to these dormant cones, either artificially through optogenetic techniques or through metabolic and cellular manipulations to reactive these cells, is another promising approach to restoring vision at the level of the photoreceptor. One of the major challenges in vision restoration is retinal remodeling, and no matter which approach is used, it may not be possible to restore normal vision if there are permanent remodeling changes to the inner retinal circuitry. Nonetheless, restoration of even crude light perception can have a significant impact on patient quality of life.

Degenerative Processes in RP: Mechanisms of Primary Rod Death

The mechanism of primary rod death in RP differs depending on the causative mutation. Figure 1.10 illustrates some of the cellular systems that can be disrupted in RP. Because photoreceptors are among the most metabolically active cells in the body, they are particularly susceptible to mitochondrial dysfunction and other defects in retinal metabolism. Mutations that lead to ciliary dysfunction are associated with syndromic forms of RP, which often present with concurrent hearing loss due to degeneration of cochlear hair cells. Mutations in a wide variety of genes can lead to protein misfolding, and the accumulation of misfolded proteins results in endoplasmic reticulum stress that activates pro-apoptotic pathways.

Defects in rod phototransduction are among the most common causes of RP. Phototransduction dysfunction can be roughly categorized into two groups: 1) mutations leading to inactivation of the phototransduction cascade, and 2) mutations leading to over-activation of the phototransduction cascade. Inactivation of the phototransduction cascade will result in permanently elevated levels of cGMP and open CNG channels (refer to Fig 1.4). These defects effectively keep rods in a “dark” state and can be expected to result in persistent glutamate release

at the synaptic terminal. Examples of mutations leading to phototransduction inactivation include loss-of-function mutations in rod phosphodiesterase genes, such as those seen in rd1 and rd10 mouse models. Over-activation of phototransduction results in closure of the CNG channels, effectively keeping the rods in a “light activated” state and are predicted to cause chronically low levels of glutamate release at the synaptic terminal. Given that these two types of phototransduction defects may have opposite effects on synaptic glutamate release, they may also result in different mechanisms of downstream retinal remodeling, especially early remodeling changes at the rod-to-rod bipolar cell synapse. Such differences could have significant implications for therapeutic approaches. There is a need for more research into the mechanisms of downstream retinal remodeling, and how different forms of RP affect these mechanisms.

Degenerative Processes in RP: Retinal Remodeling

Photoreceptor death results in changes to downstream retinal neurons, including synaptic rewiring, changes in expression of synaptic structures, cell migration, and growth of abnormal neuronal processes[40,69–72]. Together, these changes are known as retinal remodeling. Retinal remodeling disrupts normal retinal circuitry, may interfere with early interventions, and poses a significant challenge to restoring functional vision to patients with late stage RP. Understanding the mechanisms behind retinal remodeling is critical for the development of vision restoration therapies.

Retinal remodeling in the outer retina begins at the synapse between rods and rod bipolar cells (see Fig. 1.11). Rod dysfunction in early degeneration is accompanied by retraction of rod spherules and downregulation of presynaptic and postsynaptic structures[73–75]. As rods die, rod bipolar cells begin to extend aberrant dendritic processes, searching for new synaptic partners in an attempt to restore normal synaptic input[76]. Studies have shown that prior to rod death, there is a disruption in the synaptic transmission between rods and rod bipolar cells. Figure 1.12 shows

ex vivo ERG recordings, comparing retinal responses between wildtype mice and Cngb1 knockout mice, a model of RP[73]. These recordings reveal a larger relative desensitization of the rod bipolar-dominated b-wave compared to the rod-driven a-wave, indicating a functional uncoupling of the rod-to-rod bipolar synapse. The functional deficit seen from the ERG is disproportionate to histological changes (see Fig. 1.13) and cannot be explained simply by the loss of synaptic connections. Investigating the mechanism underlying this functional uncoupling is the focus of the second chapter of my thesis.

As photoreceptor degeneration progresses and the retina loses light driven input, the outer retina continues to undergo remodeling. Despite significant disruption of the outer retina, inner retinal structures appear to remain largely intact until the end stages of degeneration[77–79]. Some retinal ganglion cells show abnormally small dendritic arborizations[80], but they continue to maintain cell-type specific stratification into ON, OFF, and ON-OFF inner plexiform layers.

Although the inner retinal structure remains relatively intact, the inner retina does exhibit functional abnormalities. Paradoxically, the loss of photoreceptor input results in increased spontaneous activity which manifests as oscillatory waves of retinal activity[81–83]. This retinal hyperactivity is likely responsible for some of the visual hallucinations that patients experience in the late stages of RP. At the end stage of RP, the inner retina also undergoes degeneration with cellular migration, neurite formation, and reactive gliosis resulting in significant disorganization across the entire retina. At the end stage of retinal degeneration, it is highly unlikely that any vision restoration treatments will be able to restore functional vision.

Degenerative Processes in RP: Mechanisms of Secondary Cone Death

Currently, the mechanisms of secondary cone degeneration in RP are only partially understood. Secondary cone degeneration begins only after rod death has reached a critical threshold. Prior to cell death, cones undergo a degenerative process, progressively losing their outer segment

and cone pedicle[84]. The resulting dormant cone cell bodies can remain alive in the retina into the late stages of RP[85]. Early proposed mechanisms for secondary cone death, such as the release of toxins during rod death[86,87], failed to explain the delay in cone death or the preceding degeneration of cones into dormant cells. Recently, a significant amount of research has begun to elucidate the complex mechanisms behind secondary cone degeneration.

One of the first discoveries directly linking rod death to secondary cone dysfunction was the identification of rod-derived cone viability factor (RdCVF), a soluble protein secreted by rods that regulates cone glucose metabolism[88–90],. RdCVF modulates the activity of the GLUT-1 glucose transporter, promoting increased glucose uptake and stimulating aerobic glycolysis[91]. Loss of RdCVF with rod death leads to a decrease in the ability of cones to take up glucose. Cones must balance glucose utilization between three major metabolic pathways: ATP production for maintaining ion gradients, reducing agents for an antioxidant defense system, and anabolic pathways for outer segment regeneration. The glucose deficiency caused by the loss of RdCVF disrupts the careful balance between these three processes. Since the discovery of RdCVF, there has been a growing body of evidence linking secondary cone degeneration to metabolic dysregulation[92–96] .

In addition to metabolic dysfunction, oxidative stress has been shown to play an important role in secondary cone degeneration [97–99]. As rods die, the oxygen demand in the outer retina decreases. Unfortunately, the choroid is unable to downregulate the oxygen supply in response to this decreased demand, and the loss of rods is accompanied by an increase in outer-retina oxygen tension. The resulting hyperoxia leads to formation of toxic reactive oxygen species, which can cause irreversible damage to proteins, lipids and DNA. In addition to directly damaging surviving cones, oxidative stress also leads to microglial activation.

Microglial cells are the resident immune cells in the retina, and one of their primary functions is to monitor tissue health and to remove damaged cells[100,101]. Microglial activation is

complex; depending on the pathways involved, it can lead to pro- or anti-inflammatory responses. Unfortunately, in RP, over-activation of the inflammatory response can cause the release of toxic inflammatory cytokines and excessive phagocytosis, resulting in further retinal damage. Microglial cells are an important target for the treatment of RP, and it may be possible to reprogram them to decrease their cytotoxic effects and promote their cytoprotective effects.

Although we are making advances in our understanding of the mechanisms involved in secondary cone degeneration, there is still little known about how cone membrane physiology changes during this process. One unexpected finding is that dormant cone cell bodies maintain a depolarized resting membrane potential[102]. This is surprising because the loss of the cone outer segment, along with the outer segment CNG channels, should result in the hyperpolarization of the cell. Additionally, degenerating cones are essentially in an energy deficient state. Because the most energetically demanding process in a photoreceptor is the maintenance of the ion gradients required to generate membrane currents (see Fig 1.6)[31,32], it is reasonable to hypothesize that degenerating cones may make significant changes to their membrane physiology in order to reduce their energy requirements. Investigating changes in cone membrane physiology during secondary cone degeneration is the focus of the third chapter of my thesis.

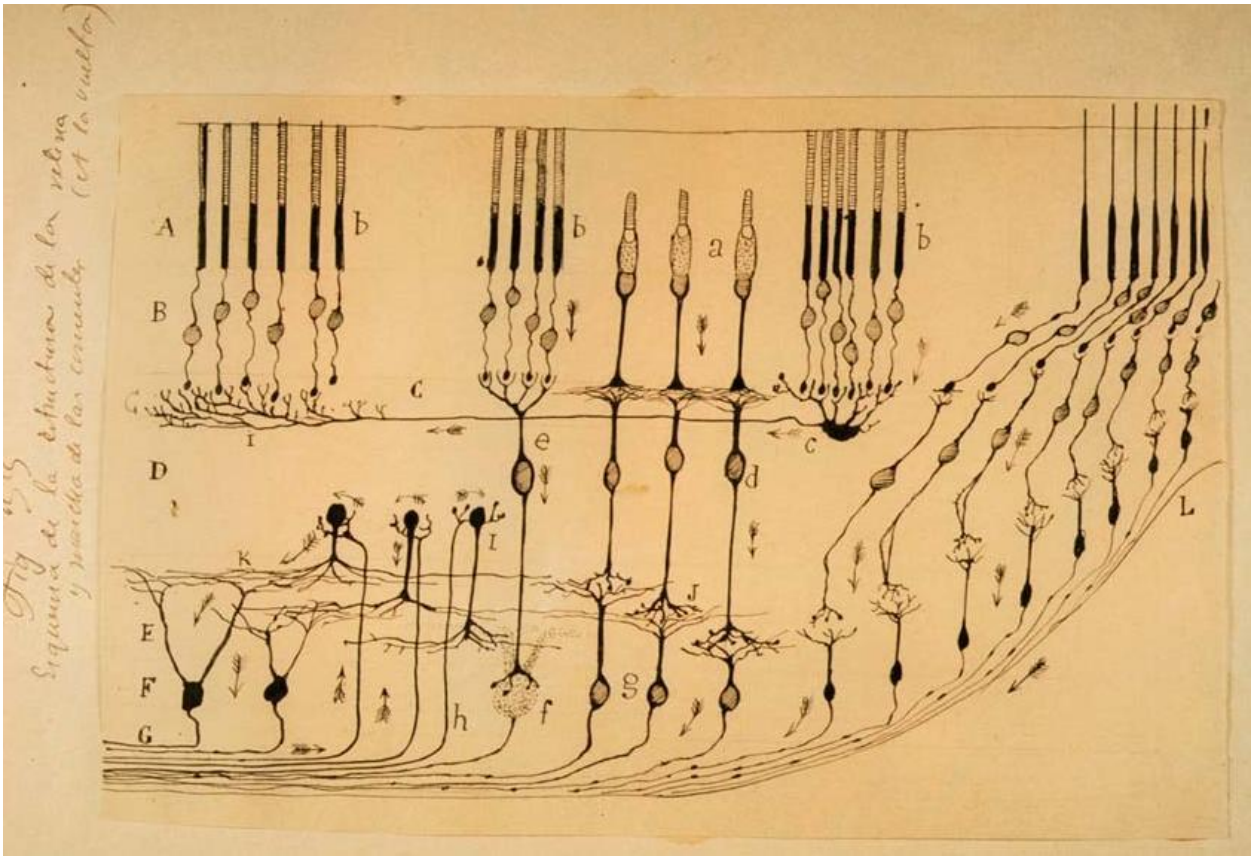

Figure 1.1 Structure of the retina illustrated by Ramon y Cajal

Ramon y Cajal depicted the major layers of the retina: photoreceptor outer segments (A), outer nuclear layer with photoreceptor cell bodies (B), outer plexiform layer with photoreceptor and bipolar cell synaptic connections (C), inner nuclear layer with bipolar cell bodies (D), inner plexiform layer with bipolar cell and retinal ganglion cell synaptic connections (E), retinal ganglion cell layer (F) and retinal nerve fiber layer with retinal ganglion cell axons which project to the brain through the optic nerve (G). He also predicted the flow of visual information from rods (b) and cones (a) through bipolar cells (e and d) to retinal ganglion cells (g). Additionally, he depicted the lateral connections of horizontal cells (c), and amacrine cells (k and l). Figure adapted from: https://braintour.harvard.edu/archives/portfolio-items/seeing-is-believing.

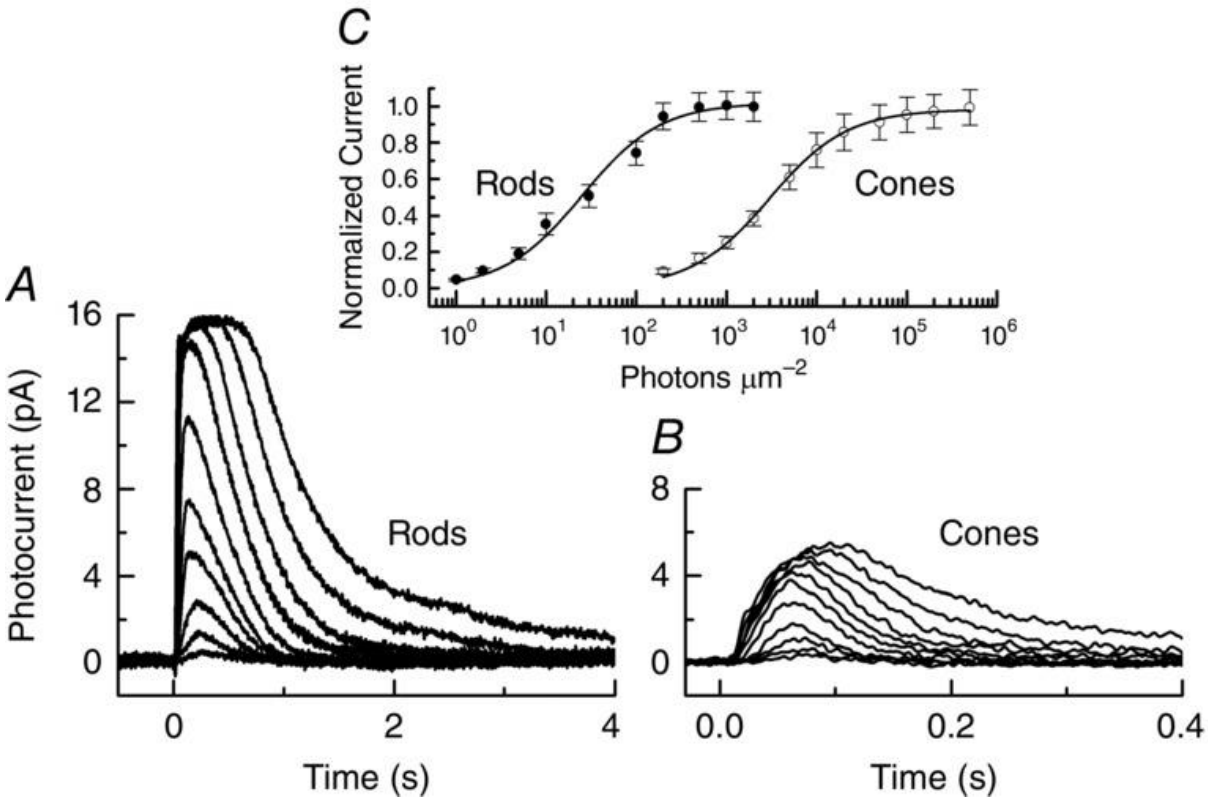

Figure 1.2 Sensitivity of rod and cone photoreceptors

Responses of mouse rod photoreceptors **(A)** and cone photoreceptors **(B)** to flashes of light of increasing intensity. Note the difference in time scales, with significantly faster response rates in cones. Using the peak responses at each light intensity, normalized to the saturating response, a response intensity curve can be generated **(C)** to show the functional range of light intensities for rods and cones. Figure adapted from Ingram et al (2016)

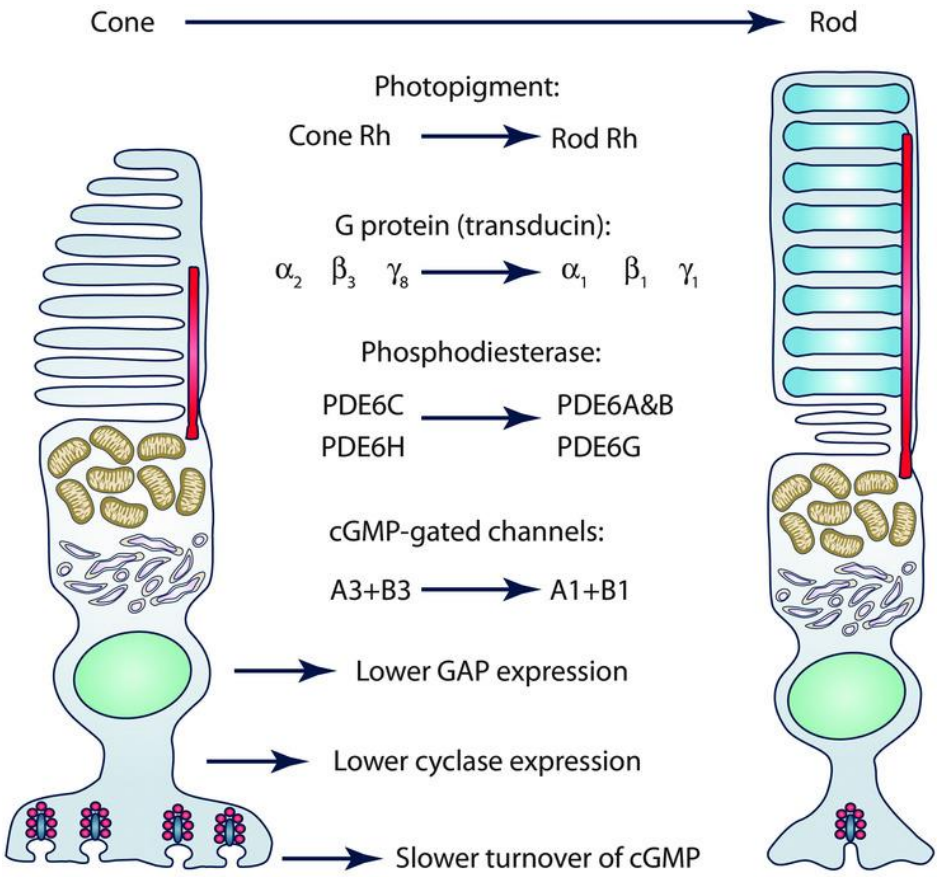

Figure 1.3 Anatomical and molecular differences between rod and cone photoreceptors

Anatomically, cones (left) have shorter outer segments with disks formed from membrane invaginations, while rods (right) have longer outer segments with intracellular disks. The cone synaptic pedicle has multiple synaptic ribbons transmitting information into diverging circuits. In contrast, rods have a single synaptic ribbon and transmit information into converging circuits. Different isoforms of phototransduction proteins result in the major differences in cone and rod photoreceptor sensitivity and other response properties. Abbreviations: Rh, photoreceptor photopigment; cGMP, guanosine 3′,5′-cyclic monophosphate; GAP, GTPase-accelerating protein. Figure adapted from Ingram et al (2016)

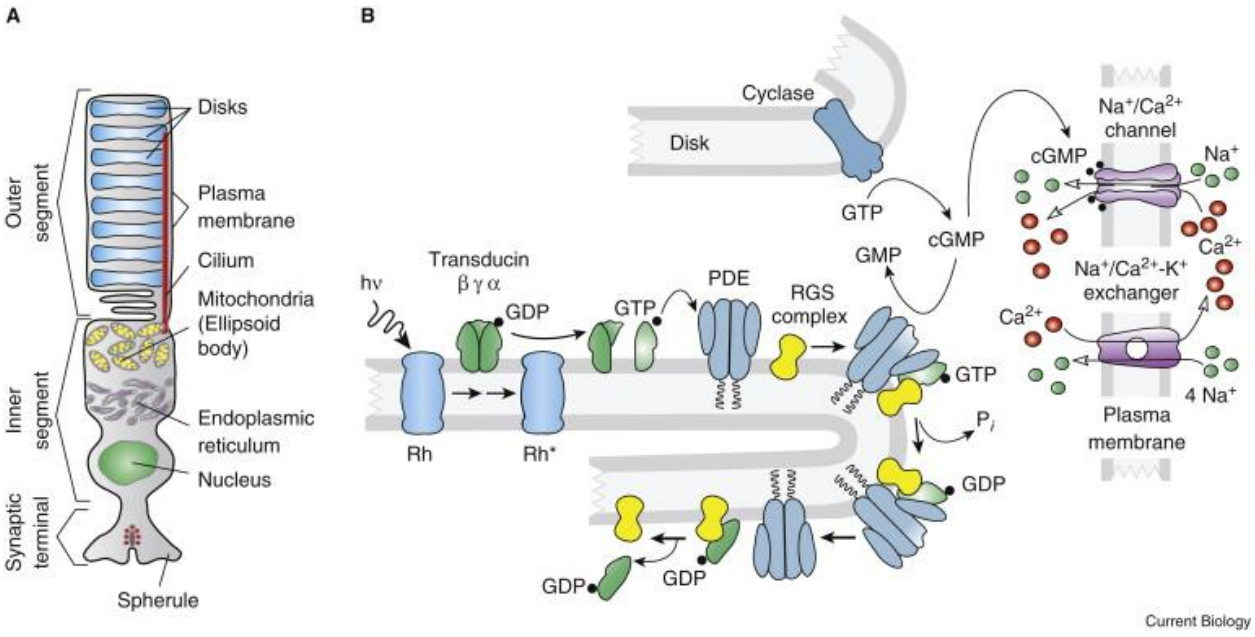

Figure 1.4 Phototransduction in the vertebrate photoreceptor

A) The basic structure of a vertebrate ciliary photoreceptors. **B).** Phototransduction occurs in the disks of the photoreceptor outer segment. cGMP levels in the outer segment are maintained through the balance of cGMP production by cyclase and hydrolysis by phosphodiesterase (PDE). In the dark, cGMP levels remain elevated, allowing cyclic nucleotide-gated channels (CNG channels) to remain open. Light absorption leads to photoisomerization and activation of the photoreceptor opsin. This in turn activates the G-protein transducin, which then activates PDE. Activated PDE hydrolyzes cGMP to GMP, resulting in a decrease in cGMP levels and closure of CNG channels. Abbreviations: hv, light; Rh, rod photopigment rhodopsin; Rh∗, activated rhodopsin; GTP, guanosine triphosphate; GDP, guanosine diphosphate; cGMP, guanosine 3′,5′-cyclic monophosphate; GMP, guanosine monophosphate; PDE, guanosine nucleotide phosphodiesterase; RK, rhodopsin kinase; RGS complex, group of three proteins including RGS9 which accelerate the hydrolysis of GTP by the alpha subunit of transducin; and Pi, inorganic phosphate. Figure adapted from Fain et al (2010)

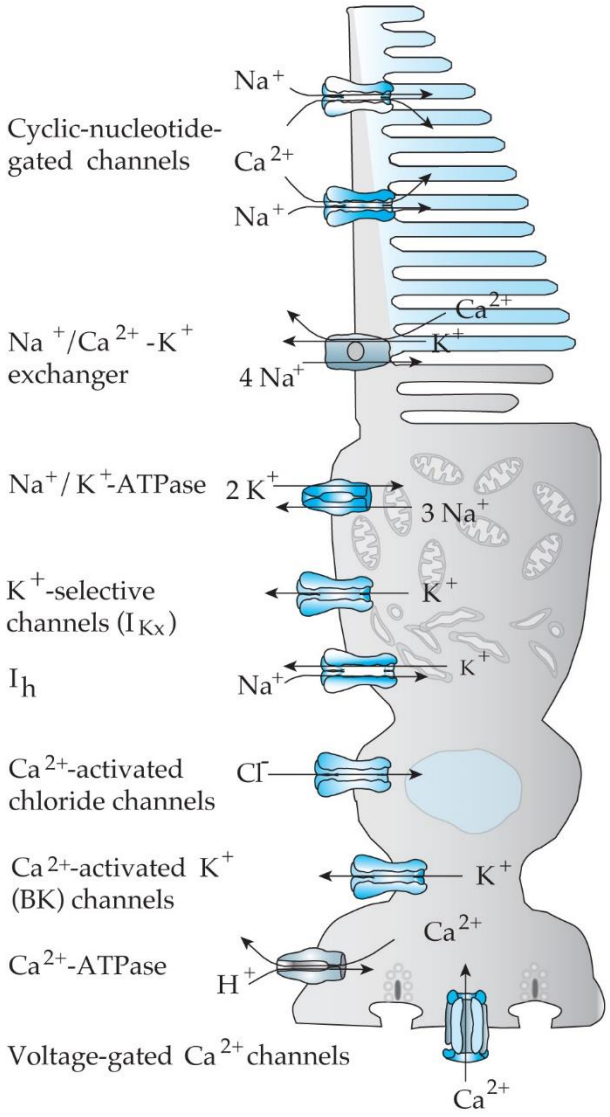

Figure 1.5 Major membrane conductances of the cone photoreceptor

Illustration of the major cone conductances of the cone. The primary ion channel of the outer segment is the CNG channel, which is responsible for generating the photoresponse. Inner segment conductances, including I_h and voltage-gated K^+ channels, help to shape the photoresponse. Synaptic voltage-gated Ca^{2+} channels mediate synaptic glutamate release. Schematic by Margie Fain

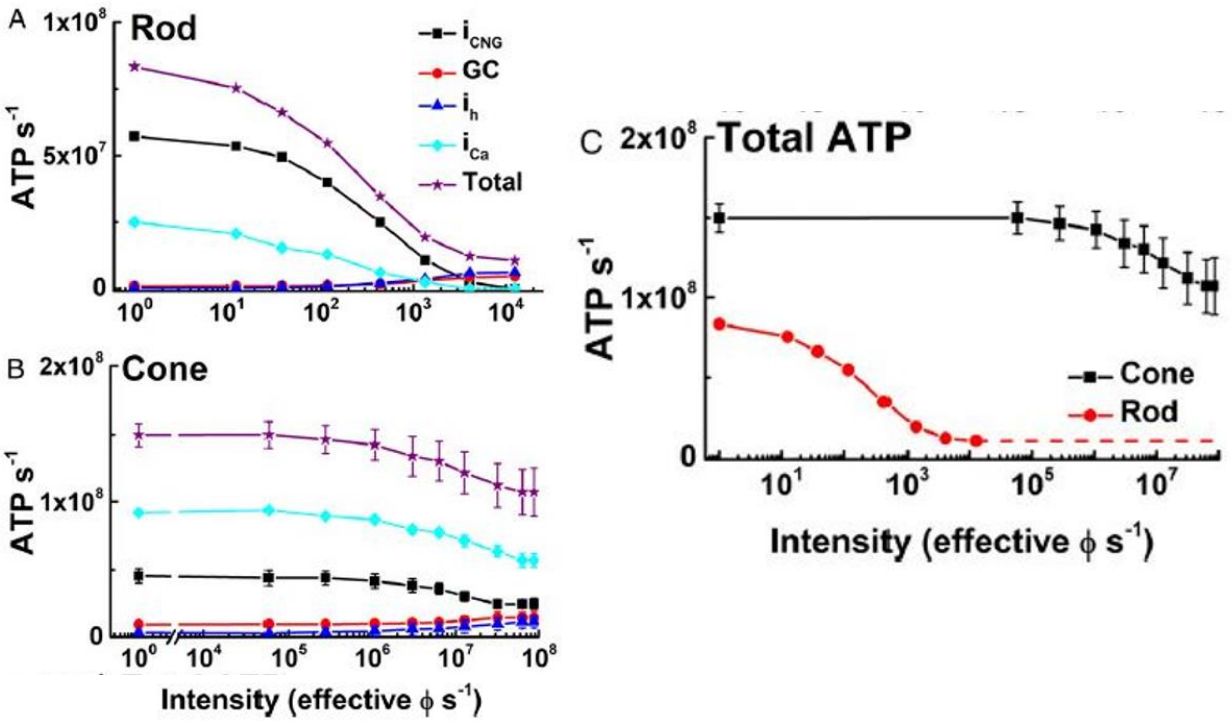

Figure 1.6 ATP consumption of rods and cones in steady light

ATP consumption required to maintain photoreceptor membrane conductances in rods **(A)** compared to cones **(B)** as a function of light intensity. A direct comparison of the total ATP required for cones vs rods **(C)** shows that cones require significantly more ATP than rods at all light levels. Note that rod energy requirements drop off quickly with increasing light levels, and are minimal in bright light. Cones, on the other hand, have only a small decrease in their ATP requirement at bright light levels. When comparing the relative contributions of different conductances, note the significantly larger contribution of the synaptic Ca^{2+} current (cyan) to the energy requirement of cones compared to rods. Abbreviations: i_{CNG}, CNG channel conductance; GC, guanine cyclase; i_h, HCN channel conductance; i_{Ca}, synaptic voltage-gated Ca^{2+} channel conductance; Adapted from Ingram et al. (2020)

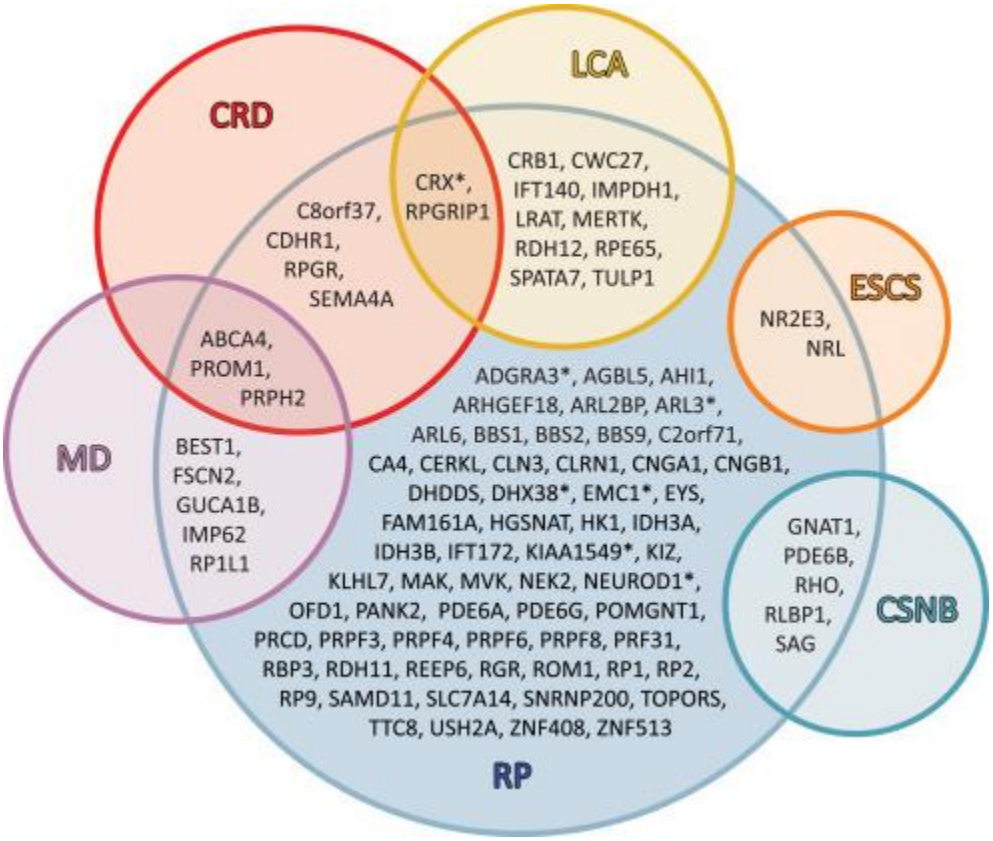

Figure 1.7 Genetic diversity of RP and overlap with other inherited retinal dystrophies

This Venn diagram illustrates the genetic diversity of RP, listing the genes that have been associated with RP within the central blue circle. Different mutations in these same genes can result in other forms of inherited retinal dystrophies that have a different clinical phenotype. Abbreviations: CRD, cone-rod dystrophy; CSNB, congenital stationary night blindness; ESCS, enhanced S-cone syndrome; LCA, Leber congenital amaurosis; MD, macular dystrophy; RP, retinitis pigmentosa. Figure adapted from Verbakel et al (2018)

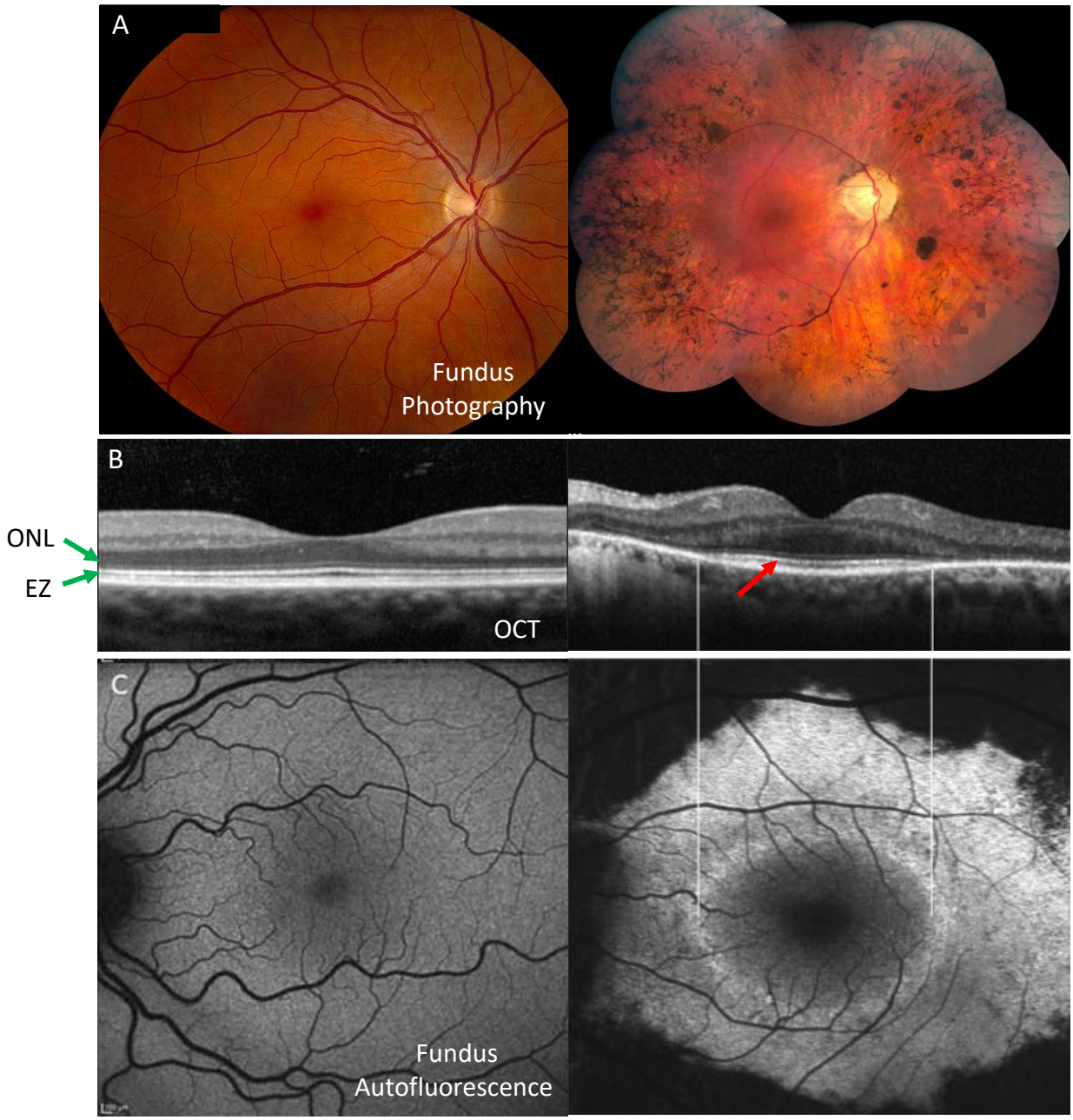
A
Fundus
Photography
B
ONL
EZ
OCT
C
Fundus
Autofluorescence

Figure 1.8 Retinal imaging in RP

Retinal imaging can be a useful tool for the diagnoisis of RP and to monitor disease progression. In this figure you can see retinal imaging studies from an RP patient (right) compared to a normal healthy patient (left) **A)** Fundus photography of an RP patient showing characteristic retinal findings. Note the intraretinal pigment deposits, arteriolar attenuation, and waxy pallor of the optic disc. **B)** Optical coherence tomography (OCT) imaging studies. The green arrows on the healthy retina (left) highlight the thick dark band of outer nuclear layer (ONL) and a prominent bright ellipsoide zone (EZ) band indicating healthy photoreceptors. The RP patient (right) shows perifoveal loss of the ONL and EZ band indicating photoreceptor loss, with a preserved island of ONL and EZ layers (red arrow). **C)** Fundus autofluorescence shows a hyperautofluorescent ring, corresponding to the area of active degeneration around the edges of the preserved central retina. Figures adapted from http://eyerounds.org/index.htm

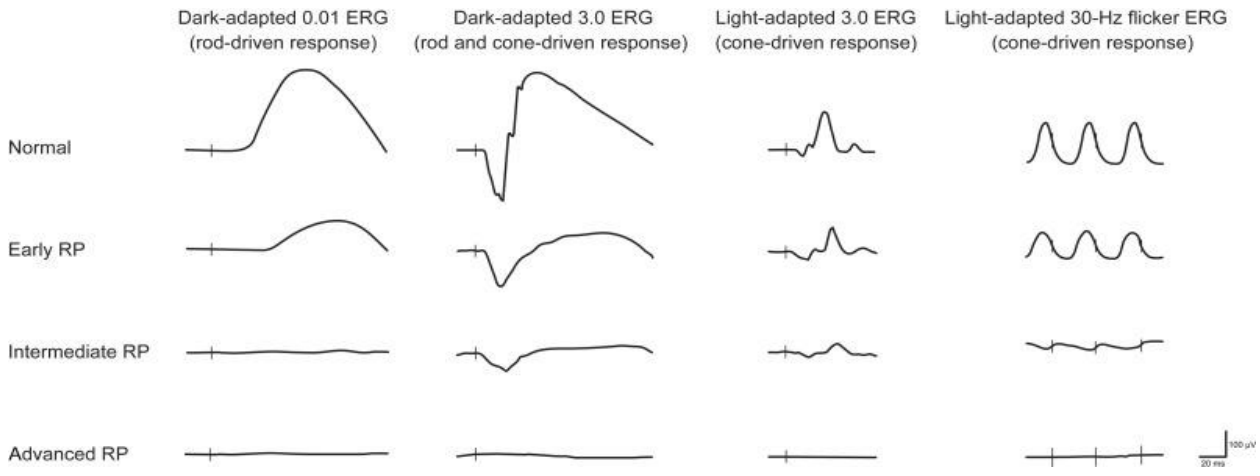

Figure 1.9 ERG findings in RP

This schematic shows the electroretinogram (ERG) findings at various stages of RP compared to a normal study (top). In the early stages of RP there are decreased responses in the dark adapted scotopic and dark adapted photopic conditions, with relatively normal light-adapted photopic and flicker responses. This indicates abnormal rod function with grossly normal cone function and these early ERG changes can be detected prior to the development of visual symptoms. As RP progresses, rod function continues to decline and cone function eventually also becomes impaired. In advanced RP, the ERG responses are extinguished under all four testing conditions. Figure adapted from Verbakel et al (2018)

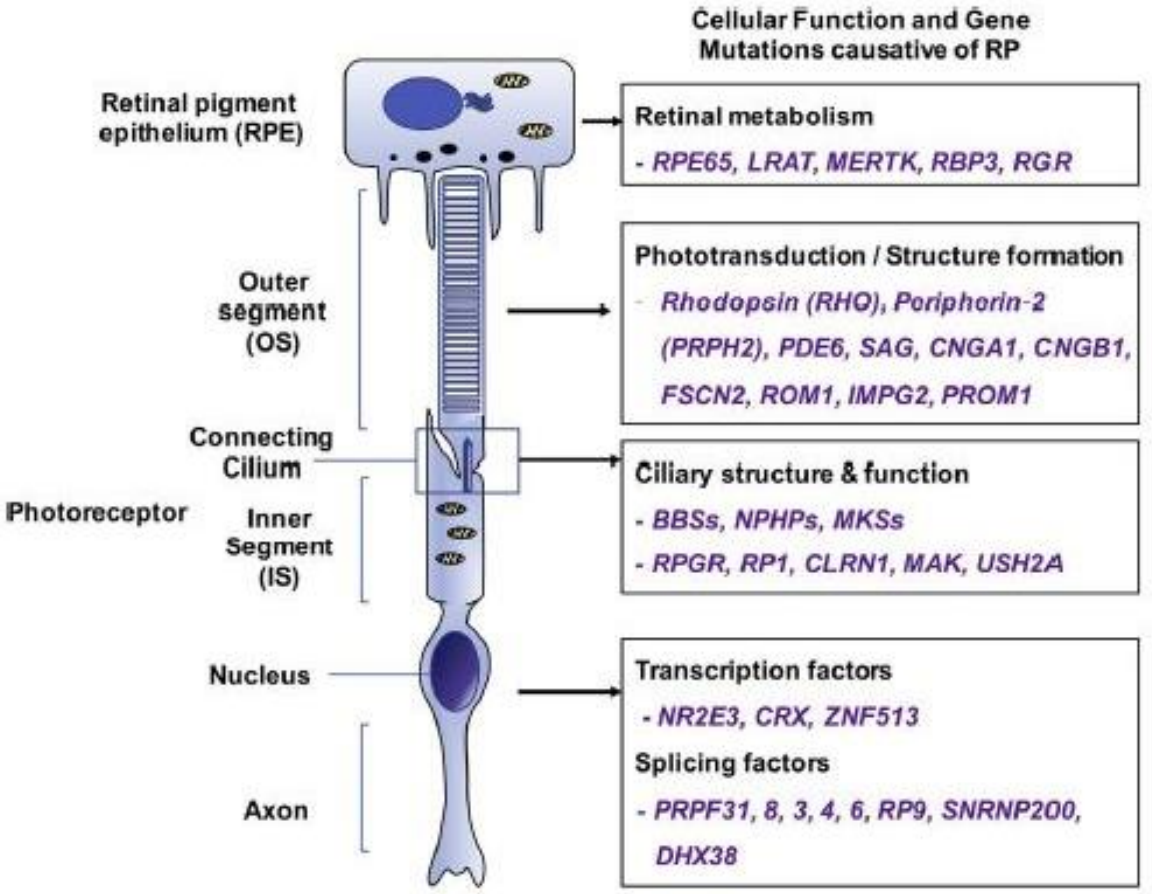

Figure 1.10 Mechanisms of rod death in RP

The mechanism of rod death in RP depends on the underlying genetic defect. This schematic illustrates a number of systems that can be disrupted with RP, and lists some of the RP associated genes that affect these systems. Figure adapted from Dias et al. (2018)

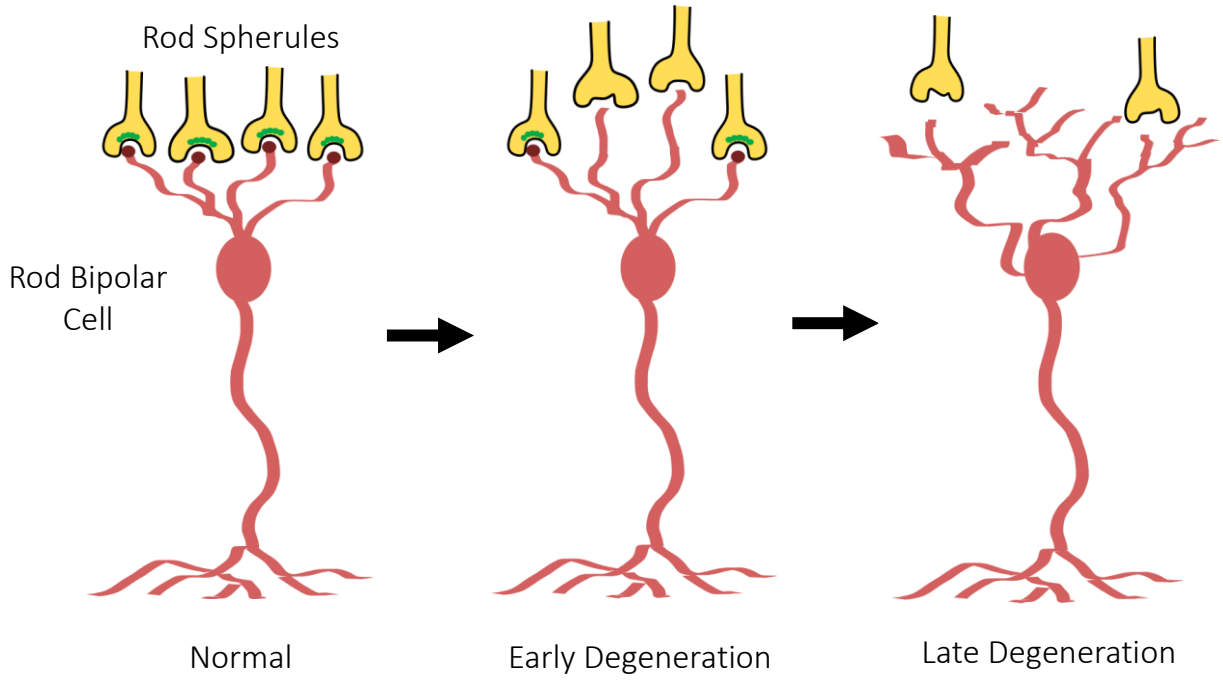

Figure 1.11 Retinal remodeling between rod photoreceptors and rod bipolar cells

Schematic of retinal remodeling between rods and rod bipolar cells. During early stages of retinal degeneration, rod dysfunction is accompanied by retraction of rod spherules and down regulation of synaptic structures, including loss of the rod synaptic ribbons (illustrated in green) presynaptically and rod bipolar cell mGluR6 receptors (illustrated in dark red) postsynaptically. As rods die, rod bipolar cells begin to extend aberrant dendritic processes in search of new synaptic partners in an attempt to restore normal synaptic input. Schematic by Erika Ellis

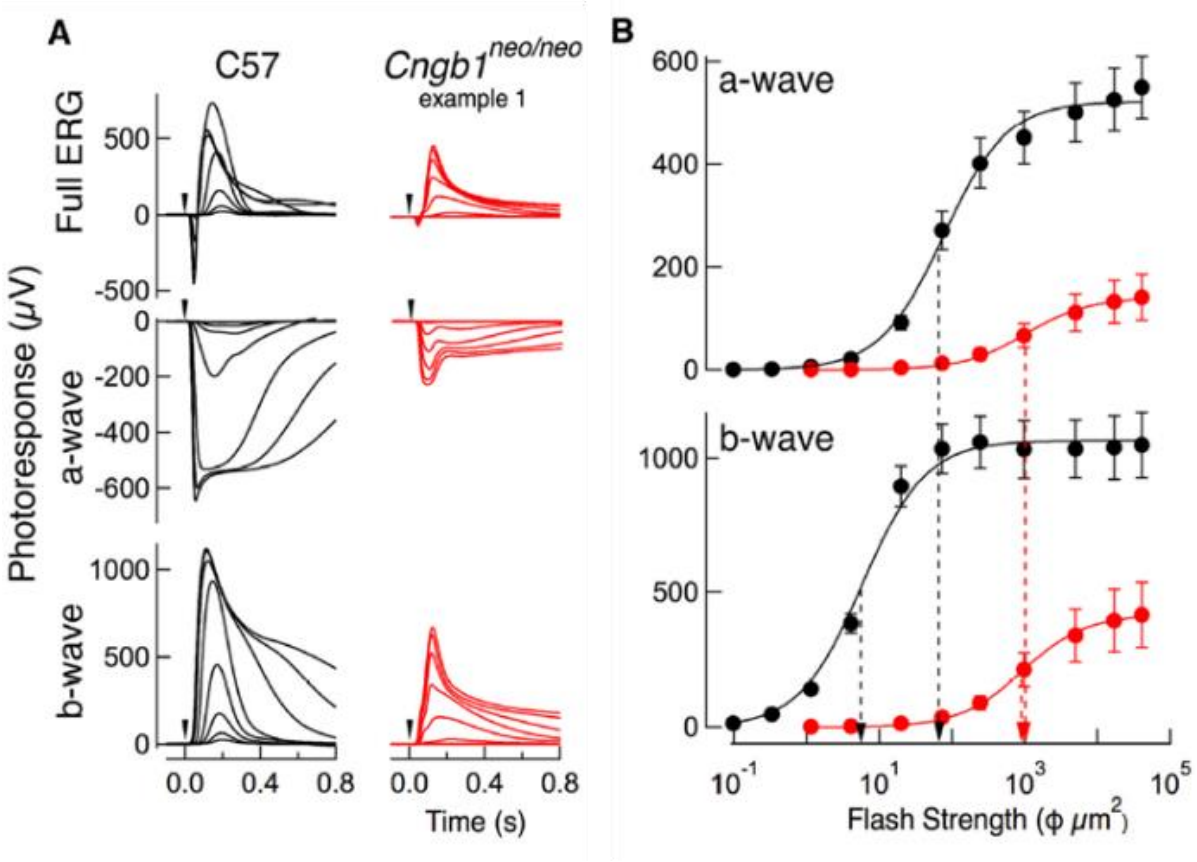

Figure 1.12 Characterization of rod and rod bipolar function by ex vivo ERGs

A) ERG recordings from a C57 wildtype mouse (black) and from a 1-month-old Cngb1 knockout mouse (red) show photoresponses of the retina following flashes of light of increasing intensity. The rod-driven a-wave was isolated using pharmacological blockers of synaptic transmission. The b-wave, which is dominated by rod bipolar cell responses, was then derived by subtracting the a-wave from the Full ERG recording. **B)** A-wave (top) and b-wave (bottom) response intensity curves show the sensitivity of rods and rod bipolar cell responses in WT mice compared to Cngb1 knockout mice. Note the b-wave shows a larger desensitization compared to the a-wave, suggesting defective synaptic transmission between rods and rod bipolar cells. Adapted from Wang et al. (2019)

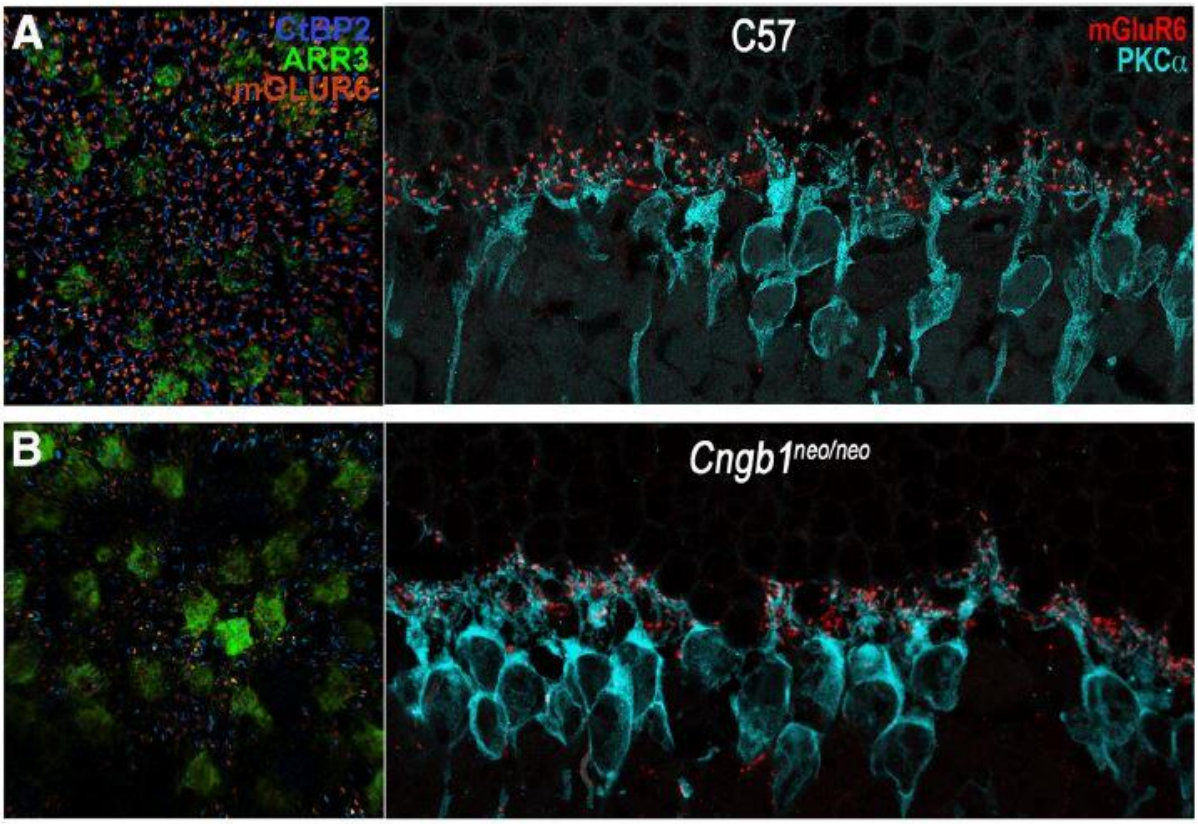

Figure 1.13 Rod-to-rod bipolar cell synaptic remodeling

Retinal flat mounts (left) and retinal sections (right) from P30 C57 wildtype (top) and Cngb1 knockout (bottom) mice. Flat mounts are stained for presynaptic ribbon CtBP2 (blue), postsynaptic mGluR6 (red), and cone arrestin (green). Sections are stained for mGluR6 (red) and rod bipolar cell PkCα (cyan). Note that the Cngb1 knockout retina has fewer presynaptic ribbons and postsynaptic mGluR6, smaller mGluR6 puncta, and migration of synaptic structures into the outer nuclear layer. Adapted from Wang et al. (2019)

RESOURCES

1. Fu, Y., Liao, H.-W., Do, M. T. H. & Yau, K.-W. Non-image-forming ocular photoreception in vertebrates. *Current Opinion in Neurobiology* **15**, 415–422 (2005).

2. Shimojo, S., Paradiso, M. & Fujita, I. What visual perception tells us about mind and brain. *Proceedings of the National Academy of Sciences* **98**, 12340–12341 (2001).

3. Harvard Brain Science Initiative. Harvard Brain Tour: Seeing is Believing. https://braintour.harvard.edu/archives/portfolio-items/seeing-is-believing (2022).

4. Tikidji-Hamburyan, A. *et al.* Rods progressively escape saturation to drive visual responses in daylight conditions. *Nature Communications* **8**, 1813 (2017).

5. Fain, G. L. & Dowling, J. E. Intracellular Recordings from Single Rods and Cones in the Mudpuppy Retina. *Science (1979)* **180**, 1178–1181 (1973).

6. Nickle, B. & Robinson, P. R. The opsins of the vertebrate retina: insights from structural, biochemical, and evolutionary studies. *Cellular and Molecular Life Sciences* **64**, 2917–2932 (2007).

7. Shichida, Y. & Matsuyama, T. Evolution of opsins and phototransduction. *Philosophical Transactions of the Royal Society B: Biological Sciences* **364**, 2881–2895 (2009).

8. Lamb, T. D. Evolution of phototransduction, vertebrate photoreceptors and retina. *Progress in Retinal and Eye Research* **36**, 52–119 (2013).

9. Morshedian, A. & Fain, G. L. The evolution of rod photoreceptors. *Philosophical Transactions of the Royal Society B: Biological Sciences* **372**, 20160074 (2017).

10. Morshedian, A. & Fain, G. L. Light adaptation and the evolution of vertebrate photoreceptors. *The Journal of Physiology* **595**, 4947–4960 (2017).

11. Hecht, S., Shlaer, S. & Pirenne, M. H. ENERGY, QUANTA, AND VISION. *Journal of General Physiology* **25**, 819–840 (1942).

12. Baylor, D., Lamb, T. & Yau, K. Responses of retinal rods to single photons. *The Journal of Physiology* 613–634 (1979).

13. Baylor, D. Photoreceptor signals and vision. Proctor lecture. *Investigative Ophthalmology and Visual Science* **28**, 34–49 (1987).

14. Zhang, C. *et al.* Circuit Reorganization Shapes the Developing Human Foveal Midget Connectome toward Single-Cone Resolution. *Neuron* **108**, 905-918.e3 (2020).

15. Baylor, D. A. & Fettiplace, R. Transmission of Signals from Photoreceptors to Ganglion Cells in the Eye of the Turtle. *Cold Spring Harbor Symposia on Quantitative Biology* **40**, 529–536 (1976).

16. Fain, G. L., Hardie, R. & Laughlin, S. B. Phototransduction and the Evolution of Photoreceptors. *Current Biology* **20**, R114–R124 (2010).

17. Fain, G. L. & Sampath, A. P. Light responses of mammalian cones. *Pflügers Archiv - European Journal of Physiology* **473**, 1555–1568 (2021).

18. van Hook, M. J., Nawy, S. & Thoreson, W. B. Voltage- and calcium-gated ion channels of neurons in the vertebrate retina. *Progress in Retinal and Eye Research* **72**, 100760 (2019).

19. Ingram, N. T., Sampath, A. P. & Fain, G. L. Membrane conductances of mouse cone photoreceptors. *Journal of General Physiology* **152**, (2020).

20. Koch, K.-W. & Stryer, L. Highly cooperative feedback control of retinal rod guanylate cyclase by calcium ions. *Nature* **334**, 64–66 (1988).

21. Dizhoor, A. M. *et al.* Recoverin: a Calcium Sensitive Activator of Retinal Rod Guanylate Cyclase. *Science (1979)* **251**, 915–918 (1991).

22. Hsu, Y.-T. & Molday, R. S. Modulation of the cGMP-gated channel of rod photoreceptor cells by calmodulin. *Nature* **361**, 76–79 (1993).

23. Nakatani, K. & Yau, K.-W. Calcium and light adaptation in retinal rods and cones. *Nature* **334**, 69–71 (1988).

24. FAIN, G. L., QUANDT, F. N., BASTIAN, B. L. & GERSCHENFELD, H. M. Contribution of a caesium-sensitive conductance increase to the rod photoresponse. *Nature* **272**, 467–469 (1978).

25. Barnes, S. & Hille, B. Ionic channels of the inner segment of tiger salamander cone photoreceptors. *Journal of General Physiology* **94**, 719–743 (1989).

26. Barrow, A. J. & Wu, S. M. Complementary conductance changes by I_{kx} and I_{h} contribute to membrane impedance stability during the rod light response. *Channels* **3**, 301–307 (2009).

27. Beech, D. J. & Barnes, S. Characterization of a voltage-gated K+ channel that accelerates the rod response to dim light. *Neuron* **3**, 573–581 (1989).

28. Lalonde, M., Kelly, M. & Barnes, S. Calcium-activated chloride channels in the retina. *Channels* **2**, 252–260 (2008).

29. Pelucchi, B., Grimaldi, A. & Moriondo, A. Vertebrate rod photoreceptors express both BK and IK calcium-activated potassium channels, but only BK channels are involved in receptor potential regulation. *Journal of Neuroscience Research* **86**, 194–201 (2008).

30. Grassmeyer, J. J. *et al.* Ca2+ sensor synaptotagmin-1 mediates exocytosis in mammalian photoreceptors. *Elife* **8**, (2019).

31. Okawa, H., Sampath, A. P., Laughlin, S. B. & Fain, G. L. ATP Consumption by Mammalian Rod Photoreceptors in Darkness and in Light. *Current Biology* **18**, 1917–1921 (2008).

32. Ingram, N. T., Fain, G. L. & Sampath, A. P. Elevated energy requirement of cone photoreceptors. *Proceedings of the National Academy of Sciences* **117**, 19599–19603 (2020).

33. Daiger, S. P., Bowne, S. J. & Sullivan, L. S. Genes and mutations causing autosomal dominant retinitis pigmentosa. *Cold Spring Harbor Perspectives in Medicine* **5**, a017129 (2015).

34. Verbakel, S. K. *et al.* Non-syndromic retinitis pigmentosa. *Progress in Retinal and Eye Research* **66**, 157–186 (2018).

35. van Trigt, A. C. De oogspiegel. *Nederlandisch Lancet, third series, Utrecht* 417–509 (1853).

36. Donders, F. C. Beiträge zur pathologischen Anatomie des Auges. *Archiv Für Ophthalmologie* **1**, 106–118 (1855).

37. Daiger, S. P., Sullivan, L. S. & Bowne, S. J. RetNet: Retinal Information Network. https://sph.uth.edu/retnet/home.htm (2021).

38. Daiger, S. P., Sullivan, L. S. & Bowne, S. J. Genes and mutations causing retinitis pigmentosa. *Clinical Genetics* **84**, 132–141 (2013).

39. Birtel, J. *et al.* Next-generation sequencing identifies unexpected genotype-phenotype correlations in patients with retinitis pigmentosa. *PLOS ONE* **13**, e0207958 (2018).

40. Strettoi, E. & Pignatelli, V. Modifications of retinal neurons in a mouse model of retinitis pigmentosa. *Proceedings of the National Academy of Sciences* **97**, 11020–11025 (2000).

41. University of Iowa Carver College of Medicine. EyeRounds. http://eyerounds.org/ (2022).

42. Dias, M. F. *et al.* Molecular genetics and emerging therapies for retinitis pigmentosa: Basic research and clinical perspectives. *Progress in Retinal and Eye Research* **63**, 107–131 (2018).

43. Russell, S. *et al.* Efficacy and safety of voretigene neparvovec (AAV2-hRPE65v2) in patients with RPE65 -mediated inherited retinal dystrophy: a randomized, controlled, open-label, phase 3 trial. *The Lancet* **390**, 849–860 (2017).

44. Tsai, Y.-T. *et al.* Clustered Regularly Interspaced Short Palindromic Repeats-Based Genome Surgery for the Treatment of Autosomal Dominant Retinitis Pigmentosa. *Ophthalmology* **125**, 1421–1430 (2018).

45. Bakondi, B. *et al.* In Vivo CRISPR/Cas9 Gene Editing Corrects Retinal Dystrophy in the S334ter-3 Rat Model of Autosomal Dominant Retinitis Pigmentosa. *Molecular Therapy* **24**, 556–563 (2016).

46. Li, P. *et al.* Allele-Specific CRISPR-Cas9 Genome Editing of the Single-Base P23H Mutation for Rhodopsin-Associated Dominant Retinitis Pigmentosa. *The CRISPR Journal* **1**, 55–64 (2018).

47. O'Reilly, M. *et al.* RNA Interference–Mediated Suppression and Replacement of Human Rhodopsin In Vivo. *The American Journal of Human Genetics* **81**, 127–135 (2007).

48. Cideciyan, A. v. *et al.* Mutation-independent rhodopsin gene therapy by knockdown and replacement with a single AAV vector. *Proceedings of the National Academy of Sciences* **115**, (2018).

49. Mookherjee, S. *et al.* Long-term rescue of cone photoreceptor degeneration in retinitis pigmentosa 2 (*RP2*)-knockout mice by gene replacement therapy. *Human Molecular Genetics* **24**, 6446–6458 (2015).

50. Millington-Ward, S. *et al.* Suppression and Replacement Gene Therapy for Autosomal Dominant Disease in a Murine Model of Dominant Retinitis Pigmentosa. *Molecular Therapy* **19**, 642–649 (2011).

51. Murray, S. F. *et al.* Allele-Specific Inhibition of Rhodopsin with an Antisense Oligonucleotide Slows Photoreceptor Cell Degeneration. *Investigative Ophthalmology & Visual Science* **56**, 6362 (2015).

52. NIH US National Library of Medicine. ClinicalTrials.gov. https://clinicaltrials.gov/ct2/home (2022).

53. Cayouette, M., Behn, D., Sendtner, M., Lachapelle, P. & Gravel, C. Intraocular Gene Transfer of Ciliary Neurotrophic Factor Prevents Death and Increases Responsiveness of Rod Photoreceptors in the *retinal degeneration slow* mouse. *The Journal of Neuroscience* **18**, 9282–9293 (1998).

54. Thanos, C. & Emerich, D. Delivery of neurotrophic factors and therapeutic proteins for retinal diseases. *Expert Opinion on Biological Therapy* **5**, 1443–1452 (2005).

55. Komeima, K., Rogers, B. S. & Campochiaro, P. A. Antioxidants slow photoreceptor cell death in mouse models of retinitis pigmentosa. *Journal of Cellular Physiology* **213**, 809–815 (2007).

56. Komeima, K., Rogers, B. S., Lu, L. & Campochiaro, P. A. Antioxidants reduce cone cell death in a model of retinitis pigmentosa. *Proceedings of the National Academy of Sciences* **103**, 11300–11305 (2006).

57. Lipinski, D. M. *et al.* CNTF Gene Therapy Confers Lifelong Neuroprotection in a Mouse Model of Human Retinitis Pigmentosa. *Molecular Therapy* **23**, 1308–1319 (2015).

58. Wang, S. K., Xue, Y. & Cepko, C. L. Microglia modulation by TGF-β1 protects cones in mouse models of retinal degeneration. *Journal of Clinical Investigation* **140**, 4360–4369 (2020).

59. Wang, S. K., Xue, Y. & Cepko, C. L. Augmentation of CD47/SIRPα signaling protects cones in genetic models of retinal degeneration. *JCI Insight* **6**, (2021).

60. Wang, S. K., Xue, Y., Rana, P., Hong, C. M. & Cepko, C. L. Soluble CX3CL1 gene therapy improves cone survival and function in mouse models of retinitis pigmentosa. *Proceedings of the National Academy of Sciences* **116**, 10140–10149 (2019).

61. Venkatesh, A. *et al.* Activated mTORC1 promotes long-term cone survival in retinitis pigmentosa mice. *Journal of Clinical Investigation* **125**, 1446–1458 (2015).

62. Xue, Y. *et al.* AAV-Txnip prolongs cone survival and vision in mouse models of retinitis pigmentosa. *Elife* **10**, (2021).

63. Park, K. S., Xu, C. L., Cui, X. & Tsang, S. H. Reprogramming the metabolome rescues retinal degeneration. *Cellular and Molecular Life Sciences* **75**, 1559–1566 (2018).

64. Zhang, L. *et al.* Reprogramming metabolism by targeting sirtuin 6 attenuates retinal degeneration. *Journal of Clinical Investigation* **126**, 4659–4673 (2016).

65. Zhang, L. *et al.* Reprogramming towards anabolism impedes degeneration in a preclinical model of retinitis pigmentosa. *Hum Mol Genet* **25**, 4244–4255 (2016).

66. McDougald, D. S., Papp, T. E., Zezulin, A. U., Zhou, S. & Bennett, J. AKT3 Gene Transfer Promotes Anabolic Reprogramming and Photoreceptor Neuroprotection in a Pre-clinical Model of Retinitis Pigmentosa. *Molecular Therapy* **27**, 1313–1326 (2019).

67. Tezel, T. H. & Ruff, A. Retinal cell transplantation in retinitis pigmentosa. *Taiwan Journal of Ophthalmology* **11**, 336 (2021).

68. Barnea-Cramer, A. O. *et al.* Function of human pluripotent stem cell-derived photoreceptor progenitors in blind mice. *Scientific Reports* **6**, 29784 (2016).

69. Barhoum, R. *et al.* Functional and structural modifications during retinal degeneration in the rd10 mouse. *Neuroscience* **155**, 698–713 (2008).

70. Gargini, C., Terzibasi, E., Mazzoni, F. & Strettoi, E. Retinal organization in the retinal degeneration 10 (rd10) mutant mouse: A morphological and ERG study. *The Journal of Comparative Neurology* **500**, 222–238 (2007).

71. Jones, B. W. *et al.* Retinal remodeling triggered by photoreceptor degenerations. *The Journal of Comparative Neurology* **464**, 1–16 (2003).

72. Marc, R. E. *et al.* Neural Reprogramming in Retinal Degeneration. *Investigative Ophthalmology & Visual Science* **48**, 3364 (2007).

73. Wang, T. *et al.* Activation of Rod Input in a Model of Retinal Degeneration Reverses Retinal Remodeling and Induces Formation of Functional Synapses and Recovery of Visual Signaling in the Adult Retina. *The Journal of Neuroscience* **39**, 6798–6810 (2019).

74. Varela, C., Igartua, I., de la Rosa, E. J. & de la Villa, P. Functional modifications in rod bipolar cells in a mouse model of retinitis pigmentosa. *Vision Research* **43**, 879–885 (2003).

75. Puthussery, T., Gayet-Primo, J., Pandey, S., Duvoisin, R. M. & Taylor, W. R. Differential loss and preservation of glutamate receptor function in bipolar cells in the *rd10* mouse model of retinitis pigmentosa. *European Journal of Neuroscience* **29**, 1533–1542 (2009).

76. Peng, Y.-W., Hao, Y., Petters, R. M. & Wong, F. Ectopic synaptogenesis in the mammalian retina caused by rod photoreceptor-specific mutations. *Nature Neuroscience* **3**, 1121–1127 (2000).

77. Telias, M., Nawy, S. & Kramer, R. H. Degeneration-Dependent Retinal Remodeling: Looking for the Molecular Trigger. *Frontiers in Neuroscience* **14**, (2020).

78. Mazzoni, F., Novelli, E. & Strettoi, E. Retinal Ganglion Cells Survive and Maintain Normal Dendritic Morphology in a Mouse Model of Inherited Photoreceptor Degeneration. *Journal of Neuroscience* **28**, 14282–14292 (2008).

79. Lin, B. & Peng, E. B. Retinal Ganglion Cells are Resistant to Photoreceptor Loss in Retinal Degeneration. *PLoS ONE* **8**, e68084 (2013).

80. Damiani, D., Novelli, E., Mazzoni, F. & Strettoi, E. Undersized dendritic arborizations in retinal ganglion cells of the rd1 mutant mouse: A paradigm of early onset photoreceptor degeneration. *The Journal of Comparative Neurology* **520**, 1406–1423 (2012).

81. Euler, T. & Schubert, T. Multiple Independent Oscillatory Networks in the Degenerating Retina. *Frontiers in Cellular Neuroscience* **9**, (2015).

82. Trenholm, S. & Awatramani, G. B. Origins of spontaneous activity in the degenerating retina. *Frontiers in Cellular Neuroscience* **9**, (2015).

83. Margolis, D. J. & Detwiler, P. B. Cellular Origin of Spontaneous Ganglion Cell Spike Activity in Animal Models of Retinitis Pigmentosa. *Journal of Ophthalmology* **2011**, 1–6 (2011).

84. Lin, B., Masland, R. H. & Strettoi, E. Remodeling of cone photoreceptor cells after rod degeneration in rd mice. *Experimental Eye Research* **88**, 589–599 (2009).

85. Wong, F. & Kwok, S. Y. The Survival of Cone Photoreceptors in Retinitis Pigmentosa. *JAMA Ophthalmology* **134**, 249 (2016).

86. Ripps, H. Cell death in retinitis pigmentosa: gap junctions and the 'bystander' effect. *Experimental Eye Research* **74**, 327–336 (2002).

87. Kranz, K., Paquet-Durand, F., Weiler, R., Janssen-Bienhold, U. & Dedek, K. Testing for a Gap Junction-Mediated Bystander Effect in Retinitis Pigmentosa: Secondary Cone Death Is Not Altered by Deletion of Connexin36 from Cones. *PLoS ONE* **8**, e57163 (2013).

88. Léveillard, T. *et al.* Identification and characterization of rod-derived cone viability factor. *Nature Genetics* **36**, 755–759 (2004).

89. Byrne, L. C. *et al.* Viral-mediated RdCVF and RdCVFL expression protects cone and rod photoreceptors in retinal degeneration. *Journal of Clinical Investigation* **125**, 105–116 (2015).

90. Yang, Y. *et al.* Functional cone rescue by RdCVF protein in a dominant model of retinitis pigmentosa. *Molecular Therapy* **17**, 787–795 (2009).

91. Aït-Ali, N. *et al.* Rod-derived cone viability factor promotes cone survival by stimulating aerobic glycolysis. *Cell* **161**, 817–832 (2015).

92. Cheng, S. *et al.* Altered photoreceptor metabolism in mouse causes late stage age-related macular degeneration-like pathologies. *Proceedings of the National Academy of Sciences* **117**, 13094–13104 (2020).

93. Camacho, E. T., Punzo, C. & Wirkus, S. A. Quantifying the metabolic contribution to photoreceptor death in retinitis pigmentosa via a mathematical model. *Journal of Theoretical Biology* **408**, 75–87 (2016).

94. Léveillard, T., Philp, N. & Sennlaub, F. Is retinal metabolic dysfunction at the center of the pathogenesis of age-related macular degeneration? *International Journal of Molecular Sciences* **20**, 762 (2019).

95. Kurihara, T. *et al.* Hypoxia-induced metabolic stress in retinal pigment epithelial cells is sufficient to induce photoreceptor degeneration. *Elife* **5**, 1–22 (2016).

96. Wang, W. *et al.* Metabolic deregulation of the blood-outer retinal barrier in retinitis pigmentosa. *Cell Reports* **28**, 1323-1334.e4 (2019).

97. Punzo, C., Xiong, W. & Cepko, C. L. Loss of daylight vision in retinal degeneration: are oxidative stress and metabolic dysregulation to blame? *Journal of Biological Chemistry* **287**, 1642–1648 (2012).

98. Murakami, Y., Nakabeppu, Y. & Sonoda, K.-H. Oxidative Stress and Microglial Response in Retinitis Pigmentosa. *International Journal of Molecular Sciences* **21**, 7170 (2020).

99. Roberts, P. A., Gaffney, E. A., Luthert, P. J., Foss, A. J. E. & Byrne, H. M. Mathematical models of retinitis pigmentosa: The oxygen toxicity hypothesis. *Journal of Theoretical Biology* **425**, 53–71 (2017).

100. Zeng, H. *et al.* Identification of sequential events and factors associated with microglial activation, migration, and cytotoxicity in retinal degeneration in rd mice. *Investigative Ophthalmology & Visual Science* **46**, 2992 (2005).

101. Gupta, N., Brown, K. E. & Milam, A. H. Activated microglia in human retinitis pigmentosa, late-onset retinal degeneration, and age-related macular degeneration. *Experimental Eye Research* **76**, 463–471 (2003).

102. Busskamp, V. *et al.* Genetic reactivation of cone photoreceptors restores visual responses in retinitis pigmentosa. *Science (1979)* **329**, 413–417 (2010).

CHAPTER 2:

Changes in Signaling at Synapses Between Rods and Rod Bipolar Cells in the Early Stages of Retinal Degeneration

ABSTRACT

Retinal remodeling poses a major obstacle to restoring normal retinal function to patients with retinitis pigmentosa (RP). Understanding the mechanisms underlying retinal remodeling is vital for research into new RP treatments. To investigate early changes in the rod-to-rod bipolar cell synapse, I used an RP mouse model with knockout of the rod-specific β-subunit of the cyclic nucleotide-gated channel (CNGβ1 KO). The CNGβ1 KO mouse displays a relatively slow retinal degeneration over approximately 6 months, making it an ideal model for studying early changes in retinal degeneration. Previous studies from CNGβ1 KO mice have shown that rod bipolar cells lack light-evoked responses prior to the loss of light responses in rods, despite histological evidence of intact rod-to-rod bipolar cell synapses at this stage of degeneration. To test whether the lack of rod bipolar cell light-evoked responses is due to impaired glutamate release from rods or due to deficient mGluR6 transduction in rod bipolar cell dendrites, I performed whole-cell patch clamp recordings from rod bipolar cells in retinal slices from CNGβ1 KO mice 2 – 3 months old. Light responses were evoked with bright flashes from a 405-nm LED. To test for mGluR6-driven responses in the absence of light, a weak mGluR6 antagonist, CPPG, was puffed onto the bipolar-cell dendrites. Consistent with previous studies, I showed that light-evoked responses of rod bipolar cells in CNGβ1 KO mice 2 – 3 months old are impaired. These same bipolar cells, however, produced an mGluR6-driven response with exposure to 1 mM CPPG. These results suggest that impaired synaptic transmission between rods and rod bipolar cells is due to presynaptic dysfunction in rods rather than post-synaptic dysfunction in rod bipolar cells. This finding may explain why synaptic transmission between rods and rod bipolar cell can be restored following the early rescue of rod function.

INTRODUCTION

Retinitis pigmentosa (RP) is an inherited retinal dystrophy characterized by autonomous rod photoreceptor degeneration followed by non-autonomous cone photoreceptor degeneration, with concurrent remodeling of downstream retinal circuits. RP is the most common form of inherited retinal dystrophy, affecting approximately two million people worldwide[1]. At the present time, there are no disease-modifying treatments that can slow or stop the progression of retinal degeneration in RP. Substantial progress is being made in the development of treatments, including gene therapy to rescue rod function and treatments to restore light sensitivity to the retina after photoreceptors have been lost[2,3]. A major obstacle to restoring normal retinal function to patients with RP is retinal remodeling, which disrupts the normal retinal circuits and interferes with visual information processing[4]. Understanding the mechanisms underlying remodeling is critical for the development of RP treatments.

During early retinal remodeling, rod bipolar cells undergo dendritic retraction and develop aberrant dendritic processes[5–8]. In an attempt to maintain normal synaptic input, rod bipolar cells can form ectopic synaptic connections with cones[4,9–11]. Bipolar cells also show changes in the expression of synaptic receptors, with downregulation and miss-location of metabotropic glutamate receptors (mGluR6)[12,13]. Studies investigating the effect remodeling on rod bipolar cell function reveal conflicting results. Varela et al. (2003) found that rod bipolar cells from adult rd1 mice lacked responses to glutamate[13]. Degeneration in rd1 mice begins, however, before retinal development is complete, and abnormal rod-to-rod bipolar synaptic development in the rd1 retina could have confounded these results[14]. Barhoum et al. (2008) performed similar experiments with rd10 mice, in which degeneration begins later, and found no difference in rod bipolar-cell glutamate responses between wildtype mice and 1-month-old rd10 mice[8]. On the other hand, Puthussery et al. (2009) showed significant changes in mGluR6-driven responses from rd10 rod bipolar cells, with initial signs of dysfunction beginning at P20 and complete loss of responses by

P45[15]. Additional studies are clearly needed to understand better the remodeling of the rod-to-rod bipolar cell synapse during retinal degeneration.

In this study, I used the CNGβ1 knockout mouse model of RP to investigate early changes in the rod-to-rod bipolar cell synapse. Knockout of CNGβ1, the rod-specific β-subunit of the cyclic nucleotide-gated channel (CNG channel), results in a slow rod-cone retinal degeneration. The CNG channel is the outer segment channel responsible for generating the photoreceptor's dark current and maintaining a depolarized resting membrane potential. It is a non-selective cation channel with a heteromeric structure composed of three α-subunits and one β-subunit[16]. The β1-subunit is specific to rod photoreceptors, and mutations in the CNGβ1 gene lead to impaired expression of rod CNG channels. Due to the formation of homomeric CNGα channels, these rods are still able to generate small light-evoked responses[17]. Retinal degeneration in the CNGβ1 knockout mouse progresses relatively slowly, with ~10% of rods lost at P21, ~20% at P30, ~40% at P60, ~60% at P90, and complete loss of rods by P120[6]. The slow rate of degeneration makes this mouse an ideal model for studying early changes in retinal degeneration.

Our lab previously showed early impairment of rod bipolar-cell light responses in CNGβ1 knockout mice. E*x vivo* ERG recordings from 1-month-old CNGβ1 knockout mice revealed a larger relative desensitization of the rod bipolar-dominated b-wave when compared to the rod photoreceptor-driven a-wave. Additionally, data from single-cell electrophysiology showed a complete loss of light-evoked rod bipolar-cell responses. Histological data from 1-month-old CNGβ1 mice showed changes in the structure of the rod-to-rod bipolar cell synapse [6]. However, the functional deficit was disproportionate to the level of observed synaptic remodeling. These findings suggest that there is early disruption in synaptic transmission between rods and rod bipolar cells in CNGβ1 knockout mice.

Early impairment of rod-to-rod bipolar cell responses could be caused by either (1), presynaptic dysfunction due to loss of glutamate release from rods; or (2), postsynaptic

dysfunction due to loss of rod bipolar-cell mGluR6 receptors or dysfunction in the mGluR6/TRPM1 transduction cascade. In this study, I used whole-cell patch-clamp recordings to determine which of these mechanisms underlies the early loss of rod bipolar-cell light responses.

MATERIALS AND METHODS

Animal Care

All experiments were performed in accordance with rules and regulations of the National Institutes of Health guidelines for research animals, as approved by the Institutional Animal Care and Use Committee of the University of California, Los Angeles, California. Mice were housed with ad libitum food and water and kept under a 12 hr light cycle (12 on/12 off). Equal numbers of female and male mice were used. The CNGβ1 knockout mice (denoted as CNGβ1 KO) were originally obtained from the lab of Jeannie Chen at the University of Southern California, then propagated and maintained in the UCLA vivarium. This is a specially designed mouse line, in which a loxP-neomycin-loxP cassette has been inserted into intron 19 of the *CNGβ1* gene to knock out expression of CNGβ1. This mouse line can be crossed with an inducible Cre-line, making it possible to restore normal CNGβ1 expression with administration of Tamoxifen. This powerful mouse model with inducible recombination not only permits the study of the process of retinal degeneration, it also enables investigation into the reversibility of retinal remodeling. This current study focuses on understanding the degenerative process itself; in consequence, the mice used in the following experiments did not express the inducible Cre. Control experiments for normal rod bipolar-cell function were performed with 129S wildtype mice, referred to simply as WT, which were obtained as needed (129SvPas from Charles River). Rod bipolar-cell function was studied in animals aged 2 – 3 months.

Solutions

After retinal dissection, retinal tissue was kept alive in a specially formulated Ames medium (pH 7.4, osmolarity 284 mOsm), either buffered with bicarbonate (Ames-bicarb) and bubbled with carbogen gas (95% O_2, 5% CO_2); or, for embedding and slicing, buffered with HEPES (Ames-HEPES) and bubbled with 100% oxygen. The standard internal solution for whole-cell patch clamp recordings was a potassium aspartate solution (K-Asp) containing (in mM): 125 potassium aspartate, 10 KCL, 10 HEPES, 5 NMDG-HEDTA, 0.5 $CaCl_2$, 0.5 $MgCl_2$, 0.1 ATP-Mg, 0.5 GTP-Tris, 2.5 NADPH (pH 7.3, osmolarity 280 mOsm). 1 mM CPPG in Ames-HEPES solution was used to test for mGluR6 driven responses in the absence of light. CPPG is a weak metabotropic glutamate-receptor antagonist. Blocking the mGluR6 receptor with CPPG mimics light-induced decrease in rod glutamate release and produces a simulated light response in the rod bipolar cell.

In some experiments, a low concentration of a strong metabotropic glutamate receptor agonist, DL-AP4 (5 μM), was added to the Ames-bicarb bath. This low level of DL-AP4 mimics the dark release of glutamate; in the setting of deficient glutamate release from rods, DL-AP4 could act to dark-adapt the rod bipolar cells artificially and increase CPPG sensitivity.

Preparation of Retinal Slices

Prior to each experiment, animals were dark-adapted overnight. The retinal dissection and preparation of retinal slices were performed under infrared illumination. Animals were euthanized by cervical dislocation. The dorsal aspect of each eye was marked prior to enucleation. After enucleation, the globes were moved to an Ames-bicarb bath. The anterior segment, including the cornea and the lens, was carefully removed. The posterior eye cup was bisected into dorsal and ventral halves. From one half, a rectangular section of retina was cut and then carefully separated from the retinal pigment epithelium. The isolated section of retina was embedded in 3% low-temperature-gelling agar dissolved in Ames-HEPES solution. The retina was sliced in cold Ames-

HEPES with a vibratome to obtain 200 µm-thick slices of retina. Slices were made perpendicular to the retina in order to obtain a cross-section of retinal tissue with intact retinal circuitry. The retinal slice selected for recording was mounted on a recording dish; the slice was held in place by a custom-made anchor, and moved to the microscope. The remaining retinal tissue and retinal slices were stored in a light-tight container with Ames-bicarb solution and kept at 32^{o}C. The tissue under the microscope was perfused with Ames-bicarb solution and kept at 35^{o}C.

Whole-cell Patch-clamp Recordings

Whole-cell patch-clamp recordings were performed with borosilicate glass micropipettes (15-19 MOhm) filled with a K-Asp internal solution. Cells were broken into in the voltage-clamp mode. Rods were held at -50 mV, while bipolar cells were held at -70 mV. Resistance was compensated at 75-80%. Light stimuli were delivered as bright flashes (10 ms) from a monochromatic 405 nm LED. Light intensities are given in photons µm^{-2} rather than in the conventional units of light-activated rhodopsin (R*). Conversion from photons µm^{-2} requires knowledge of the photoreceptor outer-segment collecting area, and degenerating photoreceptors have abnormal outer segments. CPPG was puffed onto the dendrites of rod bipolar cells with a second micropipette having a tip diameter of 1-2 µm and attached to a custom-built microinjector. Delivery of the CPPG puff was visualized with an Alexa-750 fluorescent dye, which could be imaged without evoking a light response in the retina. A lack of responses to both light and CPPG will implicate postsynaptic dysfunction, while responses to CPPG in the absence of light responses will indicate presynaptic dysfunction.

Electrophysiology data were filtered at 500 Hz, sampled at 10 kHz, and acquired with Symphony (https://open-ephys.org/symphony/), an open-source MATLAB-based data-acquisition system. All reported membrane voltages have been corrected for the liquid junction potential,

which was approximately 10 mV for the solutions used in these experiments. Data were analyzed with custom scripts written in MATLAB. All averages are reported as mean ± standard deviation.

RESULTS

Recordings of rod bipolar cells from CNGβ1 KO mice 2 – 3 months old showed impaired light-evoked responses (see Fig 2.1, and Table 2.1). For recording conditions in external Ames solution, no light response could be evoked in 4 of 5 rod bipolar cells; however, one rod bipolar cell produced a -40 pA photocurrent (see Fig 2.1E). In all five of these rod bipolar cells, an mGlur6-driven current was seen upon application of 1 mM CPPG (mean: -11 ± 10 pA, range: -5 to -24 pA, n = 5). For three of these cells, including the cell with the light-evoked response, recordings were made after washing on 5 μM DL-AP4 external solution. The application of DL-AP4 had no clear effect on the size of the CPPG induced response, with one cell showing a 14 pA decrease in response, one cell showing no change in response, and one cell showing a 5 pA increase in response. The cell that produced a light-evoked response in Ames solution also produced a 15 pA light-evoked response in the DL-AP4 solution. Light responses in DL-AP4 were not recorded from the two cells that showed no light-evoked responses in Ames. Recordings were made in one cell only in the DL-AP4 solution. This cell showed no light-evoked response and a -33 pA CPPG driven response.

WT rod bipolar cells showed light responses in Ames solution (mean: -62 ± 16 pA, n = 3). Of note, these responses were evoked with significantly less light than used in the CNGβ1 KO mice (WT light intensities, $4x10^1$ to $6x10^3$ photons μm^{-2}; versus CNGβ1 KO light intensities, $1x10^5$ to $2x10^5$ photons μm^{-2}). All three WT rod bipolar cells produced mGluR6-driven responses with application of 1 mM CPPG (mean: -36 ± 17 pA). For two of these cells, recordings were made after washing on 5 μM DL-AP4 in the external solution. The application of DL-AP4 had no clear effect on the size of the CPPG induced response, with one cell showing a large 71 pA increase

in response, and the other cell showing 14 pA decrease in response. Both cells showed persistent—but decreased—light-evoked responses in the DL-AP4 solution.

A recording from a rod in a CNGβ1 KO mouse showed persistent light-evoked responses. As expected, the CNGβ1 KO rod response was substantially smaller than the light-evoked responses seen in WT rods (see Fig 2.2).

DISCUSSION

During RP, the degeneration of photoreceptors leads to changes in downstream retinal neurons, including synaptic rewiring, changes in expression of synaptic structures, cell migration, and growth of abnormal neuronal processes[4,6,11,12]. This retinal remodeling disrupts the normal information-processing circuitry of the retina, and poses a significant challenge to developing RP treatments. Remodeling of the inner retina begins early during degeneration, and rod bipolar cell function can be disrupted prior to the death of rods. Currently, we are making progress in developing gene therapies that can restore normal rod function in certain forms of RP. The rescue of rod function will not however restore vision if rod bipolar cell function remains impaired. Understanding the early changes in retinal degeneration is critical to the development of effective treatments.

Early impairment of rod bipolar-cell function has previously been reported in the CNGβ1 KO mouse model, with evidence of disruption in rod-to-rod bipolar-cell synaptic transmission[6]. In this study, I used whole-cell patch clamp recordings to determine if the rod bipolar-cell dysfunction is presynaptic in rods or postsynaptic in the mGluR6/TRPM1 rod bipolar-cell transduction cascade. First, I tested for light-evoked responses with bright flashes from a monochromatic 405 nm LED. After testing for light-evoked responses, I tested for mGluR6-driven responses in the absence of light by puffing CPPG, a weak mGluR6 antagonist, onto the bipolar cell dendrites. The puffing of CPPG should simulate an mGluR6-driven light response in the rod bipolar cell. A lack

of responses to both light and CPPG would implicate postsynaptic dysfunction, while responses to CPPG in the absence of light-evoked responses would indicate presynaptic dysfunction. My data confirm previous findings, which show impaired light-evoked responses of rod bipolar cells in CNGβ1 KO mice[6]. Rod bipolar cells that lacked a light-evoked response were still able to produce a CPPG-driven response. These results indicate that rod bipolar cells retain mGluR6 transduction to open TRPM1 channels, even after the loss of light-evoked responses.

In the CNGβ1 KO mouse, expression of the rod CNG channel responsible for producing the rod dark current is significantly impaired. Loss of the rod CNG channel would be expected to lead to a decrease in synaptic glutamate release, simulating the effects of persistent light exposure. It is unclear, however, whether rod glutamate release is decreased in the CNGβ1 KO mouse as expected, or if changes in glutamate release are altering downstream signaling. In a healthy retina, light exposure leads to light adaptation of the rod pathway, resulting in changes in synaptic signaling of rods and rod bipolar cells[18,19]. The impaired light responses seen in CNGβ1 KO rod bipolar cells could be the result of an artificially induced "light-adapted" state due to chronically decreased rod glutamate release.

To test if CNGβ1 KO rod bipolar cells are in a light-adapted state, I recorded light-evoked and CPPG-evoked responses with and without 5 μM DL-AP4, a strong mGluR6 receptor agonist. If the rod bipolar cells are in a light-adapted state, the DL-AP4 should mimic the dark release of glutamate and return the rod bipolar cells to a dark-adapted state, increasing their sensitivity to CPPG. The results of this experiment were inconclusive, with one cell showing an increased CPPG-driven response, one cell showing no change in the CPPG-driven response, and one cell showing a decrease in the CPPG-driven response. Interpretation of these results is further confounded by the technical difficulties involved with performing these experiments. With the custom built microinjector, it was difficult to balance the solution pressure in the pipette used to deliver the CPPG puffs, resulting in inconsistencies in the amount of CPPG delivered with each

puff. This puff technique needs to be optimized, and additional data need to be collected before any conclusions can be drawn from this approach.

Future studies should directly investigate changes in rod glutamate release to confirm presynaptic dysfunction. Additionally, my findings do not rule out the possibility that the rod-to-rod bipolar cell synaptic dysfunction could be caused by structural synaptic changes that were not detectable on previous histological studies. A more thorough examination of synaptic structure with higher resolution EM imaging techniques will be needed to conclusively investigate changes in synaptic structures between rods and rod bipolar cells.

Overall, my data suggest that the impaired rod bipolar cell function seen in the CNGβ1 KO mouse model is due to presynaptic dysfunction in rods, and that rod bipolar cells retain the ability to produce mGluR6-driven responses after the loss of light-evoked responses. This may explain the findings of Wang et al (2019), showing that rod bipolar cell function in this model can be restored following the early rescue of rod function. Wang et al (2019) also showed that rescuing rod function at later stages of degeneration was not effective in restoring retinal function. It would be useful to look at rod bipolar cell function at later stages of degeneration to determine if rod bipolar cells do eventually develop defects in mGlur6-driven responses. While there is much research still to be done, this study lays the groundwork for future investigation into early retinal remodeling between rods and rod bipolar cells.

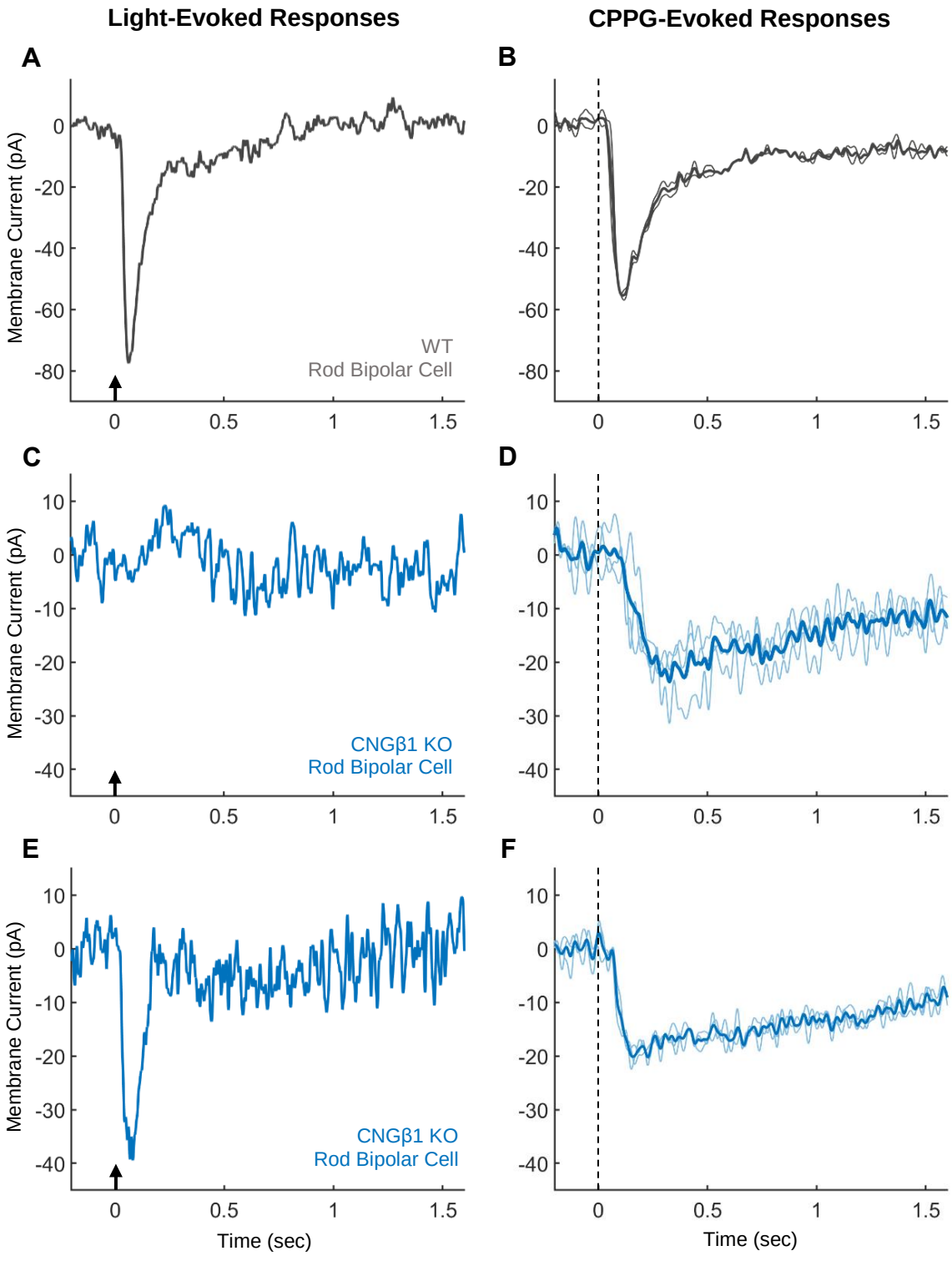
Light-Evoked Responses
CPPG-Evoked Responses
A
B
C
D
E
F
Membrane Current (pA)
WT
Rod Bipolar Cell
CNGβ1 KO
Rod Bipolar Cell
Time (sec)
0
-20
-40
-60
-80
10
-10
-30
0.5
1
1.5

Figure 2.1 Light-evoked and CPPG-evoked responses in rod bipolar cells of WT and CNGβ1 KO mice

Representative recording of a WT rod bipolar cells **(A and B)** and two CNGβ1 KO rod bipolar cells **(C-F)**. Light responses (left) were evoked using a 10 ms flash from a 405 nm LED, indicated by the arrow (light intensities used in the WT recording in A: $6x10^3$ photons μm^{-2}; and the CNGβ1 KO recordings in C and E: $1x10^5$ photons μm^{-2}). Following the recording of light-evoked responses, mGluR6 driven responses in the absence of light were evoked by puffing 1 μM CPPG onto the bipolar cell dendrites (right, delivery of the CPPG puff is indicated by the dashed line). All three of the recordings from WT rod bipolar cells showed both light-evoked and CPPG-evoked responses, as in the representative cell shown in **A and B**. 5 out of 6 CNGβ1 KO rod bipolar cells showed no response to the flash of light, but were able to generate a CPPG-evoked response, as illustrated by the representative cell in **C and D**. One CNGβ1 KO rod bipolar cell was able to produce a light response, and this cell also generated a CPPG-evoked response **(E and F).**

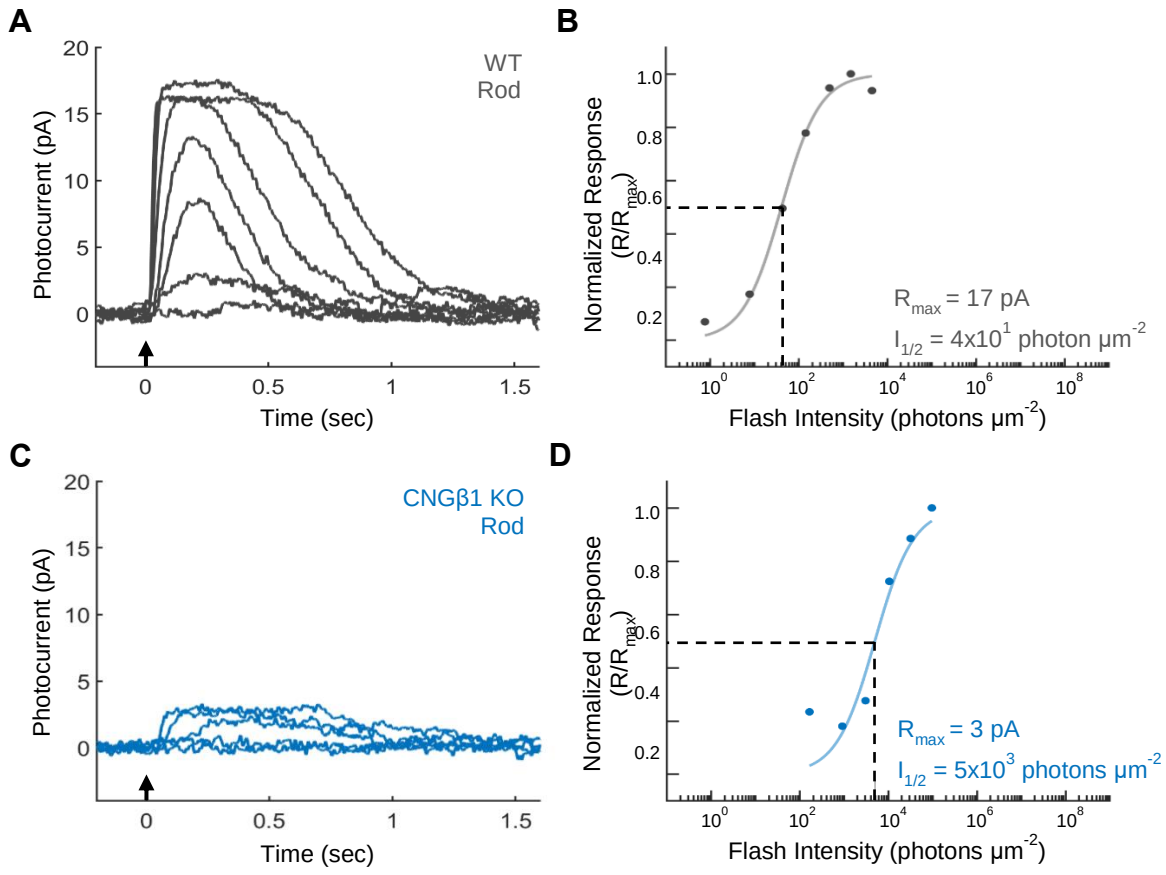

Figure 2.2 Light responses in rods of WT and CNGβ1 KO mice

Representative rod recordings from a WT **(A and B),** and a CNGβ1 KO **(C and D)**. Light responses (left) were evoked using 10 ms flashes from a 405 nm LED (arrow). Flash intensities for the WT rod: $8x10^{-1}$, $8x10^{0}$, $4x10^{1}$, $1x10^{2}$, $5x10^{2}$, $1x10^{3}$, and $4x10^{3}$ photons μm^{-2}; and for the CNGβ1 KO rod: $9x10^{2}$, $3x10^{3}$, $1x10^{4}$, $3x10^{4}$, and $1x10^{5}$ photons μm^{-2}. Note that the CNGβ1 KO rod is still able to produce a light-evoked response, although as expected this response is substantially smaller and desensitized when compared to the WT rod. The maximum response for each stimulus was normalized to the maximum response of the saturating stimulus (R/R_{max}) and plotted as a function of intensity (**B and D**). The curves represent the fit to the Michaelis-Menten equation, with the intensity of the half-maximal response ($I_{1/2}$) indicated by the dashed lines. WT rods: average R_{max} = 13 ± 2 pA, average $I_{1/2}$ = 6.2 ± 1.6 $x10^{1}$ photons μm^{-2}, n = 4); CNGβ1 KO rod: R_{max} = 3 pA, $I_{1/2}$ = $5.2x10^{3}$ photons μm^{-2}, n = 1.

RESOURCES

1. Daiger, S. P., Bowne, S. J. & Sullivan, L. S. Genes and mutations causing autosomal dominant retinitis pigmentosa. *Cold Spring Harbor Perspectives in Medicine* **5**, a017129 (2015).

2. Takahashi, V. K. L., Takiuti, J. T., Jauregui, R. & Tsang, S. H. Gene therapy in inherited retinal degenerative diseases, a review. *Ophthalmic Genetics* **39**, 560–568 (2018).

3. Cehajic-Kapetanovic, J. *et al.* Initial results from a first-in-human gene therapy trial on X-linked retinitis pigmentosa caused by mutations in RPGR. *Nature Medicine* **26**, 354–359 (2020).

4. Pfeiffer, R. L. *et al.* A pathoconnectome of early neurodegeneration: Network changes in retinal degeneration. *Experimental Eye Research* **199**, 108196 (2020).

5. Lin, B., Masland, R. H. & Strettoi, E. Remodeling of cone photoreceptor cells after rod degeneration in rd mice. *Experimental Eye Research* **88**, 589–599 (2009).

6. Wang, T. *et al.* Activation of Rod Input in a Model of Retinal Degeneration Reverses Retinal Remodeling and Induces Formation of Functional Synapses and Recovery of Visual Signaling in the Adult Retina. *The Journal of Neuroscience* **39**, 6798–6810 (2019).

7. Gargini, C., Terzibasi, E., Mazzoni, F. & Strettoi, E. Retinal organization in the retinal degeneration 10 (rd10) mutant mouse: A morphological and ERG study. *The Journal of Comparative Neurology* **500**, 222–238 (2007).

8. Barhoum, R. *et al.* Functional and structural modifications during retinal degeneration in the rd10 mouse. *Neuroscience* **155**, 698–713 (2008).

9. Peng, Y.-W., Hao, Y., Petters, R. M. & Wong, F. Ectopic synaptogenesis in the mammalian retina caused by rod photoreceptor-specific mutations. *Nature Neuroscience* **3**, 1121–1127 (2000).

10. Fariss, R. N., Li, Z.-Y. & Milam, A. H. Abnormalities in rod photoreceptors, amacrine cells, and horizontal cells in human retinas with retinitis pigmentosa. *American Journal of Ophthalmology* **129**, 215–223 (2000).

11. Jones, B. W. *et al.* Retinal remodeling triggered by photoreceptor degenerations. *The Journal of Comparative Neurology* **464**, 1–16 (2003).

12. Marc, R. E. *et al.* Neural Reprogramming in Retinal Degeneration. *Investigative Ophthalmology & Visual Science* **48**, 3364 (2007).

13. Varela, C., Igartua, I., de la Rosa, E. J. & de la Villa, P. Functional modifications in rod bipolar cells in a mouse model of retinitis pigmentosa. *Vision Research* **43**, 879–885 (2003).

14. Blanks, J. C., Adinolfi, A. M. & Lolley, R. N. Photoreceptor degeneration and synaptogenesis in retinal-degenerative (rd) mice. *The Journal of Comparative Neurology* **156**, 95–106 (1974).

15. Puthussery, T., Gayet-Primo, J., Pandey, S., Duvoisin, R. M. & Taylor, W. R. Differential loss and preservation of glutamate receptor function in bipolar cells in the *rd10* mouse model of retinitis pigmentosa. *European Journal of Neuroscience* **29**, 1533–1542 (2009).

16. Michalakis, S., Becirovic, E. & Biel, M. Retinal Cyclic Nucleotide-Gated Channels: From Pathophysiology to Therapy. *International Journal of Molecular Sciences* **19**, 749 (2018).

17. Zhang, Y. *et al.* Knockout of GARPs and the β-subunit of the rod cGMP-gated channel disrupts disk morphogenesis and rod outer segment structural integrity. *Journal of Cell Science* **122**, 1192–1200 (2009).

18. Ke, J.-B. *et al.* Adaptation to Background Light Enables Contrast Coding at Rod Bipolar Cell Synapses. *Neuron* **81**, 388–401 (2014).

19. Protti, D. A., Flores-Herr, N., Li, W., Massey, S. C. & Wässle, H. Light Signaling in Scotopic Conditions in the Rabbit, Mouse and Rat Retina: A Physiological and Anatomical Study. *Journal of Neurophysiology* **93**, 3479–3488 (2005).

CHAPTER 3:

Characterization of Cone Membrane Physiology During Secondary Cone Degeneration in the rd10 Model of Retinitis Pigmentosa

ABSTRACT

In retinitis pigmentosa, secondary degeneration of cones leads to loss of high-acuity central vision and is one of the most debilitating features of the disease. Currently, we have an incomplete understanding of the mechanisms underlying secondary cone degeneration, and there is little known about how cone membrane physiology changes during degeneration. In this study, I characterized changes in cone membrane physiology during secondary cone degeneration by performing whole-cell patch clamp recordings from degenerating cones in rd10 mice. My data support previous reports that cones maintain a normal depolarized resting membrane potential, despite the loss of their outer segment. My findings suggest that degenerating cones have ectopic expression of cyclic nucleotide-gated channels, which likely contribute to maintaining the depolarized membrane potential. Additionally, I show that degenerating cones are still able to produce small light-evoked responses, even at late stages of degeneration. The presence of a robust voltage-gated Ca^{2+} conductance suggests cones continue to express synaptic voltage-gated Ca^{2+} channels after the loss of the cone pedicle. Degenerating cones also maintain a normal hyperpolarization-activated cyclic nucleotide-gated K^+ channel conductance. Together these findings show that cones maintain much of their normal membrane physiology, an encouraging result for future research aimed at reactivating dormant cones to restore vision to patients with RP.

INTRODUCTION

Retinitis pigmentosa (RP) represents a group of inherited retinal degenerative diseases characterized by progressive photoreceptor death resulting in vision loss and eventual blindness. RP is the most common cause of inherited blindness, with an incidence of approximately 1 in 4000 people worldwide[1]. RP is highly genetically heterogeneous, with over 3000 causative mutations identified in more than 60 genes[2,3]. The majority of genes associated with RP are rod-specific genes, which lead to an intrinsic defect of the rod photoreceptors. As a result, retinal degeneration in RP progresses from primary rod photoreceptor death to secondary cone photoreceptor death. The heterogeneous nature of RP poses a major challenge to the development of treatments, and currently there are no treatments to slow or stop the progression of retinal degeneration in RP. There is progress being made towards the development of gene therapies to treat some of the more common RP mutations. However, given there are thousands of causative mutations, it is unfeasible to develop gene-specific therapies for each genetic defect. One approach to developing mutation-independent therapies is to target secondary cone degeneration. While rod photoreceptors mediate night vision and peripheral vision, cone photoreceptors provide us with high-acuity daylight vision and are of paramount importance in the majority of our functional vision. Therefore, treatments aimed at preventing secondary cone degeneration will be both broadly applicable and have the most significant impact on patient quality of life.

As rod photoreceptors die in RP, cones begin to show signs of dysfunction and progressively lose their outer segments and synaptic pedicles. These dormant cone cell bodies can persist into the late stages of RP [4,5], making them a potential target for vision restoration [6–8]. The mechanisms of secondary cone degeneration are not completely understood, but metabolic dysfunction appears to play an important role[9–13]. This effect may be due in part to the loss of rod-derived cone viability factor (RdCVF), which promotes glucose uptake in cones[14–16]. Rod death

and the loss of RdCVF ultimately leads to an energy deficiency in cones. The most energetically demanding process in a photoreceptor is the maintenance of ion gradients required to generate membrane currents[17,18]. It is therefore reasonable to predict that metabolic dysfunction during secondary cone degeneration could lead to changes in the expression of cone membrane channels. There is, however, almost nothing known at present about how cone membrane physiology changes during secondary cone degeneration.

In healthy cones, cyclic nucleotide-gated channels (CNG channels) in the outer segment remain open in the dark, allowing for a large influx of Na^+ that generates the resting dark current. The Na^+ must be removed from the outer segment by an ATP-dependent Na^+/K^+ pump. The high energy requirement for generating the dark current may partially explain why degenerating cones lose their outer segment, as shortening of the outer segment would reduce the number of CNG channels and decrease the energy required to maintain the dark current. The CNG dark current generates a depolarized resting membrane potential, which keeps voltage-gated Ca^{2+} channels at the synapse open. The Ca^{2+} influx through these channels stimulates the continuous synaptic release of glutamate in the dark. The Ca^{2+} that enters through the synaptic Ca^{2+} channels must also be removed by an ATP-dependent ion pump. Because the energy demand to maintain the synaptic Ca^{2+} current is even higher than that need for the dark current[18], it is possible that degenerating cones would downregulate synaptic voltage-gated Ca^{2+} channels to save energy.

Other membrane conductance may also play an important role in secondary cone degeneration. For example, loss of the hyperpolarization-activated cyclic nucleotide-gated K^+ channel (HCN1 channel) has been thought to accelerate photoreceptor degeneration in several models of retinal dystrophy[19]. Another mystery surrounding secondary cone degeneration is the finding that dormant cone cell bodies maintain a depolarized resting membrane potential despite the loss of the outer segment and outer segment CNG channels[7]. It is unclear which currents are responsible for maintaining the depolarized state in degenerating cones. Understanding how cone

membrane physiology is changing during secondary cone degeneration could help us understand the mechanisms underlying cone degeneration and identify potential targets to prevent cone loss or to reactivate dormant cones.

To study secondary cone degeneration, I used the well-characterized rd10 mouse model of RP. The rd10 mouse has a missense mutation in the rod-specific PDE6-β subunit[20], resulting in dysfunctional rod phosphodiesterase (PDE) and disruption of the phototransduction cascade. Cones express a different isoform of PDE6 and are not directly affected by this mutation[21]. In humans, mutations in the *PDE6-β* gene account for approximately 5% of autosomal recessive cases of RP, and mice strains with *PDE6-β* mutations are excellent models for studying RP. Compared to the rd1 mouse, which has a nonsense mutation in *PDE6-β* that completely knocks out rod PDE function[22], the rd10 rods PDE maintain a low level of enzymatic activity. Rod degeneration in the rd1 mouse is aggressive and overlaps with postnatal development, making it challenging to differentiate the effects of retinal degeneration from those of disrupted retinal development. The limited PDE activity in rd10 rods is sufficient to delay the onset of degeneration until after retinal development has completed and to slow the progression of degeneration, making the rd10 mouse a more suitable model for studying the mechanisms of retinal degeneration in RP. Rod degeneration in the rd10 mouse begins around P16 and peaks around P21, with the majority of rods lost by P30. Cone degeneration starts after rod degeneration, and cone cell bodies in the rd10 mouse can survive for up to 9 months.

In this study, I performed whole-cell patch clamp recordings from degenerating cone photoreceptors in retinal slices from rd10 mice at different stages of degeneration. Using this powerful electrophysiological technique, I measured passive membrane properties including resting membrane potential and membrane capacitance, I recorded light-evoked currents in response to flashes of light, and I used voltage-clamp protocols in combination with specific channel-blocking agents to characterize some of the major cone membrane conductances.

MATERIALS AND METHODS

Animal Care

All experiments were performed in accordance with rules and regulations of the National Institutes of Health guidelines for research animals, as approved by the Institutional Animal Care and Use Committee of the University of California, Los Angeles, California. Mice were housed with ad libitum food and water and kept under a 12 hr light cycle (12 on/12 off). Equal numbers of female and male mice were used. Rd10 mice were originally obtained from Jackson Laboratories (strain B6.CXB1-Pde6brd10/J), then propagated and maintained in the UCLA vivarium. Control experiments looking at normal cone function were performed in C57BL (C57BL/6J from Jackson Laboratories) or 129S (129SvPas from Charles River) wildtype mice, obtained as needed. No differentiation is made between C57BL and 129S mice, and in the following both are referred to simply as WT. Cone function was studied in animals ages 3 to 15 weeks.

Solutions

After retinal dissection, retinal tissue was kept alive in a specially formulated Ames medium (pH 7.4, osmolarity 284 mOsm), either buffered with bicarbonate (Ames-Bicarb) and bubbled with carbogen gas (95% O_2, 5% CO_2); or, for embedding and slicing, buffered with HEPES (Ames-HEPES) and bubbled with 100% oxygen. For certain experiments, channel-blocking agents were added to the Ames-bicarb bath solution as follows: isradipine (ISR, 10 µM), to block L-type voltage-gated Ca^{2+} channels; niflumic acid (NFA 250 µM, NFA), to block Ca^{2+}-activated Cl^- channels; tetraethylammonium (TEA, 25 mM), to block sustained voltage-gated K^+ channels; cesium (Cs^+, 5 mM), to block HCN channels; and L-cis-diltiazem (DILT, 500 µM), to block CNG channels. The standard internal solution for whole-cell patch clamp recordings was a potassium aspartate solution (K-Asp) containing (in mM): 125 potassium aspartate, 10 KCL, 10 HEPES, 5 NMDG-HEDTA, 0.5 $CaCl_2$, 0.5 $MgCl_2$, 0.1 ATP-Mg, 0.5 GTP-Tris, 2.5 NADPH (pH 7.3, osmolarity

280 mOsm). For experiments investigating the presence of CNG channels, cGMP (50-100 µM) was added to the standard internal solution. In other experiments, a cesium-TEA (Cs-TEA) based internal solution was used to block K^+ conductances. The Cs-TEA internal solution contained (in mM) 110 $CsCH_3O_3S$, 12 TEA-Cl, 10 HEPES, 10 EGTA, 2 QX-314-Br, 11 ATP-Mg, 0.5 GTP-Tris, 0.5 $MgCl_2$, 1 NAD^+ (pH 7.3, osmolarity 280 mOsm). QX-314 is 2-[(2,6-dimethylphenyl) amino]-N,N,N-triethyl-2-oxoethanaminium; it is a derivative of the anesthetic lidocaine and is a blocker of voltage-gated Na^+ channels.

Preparation of retinal slices

Prior to each experiment, animals were dark adapted overnight. The retinal dissection and preparation of retinal slices were performed under infrared illumination. Animals were euthanized by cervical dislocation. The dorsal aspect of each eye was marked prior to enucleation. After enucleation, the globes were moved to an Ames-bicarb bath. The anterior segment, including the cornea and the lens, was carefully removed. The posterior eye cup was bisected into dorsal and ventral halves. From one half, a rectangular section of retina was cut and then carefully separated from the retinal pigment epithelium. The isolated section of retina was embedded in 3% low-temperature-gelling agar dissolved in Ames-HEPES solution. The retina was sliced in cold Ames-HEPES with a vibratome to obtain 200 µm-thick slices of retina. Slices were made perpendicular to the retina in order to obtain a cross-section of retinal tissue with intact retinal circuitry. The retinal slice selected for recording was mounted on a recording dish; the slice was held in place by a custom-made anchor and moved to the microscope. The remaining retinal tissue and retinal slices were stored in a light-tight container with Ames-bicarb solution and kept at 32^{o}C. The tissue under the microscope was perfused with Ames-bicarb solution and kept at 35^{o}C.

Identifying Cones

Infrared illumination was used to view the tissue under the microscope. In WT tissue, cones can be easily distinguished from rods by their characteristic morphological and somatic features. Cone cell bodies are larger and slightly more elongated than rod cell bodies, and cone somata sit primarily on the outermost layer of the outer nuclear layer (ONL). Another prominent feature of cones is their nuclear architecture. Cone nuclei have multiple chromocenters, which create a distinct pattern under the microscope when compared to the single chromocenter in rod nuclei. Identifying cones in the degenerated tissue was more challenging than in WT tissue, as many of the rod somata are swollen and have disrupted nuclear architecture. Additionally, it was difficult to remove cell layers from the ONL of the degenerating tissue with a vacuum pipette, as is normally done in WT tissue to expose healthy cell bodies deeper in the retinal slice. I found that in the degenerating tissue, cones could be found along the top edge of the outer nuclear layer and had a prominent inner segment. Targeting the inner segment was the most reliable way to make patch-clamp recordings from cones in degenerating tissue.

Whole-cell patch clamp recordings

Whole-cell patch-clamp recordings were performed with borosilicate glass micropipettes (15-19 MOhm) filled with a K-Asp internal solution. Different internal solutions were used for specific experiments, as noted below. Cells were broken into in the voltage-clamp mode and initially held at -50 mV. After breaking into the cell, recordings could be made in voltage-clamp or switched to current-clamp mode. Specific electrophysiology protocols for each experiment are described in detail below. While in voltage-clamp, series resistance was compensated at 75-80%. Light stimuli were delivered as bright flashes (10-20 ms) from a monochromatic 405nm LED, which is approximately the isosbestic point of the S and M mouse cone opsins and stimulates both opsins with nearly equal efficiency. Light intensities are given in photons μm^{-2} rather than in the

conventional unit of light-activated rhodopsin (R*). Conversion from photons μm^{-2} to R* requires knowledge of the cone outer-segment collecting area, and degenerating cones lack an outer segment.

For most experiments, recording pipettes included a fluorescent dye, either Alexa-750 or Alexa-647, so that the cellular morphology could be imaged after electrophysiological recordings were completed. Electrophysiology data were filtered at 500 Hz, sampled at 10kHz, and acquired with Symphony (https://open-ephys.org/symphony/), an open-source MATLAB-based data-acquisition system. All reported membrane voltages have been corrected for the liquid junction potential, which was approximately 10 mV for the solutions used in these experiments.

Statistical Analysis

Data were analyzed with custom scripts written in MATLAB. All averages are reported as mean ± standard deviation. Comparison between WT control data and rd10 data was performed using the Wilcoxon Rank Sum test, a non-parametric comparison that does not assume equal variance. A p-value of less than 0.05 was considered a significant difference. To analyze changes in parameters over time, data as a function of time was fit with a linear regression, without fixing the y-intercept. Linear regression produced an equation of y=xb+c, with the 95% confidence intervals (CI) reported for the regression coefficients b and c. Fits in which the 95% CI for the slope (b) included 0 were considered to have no significant change over time.

RESULTS

Membrane Capacitance

Membrane capacitance correlates with total membrane area, with a relationship of approximately 1μF cm^{-2}. Therefore, I expected to see membrane capacitance in the rd10 cones decline during the degenerative process, as they lose their outer segments and pedicles. In line with this

expectation, I found that membrane capacitance in rd10 cones was significantly decreased, with an average membrane capacitance of 2 ± 1 pF in rd10 cones (n = 43) compared to 6 ± 2 in WT cones (n = 22) ($p<0.01$). Rd10 cone membrane capacitance was already significantly decreased at the earliest time point I examined of 3½ weeks (Fig 3.1), and imaging showed that rd10 cones had already lost their outer segments (see Fig 3.1C). Linear regression showed no change in WT membrane capacitance with animal age (WT slope = 0.05, 95% CI = [-0.06, 0.17]); however, for rd10 cones there was a small but statistically significant increase in membrane capacitance with age (rd10 slope = 0.14, 95% CI = [0.03, 0.26]). Rd10 cones may show an increase in membrane capacitance over time due to the growth of aberrant axonal processes, which were often seen at later time points (see Fig 3.1D, arrowheads).

Resting Membrane Potential

I found that rd10 cones maintained a normal resting membrane potential of -50 ± 9 mV (n = 40), compared to -47 ± 5 mV (n = 18) in WT cones (p = 0.085). Additionally, linear regression showed no significant change in resting membrane potential with age (Fig 3.2) for either WT or rd10 cones (WT slope = 0.51, 95% CI = [-0.46, 1.49]); (rd10 slope = -0.62, 95% CI = [-2.16, 0.92]).

To determine which channels were responsible for maintaining this depolarized state, I measured the change in resting membrane potential with application of channel blocking agents. The first channel I considered was the HCN1 channel, which is responsible for the i_h current. The HCN1 channel is a major channel in the cone inner segment. In WT cones, HCN1 is activated by the hyperpolarizing light response and acts to speed the photoreceptor response decay, returning the photoreceptor to a depolarized potential so that it can respond to the next light stimulus. It is not normally active at rest.

I hypothesized that loss of the outer segment CNG channels could cause the cones to drift to a more hyperpolarized potential, leading to abnormal activation of HCN1 channels.

Blocking the HCN1 channel with 5 mM external Cs^+ solution did not however significantly change the resting membrane potential in rd10 or WT cones (Fix 3.3A). Next, I considered the sustained voltage-gated K^+ channel that is responsible for the i_{KX} current. This channel is open at depolarized membrane potentials and inactivates with hyperpolarization. In healthy cones, i_{KX} is active at rest and helps to stabilize the resting membrane potential with a small hyperpolarizing effect. I hypothesized that degenerating cones could down-regulate expression of sustained voltage-gated K^+ channels, to decrease their normal hyperpolarizing effect. Blocking the sustained voltage-gated K^+ channel using 25 μM external TEA resulted in no significant change to the resting membrane potential in rd10 or WT cones (Fig 3.3B). In WT cones, the Ca^{2+}-activated Cl^- channel is active at rest. This channel has a hyperpolarizing effect on the membrane potential and it is thought to primarily stabilize the synaptic membrane voltage. Blocking the Ca^{2+}-activated Cl^- channel with 250 μM NFA had no significant effect of the resting membrane potential in rd10 cones (n = 3; Fig 3.3C).

In examining the resting membrane potential of these degenerating cones, I frequently saw cells with spontaneous Ca^{2+} spikes, which were suppressed with light stimulus (Fig 3.4). Although blocking sustained voltage-gated K^+ channels with TEA did not affect the resting membrane potential, it did significantly increase the presence Ca^{2+} spikes[23,24]. All four of the degenerating cones that were exposed to TEA exhibited an increase in Ca^{2+} spiking. In contrast, I did not observe spontaneous Ca^{2+} spikes in any WT cones, under normal conditions or with the addition of channel blocking agents. These data suggest that i_{kx} is still present in degenerating cones and continues to play an important role in stabilizing the membrane potential.

CNG Channels and Light-evoked Responses

In healthy cones, the depolarized resting membrane potential is produced by CNG channels in the outer segment. As degenerating cones lose their outer segments, they might be expected

also to lose these CNG channels. However, I hypothesized that degenerating cone cell bodies could have ectopic expression of CNG channels, and these channels may be contributing to the depolarized resting membrane potential in the dormant cone cell bodies. Initially I attempted to block CNG channels using L-cis-diltiazem. These experiments were unfortunately unsuccessful, so I decided to take a different approach. Under normal conditions, less than 10% of CNG channels are open in the dark. Instead of blocking these open channels, I attempted to open the remaining closed channels by dialyzing the cell with cGMP.

In Figure 3.5A, I show the change in membrane current in a WT cone as it is dialyzed with 100 μM cGMP. The recording is started immediately upon breaking into the cell. As cGMP diffuses into the outer segment, it opens CNG channels and produces a large inward current. The resulting current is still light suppressible, as can be seen in Figure 3.5B. As the cell is stimulated with light, PDE is activated and cGMP levels decrease, causing CNG channels to close. Each successive flash of light is brighter, activating PDE more and more strongly, until PDE is able to consume cGMP faster than it can diffuse into the outer segment from the pipette. As a result, the membrane current went back toward the level of the normal dark current.

Dialyzing rd10 cones with cGMP produced a similar inward current (Fig 3.5C), although this current often developed much faster in rd10 cones than in the WT cones. These results support my hypothesis that degenerating cones have ectopic expression of CNG channels either on the cell body or inner segment. The response to cGMP is more rapid because cGMP does not have to diffuse through the cone cilia into the outer segment to reach channels in the outer segment. There was no significant difference in the change in current produced by cGMP in rd10 cones at 4 weeks compared to 9 weeks (4 wks: mean = -45 ± 15 pA, n = 5; 9 wks: mean = -67 ± 23 pA, n = 4; p = 1.00). The average change in current in WT cones was almost twice that seen in rd10 cones (WT: mean = -95 ± 10 pA, n = 3; rd10: mean = -55 ± 21 pA, n = 9; p = 0.018); the

larger current seen in WT cones is expected, as WT cones should have significantly more CNG channels than rd10 cones.

The rd10 cone in Figure 3.5C initially displayed a small 9 pA light-evoked response. The presence of light-evoked responses also supports the hypothesis that degenerating cones ectopically express CNG channels. I was able to elicit light responses from many of the degenerating cones, despite the lack of an outer segment (Fig 3.6). Light responses could be found at the latest time point that was studied (9 weeks). Light responses from degenerated cones were small, with an average response of 3 ± 2 pA (n = 15), and required over two orders of magnitude more light than the WT cone saturating response ($2.7x10^7$ vs $1.5x10^5$ photons μm^{-2}). Nonetheless, it is still significant that any light response could be generated in the absence of an outer segment.

Voltage-gated Ca^{2+} Channel Conductance

For these small light responses to produce vision, they must be passed on to cone bipolar cells through functional synapses. Morphologically, the degenerating cones appear to have lost their axonal process and synaptic pedicle (see Fig 3.6); however, it is unclear if they maintain synaptic connections with downstream neurons. The synaptic voltage-gated Ca^{2+} channel is an essential component of the cone synapse and is required for synaptic release of glutamate. The presence of spontaneous Ca^{2+} spikes in degenerating cones (see Fig 3.4) suggests that, although these cones have lost their synaptic pedicle, they may continue to express voltage-gated Ca^{2+} channels.

To make direct recordings of voltage-gated Ca^{2+} current, I used a Cs-TEA internal solution to block K^+ currents (including the HCN1-channel current and the sustained voltage-gated K^+ current). The voltage-gated Ca^{2+} channel is gated open by depolarized membrane potentials and gated closed by hyperpolarization. To record the voltage-gated Ca^{2+} current, I used one of two ramp protocols. In both protocols, cells were initially held at -50 mV. In the first protocol, cells

were stepped to -70 mV and held here for 200-500 ms to allow all the Ca^{2+} channels to first close, before gradually ramping the voltage up to +20 mV. In the second protocol, cells were stepped to -100 mV and immediately ramped up to +30 mV. In both protocols, the membrane voltage was changed at a rate of 80 mV/sec. Leak subtraction was performed by calculating the leak from a select section of the trace prior to the opening of the Ca^{2+} channels, where the change in current was linear and proportional to the leak. Data from the two protocols were combined for the population analysis.

Figure 3.7 shows the average current produced as a function of membrane voltage for WT and rd10 cones. Degenerating cones showed a robust Ca^{2+} current, with an average peak current of -29 ± 10 pA (n = 19). The peak Ca^{2+} current of rd10 cones did not significantly differ from the peak current of WT cones which was -23 ± 9 pA (n = 9) (p = 0.13). Additionally, there was no significant difference in the voltage sensitivity of the channel, with the peak current in rd10 cones seen at an average membrane voltage of -40 ± 5 mV (n = 19) comparted to WT cones at -36 ± 10 mV (n = 9) (p = 0.28). When the peak current of rd10 cones was plotted as a function of age (Fig 3.7B), linear regression showed no significant change with time (slope = -1.15, 95% CI [-3.51, 1.21]). WT cone Ca^{2+} current data were primarily from 5-week-old animals, and there were insufficient time points to analyze Ca^{2+} current as a function of age in WT cones; no significant change would be expected.

Light Responses in Second-order Retinal Neurons

The data from Fig 3.7 suggest that degenerating cones continue to express synaptic voltage-gated Ca^{2+} channels. The voltage-gated Ca^{2+} channel is however only one component of the cone synapse, and these data alone are insufficient to confirm the presence of functional synaptic structures. To see if degenerating cones are able to make functional synapses, I recorded light-evoked responses from second-order retinal neurons from retinas of 8-9 week-old rd10 mice (Fig

3.8). By 6 weeks rod degeneration in the rd10 retina should be nearly complete[21]. By 8-9 weeks it is highly unlikely that any rods are present, therefore the light responses in these second-order neurons are most likely driven by input from degenerating cones. The recordings in Figure 3.8 are representative of 10 ON bipolar cells from four mice, 5 OFF bipolar cells from 2 mice, and 3 horizontal cells from 3 mice. Response amplitudes were quite variable, ranging from 3 to 52 pA for ON bipolar cells, 12 to 284 pA for OFF bipolar cells, and 34 to 240 pA for horizontal cells..

HCN1 Channel Conductance

The HCN1 channel is a major ion channel of the cone inner segment. As mentioned earlier, the HCN1 channel is activated at hyperpolarized membrane potentials, resulting in an inward current known at i_h. To characterize the HCN1 channel conductance, cells were held at -50 mV, then stepped to hyperpolarized potentials from -55 to -115 mV in increments of 10 mV. The protocol also included a single depolarizing step to -45 mV to allow for the calculation of the leak current. As can be seen in Figure 3.9A, hyperpolarizing voltage steps produced an inward current (i_h). The steady-state current was calculated from the last 500 ms of each stimulus. To compare current amplitudes of WT and rd10 cones and to look at the change in i_h as a function of animal age, we used the steady-state current in response to the -105 mV step (red trace in Fig 3.9A).

Compared to WT cones, rd10 cones showed no significant difference between the steady-state i_h current at -105 mV (WT mean = -56 ± 20pA, n = 8; rd10 mean = -74 ± 34 pA n = 23; p = 0.12). Figure 3.9B shows the steady-state i_h current in response to the -105 mV step as a function of animal age. Linear regression showed no significant change in i_h with age for either WT or rd10 cones (WT slope = -2.17, 95% CI = [-6.00,1.66], n = 8; rd10 slope = -2.12, 95% CI = [-10.51, 6.11], n = 23). Steady-state current for each stimulus was plotted as a function of membrane potential to generate a current-voltage curve (Fig 3.9C).

It should be noted that the current-voltage curve for i_h seen here is shifted left by approximately -10 mV when compared to the cone i_h current-voltage curve reported by Ingram et al. (2020). My i_h recordings were conducted with external Ames solution without the addition of blockers, while the i_h recordings made by Ingram et al included 25 mM TEA and 10 µM ISR in the bath solution in order to block i_{kx} and the voltage-gated Ca^{2+} current. Both i_{kx} and the voltage-gated Ca^{2+} current are inactive at hyperpolarized membrane potentials and activate with depolarization. Therefore, while i_{kx} and the voltage-gated Ca^{2+} currents may have contributed to my recordings at some of the more depolarized steps, producing the left shift of the current-voltage curve, both currents should be relatively negligible at the -105 mV step used to look at changes in i_h with degeneration. Additionally, my WT recordings were made in an identical manner as my rd10 recordings without blockers added to the Ames, and my data show no significant difference in voltage-dependence of i_h in WT cones and rd10 cone under these conditions.

DISCUSSION

Cone photoreceptors provide us with high-acuity central vision, and it is the secondary loss of cones that is the most debilitating feature of RP. There is a clear need for treatments that can preserve or restore cone function in RP. Treatments targeting secondary cone degeneration have the added benefit of being mutation-independent, and therefore broadly applicable to all forms of RP. To develop such treatments, we need to have a better understanding of the mechanisms of secondary cone degeneration and the changes cones undergo as they degenerate.

Research indicates that secondary cone degeneration is a complex and multifactorial process; however, metabolic dysfunction has been shown to play a central role. The loss of RdCVF after the death of rods impairs cone glucose uptake[15]. The resulting glucose deficiency disrupts normal cone metabolism. Metabolic reprogram of degenerating cones is a promising

approach to slowing cone degeneration, and recent research has identified several potential targets for intervention[25–27].

Upregulation of the mTOR pathway in cones has been shown to prolong cone survival and function by increasing glucose uptake and promoting anabolic metabolism. Zhang et al (2016) identified Sirtuin6, a protein that regulates the expression of multiple glycolytic genes, as a target for metabolic reprogramming[28]. They found that suppression of Sirtuin6 increased photoreceptor glycolysis and slowed degeneration. Xue et al (2021) recently found that increased expression of Txnip, a known regulator of glucose metabolism, promoted cone survival[29]. This finding was somewhat surprising because Txnip is known to reduce glucose uptake and inhibit antioxidant pathways, therefore increased Txnip expression might be expected to exacerbate cone degeneration. However, their study suggests that Txnip expression promoted lactate metabolism, enabling cones to use lactate as an alternative fuel source in the setting of decreased glucose availability.

These manipulations of cone metabolism slowed the progression of cone degeneration, but it is unclear if they can also reactive dormant cone cell bodies and promote the regrowth of cone outer segments and cone pedicles. Wang et al (2016) showed that dormant cones are capable of regenerating outer segments and regaining photosensitivity if provided with sufficient access to glucose. They achieved this either through replacement of RdCVF by transplanting WT rods or by direct glucose injection into the subretinal space[6]. Optogenetics is another approach that can be used to restore photosensitivity to dormant cones. Buskamp et al (2010) used halorhodopsin, a light-gated chloride ion pump, to restore photosensitivity to cones. They showed that halorhodopsin-expressing cones could drive light responses in retinal ganglion cells[7].

Despite the significant interest in treating secondary cone degeneration, there is little known about how cone membrane physiology changes during degeneration. In this work I have characterized the membrane physiology of degenerating cones in the rd10 mouse model of RP.

I found that cones lose their outer segments early in the degenerative process. At the earliest timepoint investigated (3½ weeks old), rd10 cones already had a significantly decreased membrane capacitance, and imaging showed no evidence of an outer segment or pedicle. Despite the loss of the outer segments, these cones continued to maintain a depolarized resting membrane potential, supporting previous reports by Buskamp et al (2010)[7]. I showed that the HCN1 channel responsible for i_h and the sustained voltage-gated K^+ channel responsible for generating the i_{kx} do not significantly contribute to depolarizing the membrane at rest. However, i_{kx} does appear to play a role in stabilization of the membrane potential, as blocking i_{kx} with 25 μM TEA resulted in the generation of spontaneous Ca^{2+} spikes. These results are in line with reports on the normal function of i_{kx} in healthy photoreceptors[23,24].

Dialyzing degenerated cones with cGMP resulted in a large inward current. In combination with my finding that degenerated cones have persistent light responses, these cGMP experiments suggest that degenerating cone cell bodies have ectopic expression of CNG channels. In support of this conclusion, Xu et al (2021) recently found evidence that CNG channels contribute to the depolarized membrane potential in cones without an outer segment[30]. While investigating the effects of knocking out cone opsins, they found that opsin-deficient cones maintain a depolarized resting membrane potential in the absence of an outer segment. Additionally, they showed that the current maintaining the depolarized potential is carried by Na^+, as would be expected for the CNG channel current. It is still possible some other Na^+ channel that is sensitive to changes in cGMP could be carrying this depolarizing current, although this seems unlikely. Unfortunately, neither Xu et al nor I myself were able to successfully block cone CNG channels in WT cones using L-cis-diltiazem. Because L-cis-diltiazem is a specific blocker of CNG channels, these experiments would have provided strong evidence for the presence of ectopic CNG channels in degenerated cones. Ectopic CNG channel expression may be able to be verified in future studies with immunohistochemistry, or by measuring RNA expression in degenerating cones.

One of the most surprising findings of my study was the presence of light-evoked responses in degenerating cones. These light responses were small, averaging only 3 pA, and were significantly desensitized, requiring two orders of magnitude more light than the WT cone saturating response. In healthy cones, the outer segment is highly specialized to optimize photodetection. The probability of light absorption depends on the concentration of opsins and the length of the outer segment. Additionally, outer segment disks provide a compartmentalized region for the components of phototransduction to interact. It is therefore unsurprising that light responses recorded from cones lacking outer segments were small and significantly desensitized. Nonetheless, light-evoked responses were present in some cells even at the latest time point investigated (9 weeks-old).

A recent study looking at opsin-deficient cones also recorded light-evoked potentials from cones that lacked outer segments; however, they showed that these responses originated from rods and were transmitted to cones through gap junctions[30]. It should be noted that the cone-opsin knockout mouse model they used does not have rod degeneration. While it is possible that there was a rod component to the light-evoked responses I recorded in cones from younger rd10 mice, I continued to see light-evoked cone responses at later stages of retinal degeneration, when there were no rods remaining. This observation indicates that degenerated cones are able to generate light-evoked responses without an outer segment. If this is true, it not only supports the presence of ectopic CNG channel expression but also suggests continued expression of all the components of phototransduction including rhodopsin. Recording from degenerating cones in the presence of a gap junction blocker would confirm that the light-evoked responses seen in my experiments originate from cones. Additionally, single-cell RNA sequencing of degenerating cones would be helpful in confirming the continued expression of phototransduction proteins.

Degenerating cones showed a robust voltage-gated Ca^{2+} current that was not significantly different from the voltage-gated Ca^{2+} current in WT cones, despite the fact that the degenerating

cones lacked a cone pedicle on imaging. Continued expression of voltage-gated Ca^{2+} channels could allow for synaptic transmission of light responses, and, indeed my recordings from second order neurons in 8-9-week-old rd10 animals show that degenerating cones are able to drive light responses in downstream neurons. There data are supported by the finding of Lin et al (2008) showing the presence of synaptic ribbons on aberrant axonal processes of degenerating cones[4]. Additionally, the finding that expression of halorhodopsin allows dormant cones to drive RGC responses supports the idea that degenerating cones maintain some synaptic connections with second-order retinal neurons[7].

Overall, my results indicate that there are surprisingly few significant changes in cone membrane physiology, even at late stages of degeneration. My work characterizes only a few of the major cone conductances, and future electrophysiology studies should look at other membrane conductances, such as the Ca^{2+}-activated Cl^- and K^+ conductances, as well as transient voltage-gated K^+ conductances. Looking at the effects of knocking out individual membrane channels in RP mice may also reveal important roles for these conductances, and my lab is currently working on generating these animal lines. The electrophysiology data from my study would also be enhanced by a more detailed analysis of structural and genetic changes occurring during secondary cone degeneration. Changes in cone synaptic structure are of particular importance, as any attempts to restore vision through reactivation of dormant cones will require functional synaptic connections with downstream retinal neurons. Additionally, changes in downstream bipolar cells and retinal ganglion cell responses should also be examined more closely. While there is still much research to be done, the results of my experiments are encouraging and suggest that degenerating cones maintain much of their normal physiology, making them a promising target for vision restoration in RP.

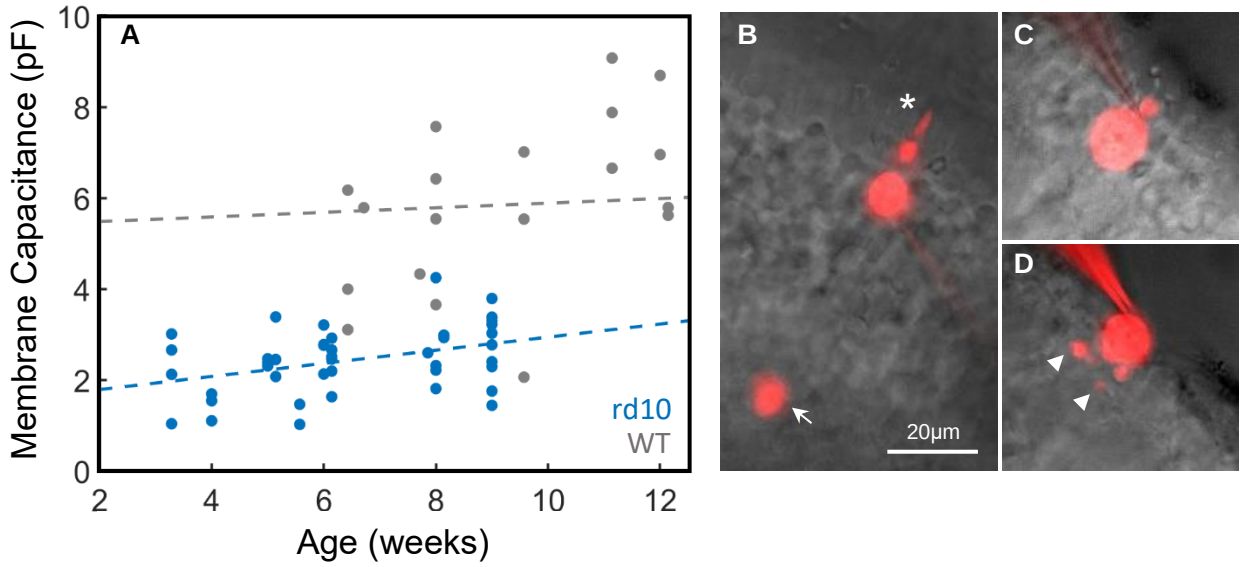

Figure 3.1 Membrane capacitance as a function of age

A) Membrane capacitance was measured for WT cones (gray, n = 22) and rd10 cones (blue, n = 42) and plotted as a function of animal age. Dash lines represent a linear fit. **B-D)** Images of cones filled with Alexa-750 from a WT mouse (B), and rd10 mice ages 4 weeks old (C), and 9 weeks old (D). Note the large outer segment (asterisk) and cone pedicle (arrow) of the WT cone. Scale bar, 20 µm. Membrane capacitance in rd10 cones was significantly decreased, with an average membrane capacitance of 2 ± 1 pF in rd10 cones (n = 43) compared to 6 ± 2 in WT cones (n = 22) ($p < 0.01$, Wilcoxon Rank Sum test). This decrease is already apparent at 3½ weeks, the earliest time points examined, and imaging shows that rd10 cones have already lost their outer segments at this age (see image C). There is no significant change in membrane capacitance with age for WT cones (WT slope = 0.05, 95% CI = [-0.06, 0.17]), however for rd10 cones there is a small but statistically significant increase in membrane capacitance with age (rd10 slope = 0.14, 95% CI = [0.03, 0.26]). This increase may be due to the growth of aberrant axonal arbors (arrowheads in D).

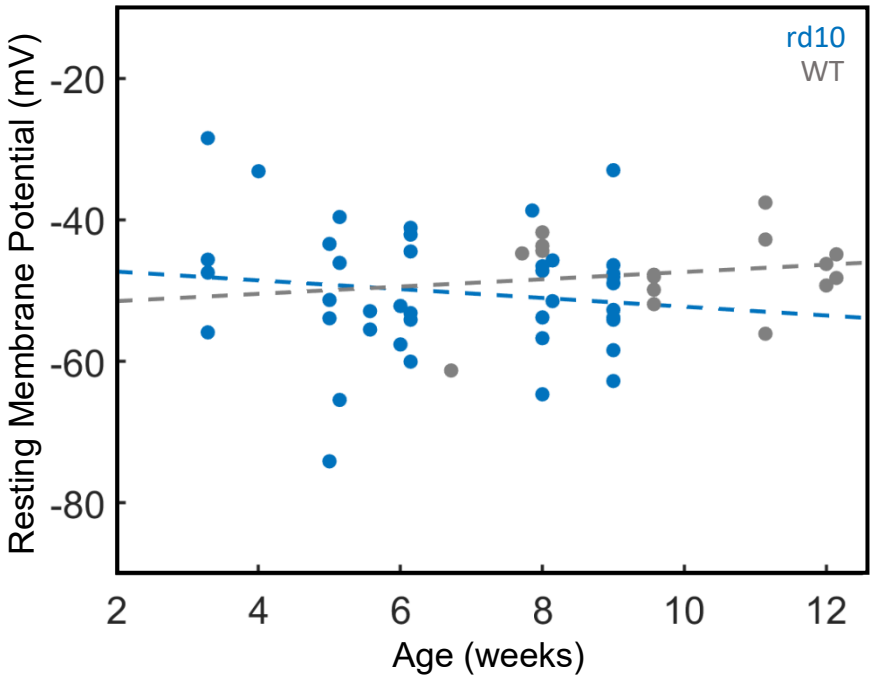

Figure 3.2 Resting membrane potential as a function of age

Resting membrane potential was measured for WT cones (gray, n = 18) and rd10 cones (blue, n = 40) and plotted as a function of age. Dashed lines represent a linear regression. There is no significant change in resting membrane potential with age for either WT or rd10 cones (WT slope=-0.51, 95% CI = (-0.46, 1.49)); (rd10 slope=-0.62, 95% CI = (-2.16, 0.92)). Additionally, the resting membrane potential of rd10 cones does not significantly differ from WT cones (rd10 mean = -50 ± 9 mV, WT mean = -47 ± 5 mV, p = 0.085, Wilcoxon rank sum test).

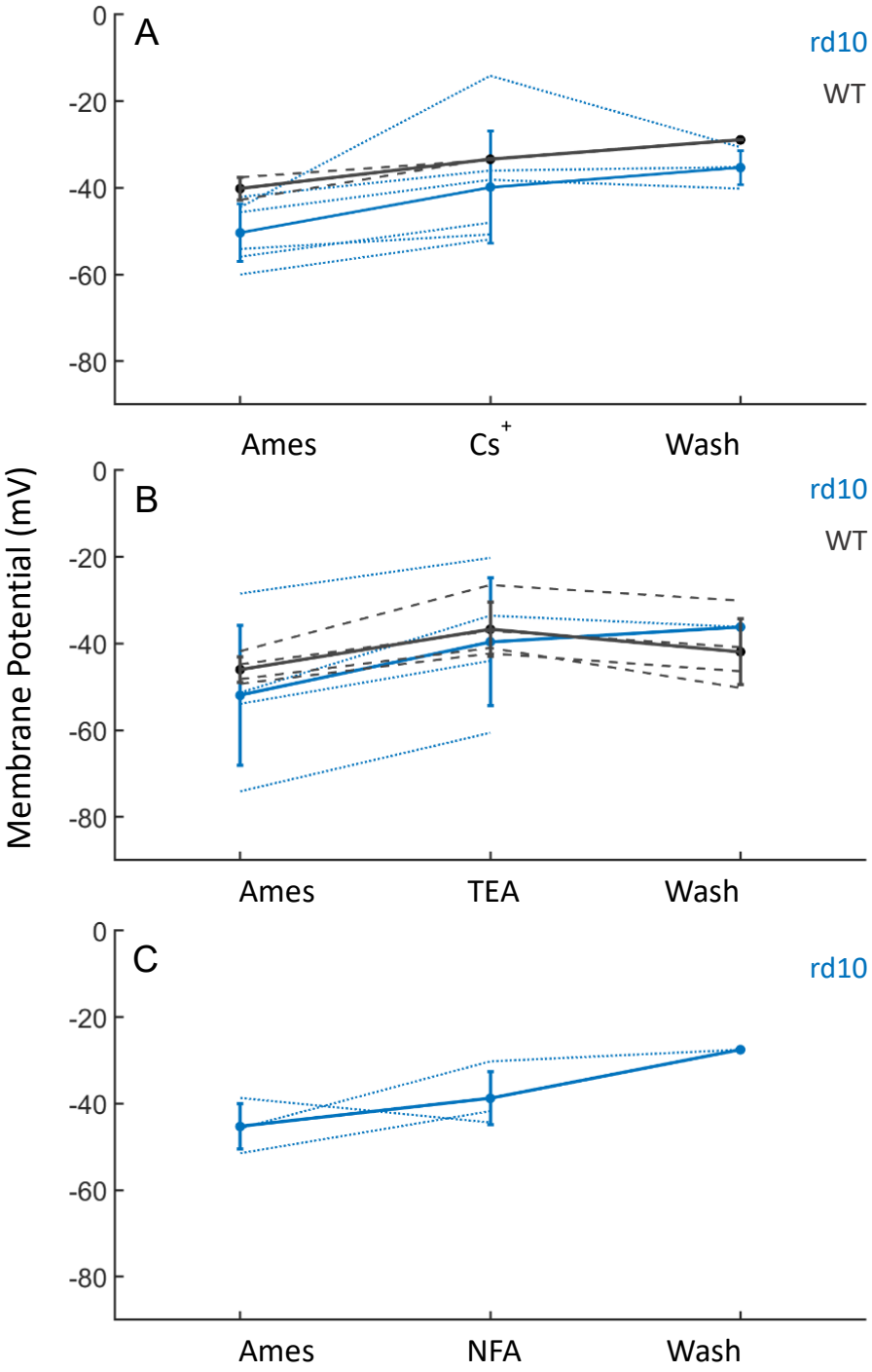
A
rd10
WT
0
-20
-40
-60
-80
Ames
Cs+
Wash
B
rd10
WT
Membrane Potential (mV)
Ames
TEA
Wash
C
rd10
Ames
NFA
Wash

Figure 3.3 Change in resting membrane potential with drug washes

To assess the contribution of I_h and I_{kx} to the resting membrane potential, the change in resting membrane potential was measured in Ames, after washing on an external channel blocking agent, and after washing off the channel blocker. WT cones are shown in black and rd10 cones in blue; dotted lines represent individual cells, solid lines represent average data, bars represent standard of deviation. **A)** Blocking I_h using 5 mM Cs^+ had no significant effect on resting membrane potential in either WT (n = 2) or rd10 cones (n = 6). **B)** Blocking I_{kx} with 25 μM TEA had no significant effect on resting membrane potential in either WT (n = 4) or rd10 cones (n = 4). **C)** Blocking Ca^{2+}-gated Cl^- channels with 250 μM NFA had no significant effect on resting membrane potential in rd10 cones (n = 3).

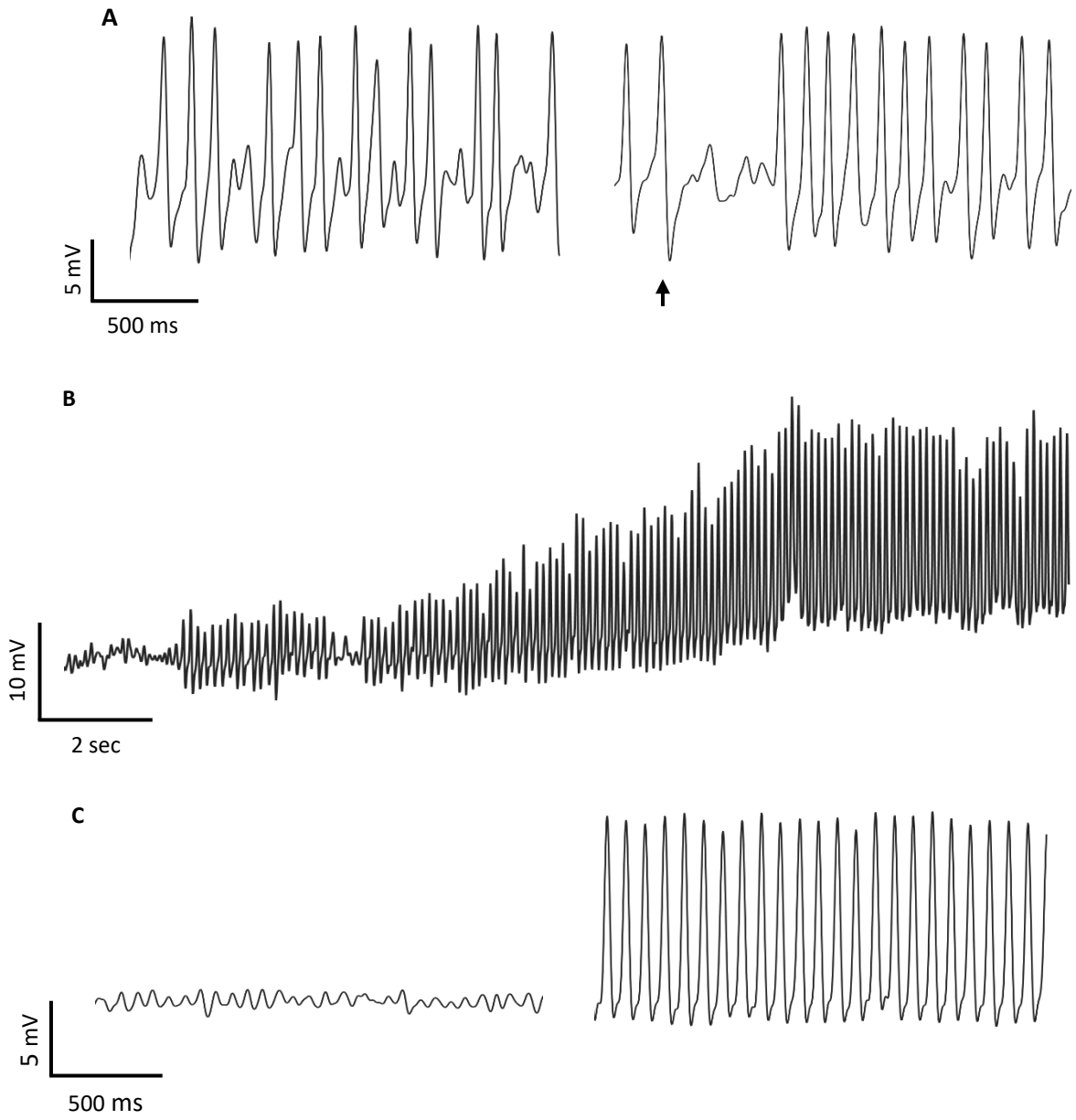

Figure 3.4 Calcium spikes in degenerating cones

A) Spontaneous calcium spike (left) in a degenerating cone from a 9-week-old rd10 animal which are suppressed by a bright flash of light (right, flash indicated by the arrow). **B)** Washing on 25μM external TEA triggers calcium spikes in a degenerating cone from a 5-week-old rd10 animal. **C)** Enlarged view the membrane voltage of the cell in B while in Ames solution (left) and after washing on TEA (right).

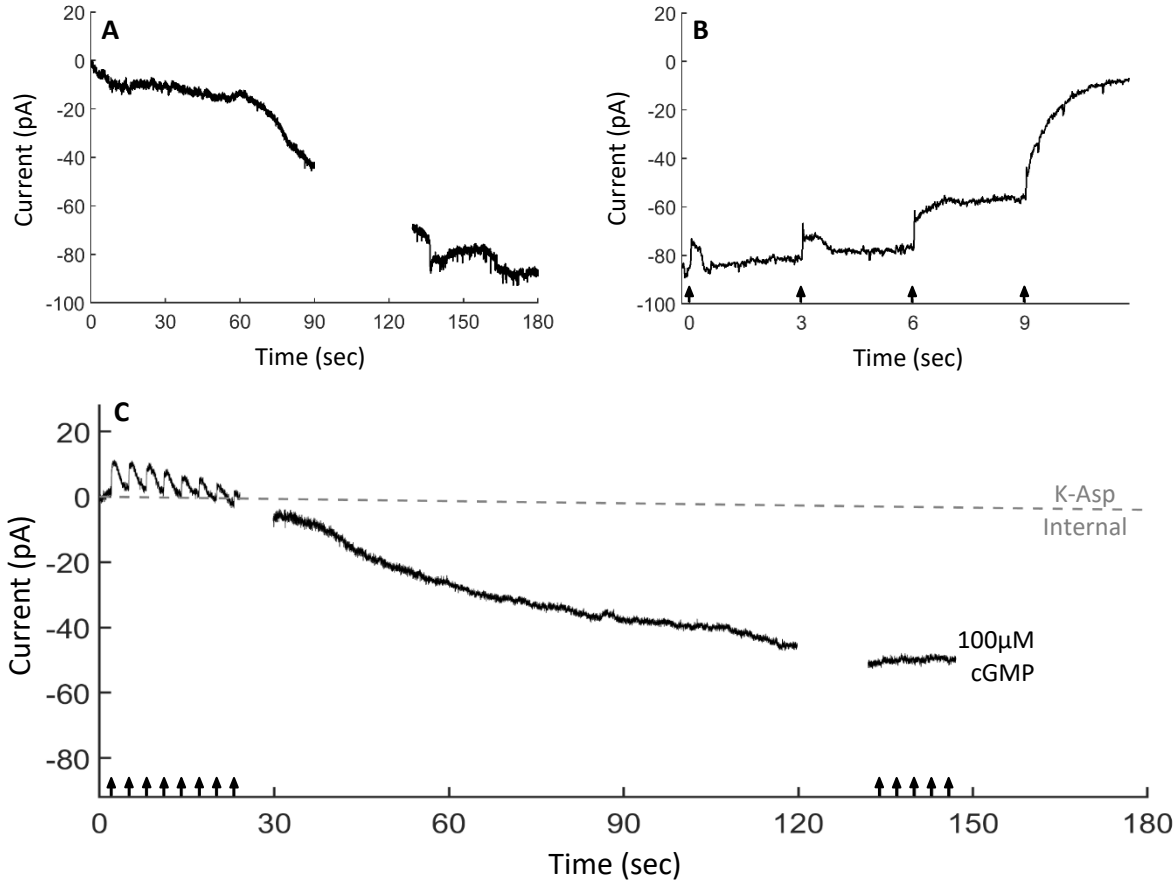

Figure 3.5 Change in resting membrane current with dialysis of cGMP

To test for the presence of CNG channels in the degenerated cones, cells were dialyzed cells with 100µM cGMP, added to the standard K-Asp internal solution. Because less than 10% of CNG channels are open at rest, the dialyzed cGMP should produce a large inward current as is opens the closed CNG channels. **A)** Change in current with cGMP in a WT cone. Recording was started immediately upon breaking into the cell. Note the delay before the inward current develops, as cGMP must diffuses out to the outer segment. **B)** The current produced by cGMP was still light suppressible. Once the cell from panel A reached a new steady state current, it was exposed to 10ms flashes from a 405nm LED as indicated by the arrows. Each successive flash increased in intensity, activating PDE more strongly. With the last flash PDE is consuming cGMP faster than it can diffuse back into the outer segment from the pipette, causing the

membrane current to return to the normal dark current. Flashes intensities: $6.0x10^{2}$, $7.5x10^{3}$, $8.0x10^{4}$, and $2.5x10^{5}$ photons $\mu m^{-2} sec^{-1}$. **C)** Change in current with cGMP in a degenerating cone from a 9-week-old rd10 retina. The recording was started immediately upon breaking into the cell. In this recording the cone was periodically flashed with a bright light at the start of the protocol, as well as at the end (indicated by the arrows). Note that this cell initially showed a relatively large light response. Light stimulus was a 10ms flash from a 405nm LED delivering $2.7x10^{7}$ photons $\mu m^{-2} sec^{-1}$. As a control, the gray dashed line represents the average change in membrane current over time when recording from rd10 cones using regular K-Asp internal (n = 13).

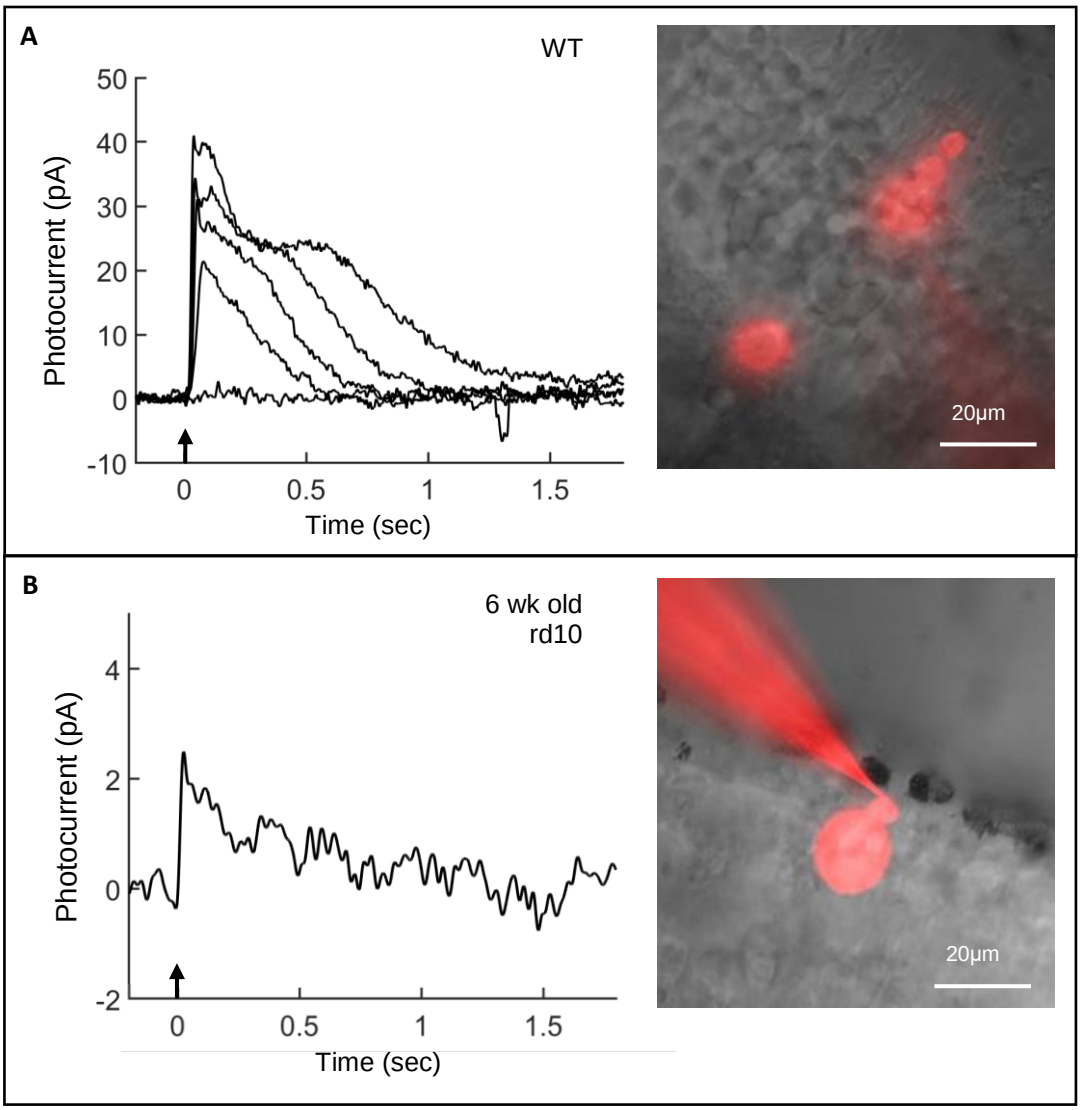

Figure 3.6 Light-evoked responses in degenerating cones

Small light responses were seen in many of the degenerating cone cell bodies. **Panel A** shows a WT cone light response (left) and image (right) **Panel B** shows a light response and image from a degenerating cone in a 6 week old rd 10 retina; note the difference of scale for the photocurrent on the x-axis. Photoresponses were produced using 10ms flashes from a 405nm LED, indicated by the arrow. The flash intensity used to evoke responses from the WT cone were: $3.0x10^{2}$, $4.0x10^{3}$, $1.5\ x10^{4}$, $4.0x10^{4}$, and $1.5x10^{5}$ photons μm^{-2} sec^{-1}. The flash intensity used for rd10 cones was: $2.7x10^{7}$ photons μm^{-2} sec^{-1}. Images of each cell were taken after the

recording. The cells were filled with Alexa-750 added to the K-Asp internal solution. Both images are oriented with the photoreceptor layer at the top-right. In B, note that the outer nuclear layer is almost entirely degenerated and only a few cone cell bodies remain. The filled cone lacks an outer segment or cone pedicle, which are both clearly visible in the WT cone from A. Scale bars 20 μm. In rd10 retinas, light-evoked responses were seen in 4 of 4 cones at 3.5-weeks-old, 7 of 10 cones at 6-weeks-old, and 1 of 3 cones at 9-weeks-old.

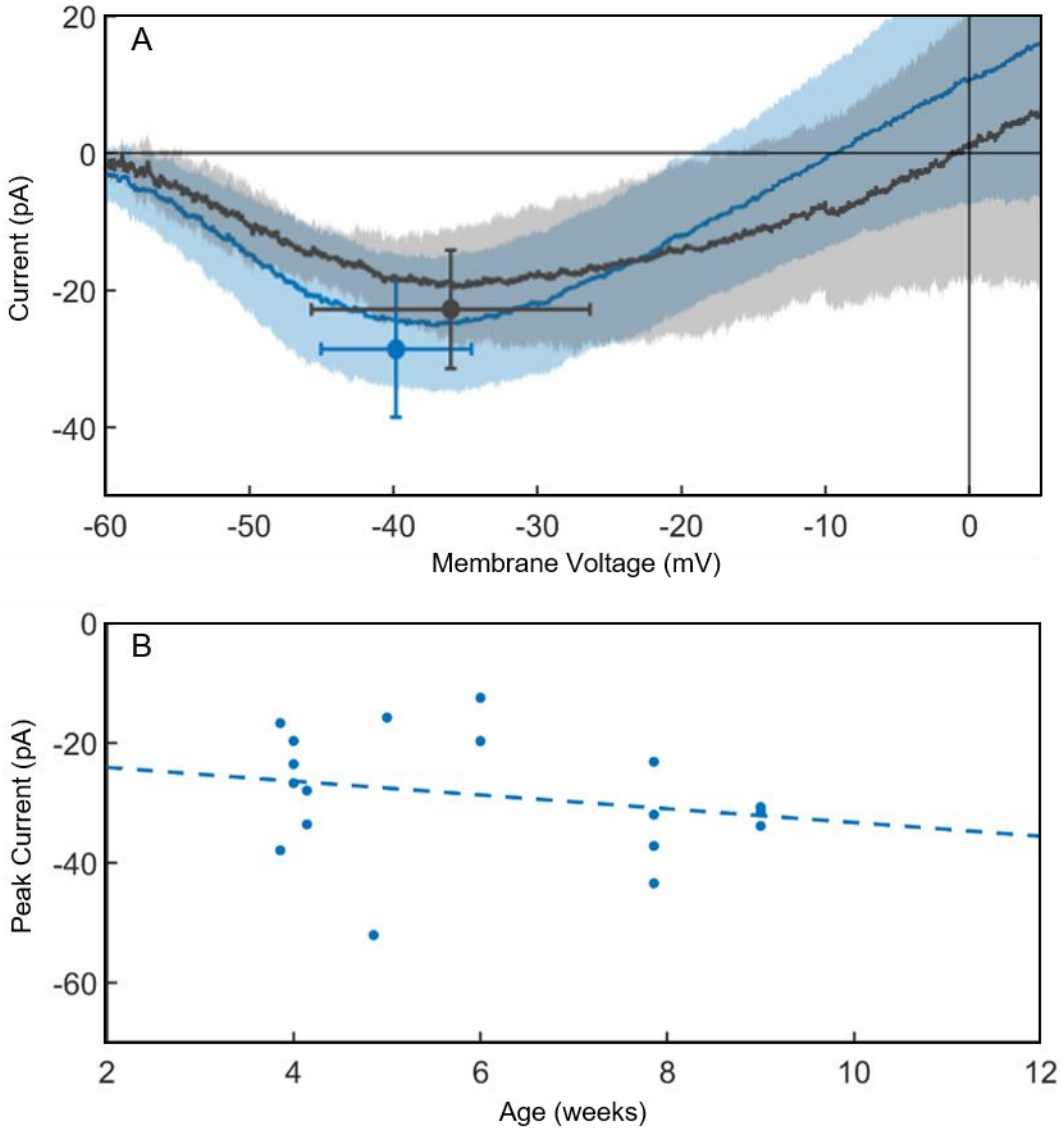

Figure 3.7 Voltage-gated Ca^{2+} current

The voltage-gated Ca^{2+} current was recorded using a ramp protocol with a Cs-TEA internal solution to block voltage-gated K^{+} currents. **Panel A** shows the average current generated as a function of membrane voltage for WT (gray, n = 9) and rd10 (blue, n = 19) cones. Shaded area represents the standard of deviation. Points indicate the average peak current, with error bars representing the standard of deviation. Degenerating cones showed a robust Ca^{2+} current, and there was no significant difference in the peak current between the rd10 and WT cones (rd10

mean = 29 ± 10 pA; WT mean = 23 ± 9 pA; p = 0.13, Wilcoxon Rank Sum test). Additionally, there was no significant difference in the voltage sensitivity of the channel, with the peak current in rd10 cones seen at an average membrane voltage of -40 ± 5 mV compared to WT cones at -36 ± 10 mV (p = 0.28, Wilcoxon Rank Sum test). **Panel B** shows the peak current of rd10 cones as a function of age. Linear regression (dashed line) showed no significant change in the peak current with time (slope = -1.15, 95% CI [-3.51, 1.21]).

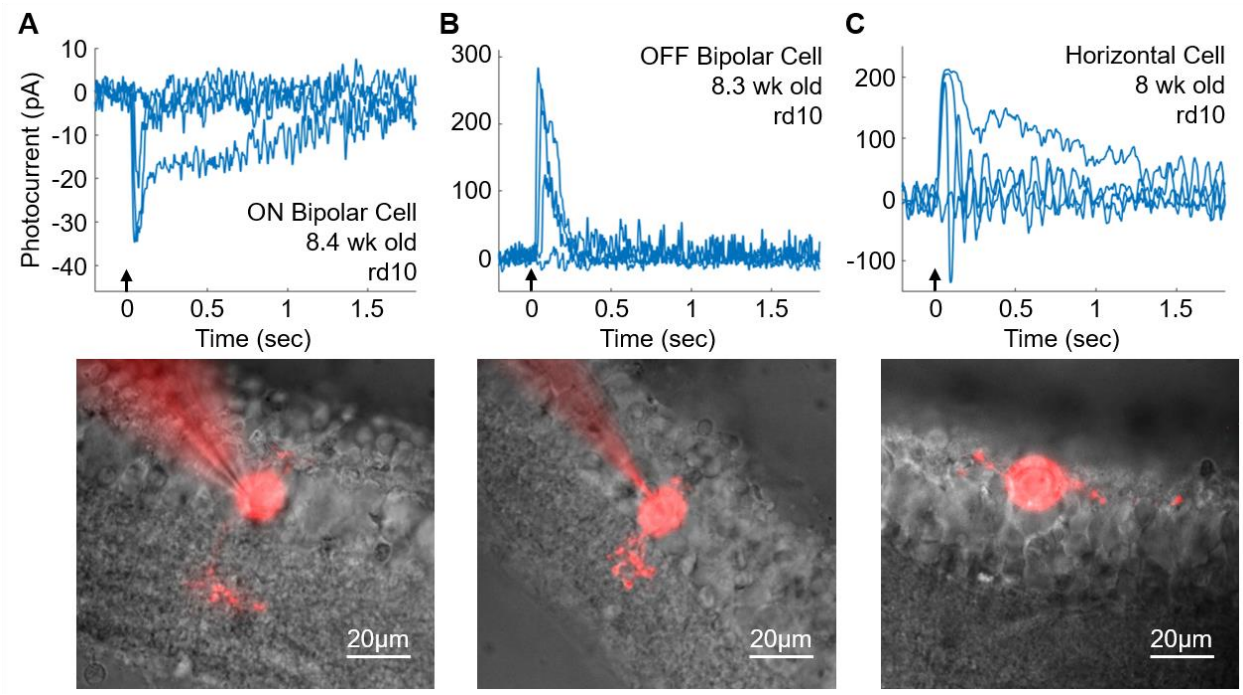

Figure 3.8 Light-evoked responses in second-order retinal neurons

Light-evoked responses (top) and images (bottom) of second-order neurons from rd10 animals ages 8-9 weeks old. **A)** an ON Bipolar Cell, **B)** an OFF bipolar cell, **C)** a horizontal cell. Stimuli were 10 ms flashes at 405 nm (arrow); flash intensities were $6.1x10^{1}$, $2.4x10^{3}$, $2.6x10^{4}$, and $1.5x10^{7}$ photons μm^{-2} in A; $2.4x10^{3}$, $2.6x10^{4}$, $2.6x10^{5}$ and $5.4x10^{7}$ photons μm^{-2} in B; and $2.6x10^{5}$, $8.7x10^{5}$, $9.1x10^{6}$, and $3.0x10^{7}$ photons μm^{-2} in C. Images of each cell were taken after the recording. The cells were filled with Alexa-750 added to the K-Asp internal solution. Images are oriented with the photoreceptor layer at the top, however note the complete absence of an outer nuclear layer. In A and B, note the long axonal process of the bipolar cell extending into the inner plexiform layer. In C, note the long dendritic processes of the horizontal cell extending along the outer edge of the inner nuclear layer. Scale bar: 20 μm.

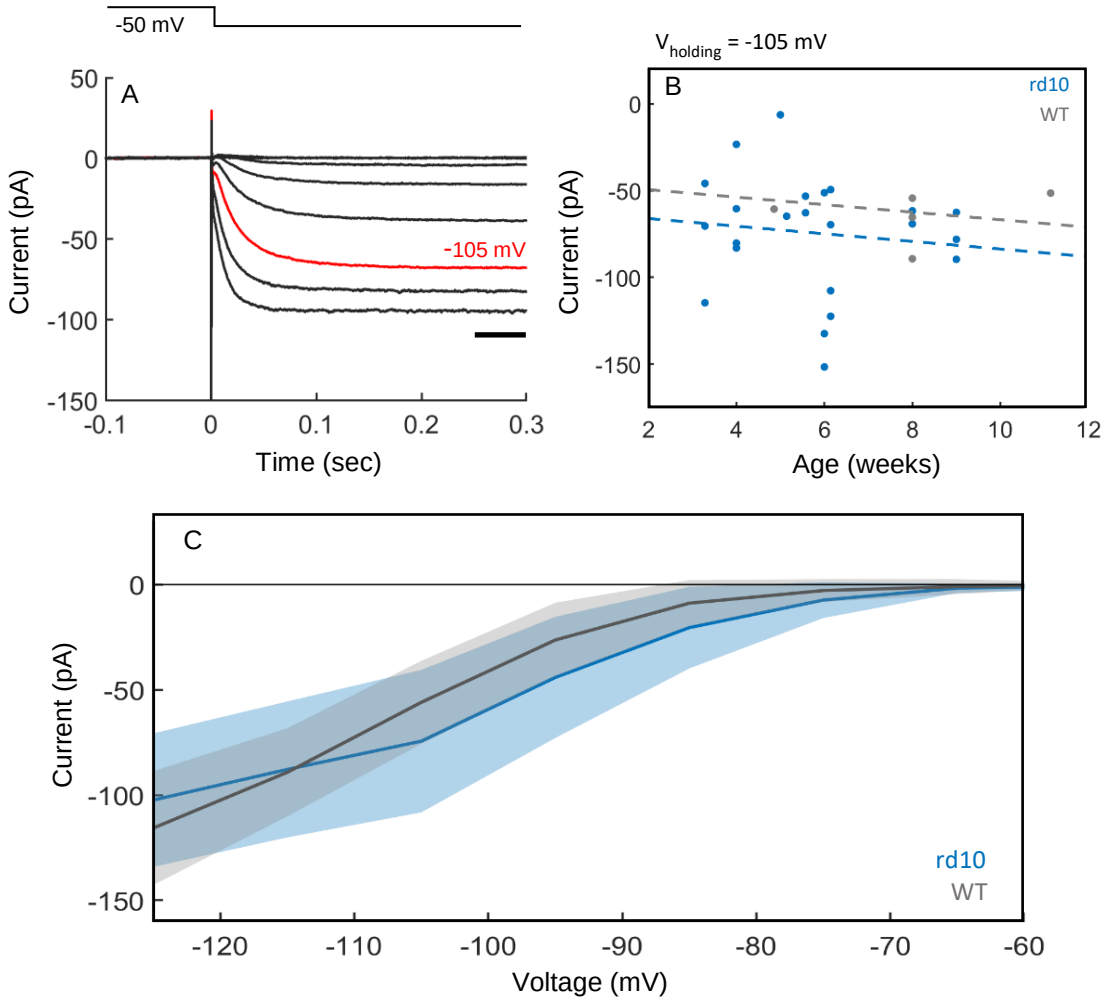

Figure 3.9 HCN1 channel current

The HCN1 channel current i_h was recorded using a step protocol. Cells were held at -50 mV, then stepped to hyperpolarized potentials from -55 to -115 mV in increments of 10 mV. **A)** Average inward i_h current produced by hyperpolarizing voltage steps seen in rd10 cones (n = 23). The steady-state current was calculated from the last 500ms of each step, indicated by the thick bar. **B)** The steady-state current of the -105 mV step (red trace in A) was plotted as a function of animal age for WT (gray, n = 8) and rd10 (blue, n = 23) cones. There was no significant difference in the steady-state i_h current at -105 mV between WT and rd10 cones (WT mean = -56 ± 20pA, n = 8; rd10 mean = -74 ± 34 pA, n = 23; p = 0.12, Wilcoxon Rank Sum

test). Linear regression (dashed lines) showed no significant change in i_h with age for either WT or rd10 cones (WT slope = -2.17, 95% CI = [-6.00,1.66], n = 8; rd10 slope = -2.12, 95% CI = [-10.51, 6.11], n = 23). **C)** Steady-state current for each stimulus was plotted as a function of membrane potential to generate a current-voltage curve. Shaded area represents SD. There was no significant difference in the voltage-dependence of i_h in WT and rd10 cones.

RESOURCES

1. Daiger, S. P., Bowne, S. J. & Sullivan, L. S. Genes and mutations causing autosomal dominant retinitis pigmentosa. *Cold Spring Harbor Perspectives in Medicine* **5**, a017129 (2015).

2. Daiger, S. P., Sullivan, L. S. & Bowne, S. J. RetNet: Retinal Information Network. https://sph.uth.edu/retnet/home.htm (2021).

3. D.N. Cooper, E.V. Ball, P.D. Stenson, A.D. Phillips, K. Evans, S. Heywood, M.J. Hayden, M.M. Chapman, M.E Mort, L. Azevedo, D. S. M. (Institute of M. G. in C. The Human Gene Mutation Database. http://www.hgmd.cf.ac.uk/ac/index.php (2020).

4. Lin, B., Masland, R. H. & Strettoi, E. Remodeling of cone photoreceptor cells after rod degeneration in rd mice. *Experimental Eye Research* **88**, 589–599 (2009).

5. Wong, F. & Kwok, S. Y. The Survival of Cone Photoreceptors in Retinitis Pigmentosa. *JAMA Ophthalmology* **134**, 249 (2016).

6. Wang, W. *et al.* Two-step reactivation of dormant cones in retinitis pigmentosa. *Cell Reports* **15**, 372–385 (2016).

7. Busskamp, V. *et al.* Genetic reactivation of cone photoreceptors restores visual responses in retinitis pigmentosa. *Science (1979)* **329**, 413–417 (2010).

8. Sahel, J.-A. *et al.* Functional rescue of cone photoreceptors in retinitis pigmentosa. *Graefe's archive for clinical and experimental ophthalmology = Albrecht von Graefes Archiv fur klinische und experimentelle Ophthalmologie* **251**, 1669–77 (2013).

9. Cheng, S. *et al.* Altered photoreceptor metabolism in mouse causes late stage age-related macular degeneration-like pathologies. *Proceedings of the National Academy of Sciences* **117**, 13094–13104 (2020).

10. Camacho, E. T., Punzo, C. & Wirkus, S. A. Quantifying the metabolic contribution to photoreceptor death in retinitis pigmentosa via a mathematical model. *Journal of Theoretical Biology* **408**, 75–87 (2016).

11. Léveillard, T., Philp, N. & Sennlaub, F. Is retinal metabolic dysfunction at the center of the pathogenesis of age-related macular degeneration? *International Journal of Molecular Sciences* **20**, 762 (2019).

12. Kurihara, T. *et al.* Hypoxia-induced metabolic stress in retinal pigment epithelial cells is sufficient to induce photoreceptor degeneration. *Elife* **5**, 1–22 (2016).

13. Wang, W. *et al.* Metabolic deregulation of the blood-outer retinal barrier in retinitis pigmentosa. *Cell Reports* **28**, 1323-1334.e4 (2019).

14. Léveillard, T. *et al.* Identification and characterization of rod-derived cone viability factor. *Nature Genetics* **36**, 755–759 (2004).

15. Krol, J. & Roska, B. Rods feed cones to keep them alive. *Cell* **161**, 706–708 (2015).

16. Yang, Y. *et al.* Functional cone rescue by RdCVF protein in a dominant model of retinitis pigmentosa. *Molecular Therapy* **17**, 787–795 (2009).

17. Okawa, H., Sampath, A. P., Laughlin, S. B. & Fain, G. L. ATP consumption by mammalian rod photoreceptors in darkness and in light. *Current Biology* **18**, 1917–1921 (2008).

18. Ingram, N. T., Fain, G. L. & Sampath, A. P. Elevated energy requirement of cone photoreceptors. *Proceedings of the National Academy of Sciences* **117**, 19599–19603 (2020).

19. Schön, C. *et al.* Loss of HCN1 enhances disease progression in mouse models of CNG channel-linked retinitis pigmentosa and achromatopsia. *Human Molecular Genetics* **25**, 1165–1175 (2016).

20. Chang, B. *et al.* Retinal degeneration mutants in the mouse. *Vision Research* **42**, 517–525 (2002).

21. Chang, B. *et al.* Two mouse retinal degenerations caused by missense mutations in the β-subunit of rod cGMP phosphodiesterase gene. *Vision Research* **47**, 624–633 (2007).

22. Bowes, C. *et al.* Retinal degeneration in the rd mouse is caused by a defect in the β subunit of rod cGMP-phosphodiesterase. *Nature* **347**, 677–680 (1990).

23. Fan, G. L., Quandt, F. N. & Gerschenfeld, H. M. Calcium-dependent regenerative responses in rods. *Nature* **269**, 707–710 (1977).

24. Fain, G. L., Gerschenfeld, H. M. & Quandt, F. N. Calcium spikes in toad rods. *The Journal of Physiology* **303**, 495–513 (1980).

25. McDougald, D. S., Papp, T. E., Zezulin, A. U., Zhou, S. & Bennett, J. AKT3 Gene Transfer Promotes Anabolic Reprogramming and Photoreceptor Neuroprotection in a Pre-clinical Model of Retinitis Pigmentosa. *Molecular Therapy* **27**, 1313–1326 (2019).

26. Zhang, L. *et al.* Reprogramming towards anabolism impedes degeneration in a preclinical model of retinitis pigmentosa. *Hum Mol Genet* **25**, 4244–4255 (2016).

27. Yao, A. & Wijngaarden, P. Metabolic pathways in context: mTOR signaling in the retina and optic nerve - A review. *Clinical & Experimental Ophthalmology* **48**, 1072–1084 (2020).

28. Zhang, L. *et al.* Reprogramming metabolism by targeting sirtuin 6 attenuates retinal degeneration. *Journal of Clinical Investigation* **126**, 4659–4673 (2016).

29. Xue, Y. *et al.* AAV-Txnip prolongs cone survival and vision in mouse models of retinitis pigmentosa. *Elife* **10**, (2021).

30. Xu, H. *et al.* Visual pigment–deficient cones survive and mediate visual signaling despite the lack of outer segments. *Proceedings of the National Academy of Sciences* **119**, (2022).

CHAPTER 4:

Separate ON and OFF Pathways in Vertebrate Vision First Arose During the Cambrian

Current Biology
Magazine

CellPress

Correspondence

Separate ON and OFF pathways in vertebrate vision first arose during the Cambrian

Erika M. Ellis[1,3], Rikard Frederiksen[1,3], Ala Morshedian[1], Gordon L. Fain[1,2,4,*], and Alapakkam P. Sampath[1,*]

A universal feature of the visual system in all previously studied vertebrates is the division of information into pathways specific for the onset and offset of illumination, called ON and OFF pathways [1]. ON and OFF pathways have a central role in the detection of contrast and combine in downstream neurons to produce complicated receptive fields, which detect diverse aspects of the visual world. This ON/OFF division occurs at the first synapse of the visual system between the photoreceptor cells — the rods and cones, and separate groups of ON and OFF bipolar cells [2]. We now show that the separation of visual information into ON and OFF pathways, and the novel metabotropic glutamate receptors which underlie ON bipolar cell light-evoked responses, are both present in the retina of lamprey. The simplest interpretation of this result is that ON and OFF bipolar cells were already present over 500 million years ago when cyclostomes diverged from other vertebrates in the late Cambrian, and that this fundamental organizing principle of the visual system probably arose not long after vertebrates first appeared.

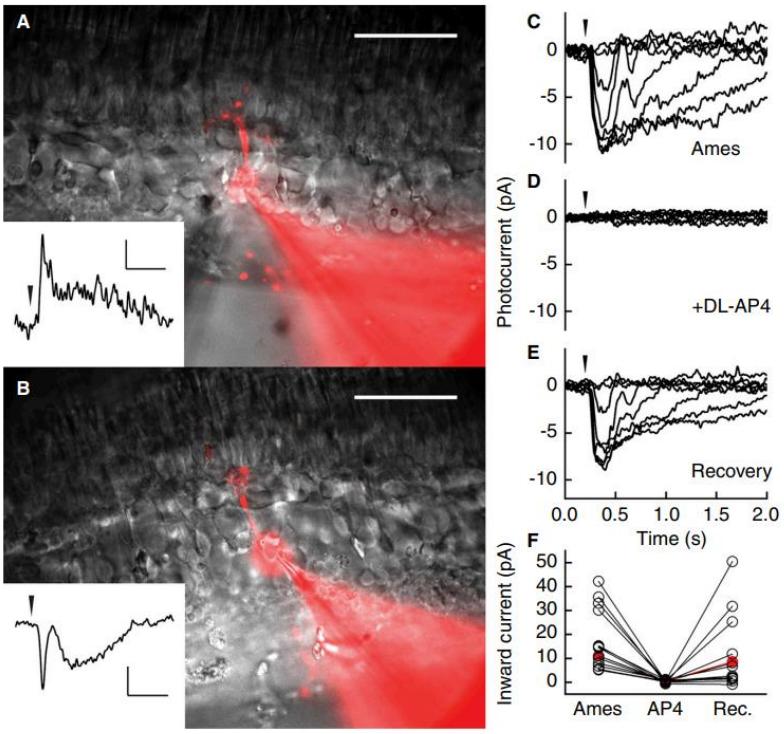

Figure 1. Voltage-clamp recordings from lamprey bipolar cells in retinal slices.
Cells were perfused in Ames' medium and maintained at a holding potential of -60 mV. (A) OFF and (B) ON bipolar cell filled with Alexa Flour 750 and imaged after the recording. The fluorescent images are overlaid with full-field infrared images. Dendritic and axonal arbors extend above and below the cell bodies. The photoreceptor layer is at the top of each image. Scale bars: 50 μm. Insets show light responses to a single, near-saturating 10-ms light stimulus indicated by arrowheads; flashes were 970 (in A) and 140 (in B) 502-nm photons μm^{-2}. Inset scale bars: 5 pA and 500 ms. (C–F) DL-AP4 blocks light response in an ON bipolar cell. (C) Responses to a series of 10 ms 405-nm flashes indicated by the arrowhead, at the following strengths: 3, 10, 30, 100, 300, 990, 3000, 9900 photons μm^{-2}. (D) Responses to the same set of light stimuli as in (C) after perfusion with Ames' medium containing 50 μM DL-AP4, which completely blocked the light response. (E) Response family after returning to Ames' medium. (F) Maximum inward current from 16 ON bipolar cells in Ames' medium, after perfusion with DL-AP4, and after returning to Ames' medium (Rec.). DL-AP4 completely blocked the light response in all cells. Ten cells recovered their light responses after returning to Ames' medium, and 6 cells showed no recovery. In two of the recordings we used L-AP4 (the active isomer) instead of DL-AP4, with results similar to the racemic mixture. The recording presented in panels C–E is highlighted in red.

Vertebrate photoreceptors remain depolarized and continuously release glutamate in darkness; light hyperpolarizes their membrane potential and decreases glutamate release. In OFF bipolar cells, the glutamate binds to AMPA/kainate receptors, with the result that the bipolar-cell membrane potential is depolarized in darkness and hyperpolarized by light. ON bipolar cells, in contrast, use a G-protein signal transduction cascade based on the mGluR6 receptor and the TRPM1 channel [2]. Glutamate binds to the mGluR6 receptor in darkness and keeps TRPM1 channels mostly closed; light decreases activation of mGluR6 and allows the channels to open, depolarizing the cell and inverting the photoreceptor signal. The ON bipolar light response is, we believe, the only known example of a metabotropic glutamate receptor acting as the primary postsynaptic mediator of synaptic transmission.

We were curious to know whether ON and OFF pathways and mGluR6 receptors are also present in the retina of lamprey. Lamprey are cyclostomes, a line that separated from all other vertebrates during the late Cambrian [3]. Earlier research has shown that lamprey rods and cones share many of the same transduction proteins as the photoreceptors of other vertebrates [4] and respond to light in a nearly identical manner [5,6], indicating that the mechanisms of phototransduction were established in vertebrates quite early. However, the organization of the remainder of the lamprey retina is rather different from other vertebrates [7]. In the lamprey, the nerve fiber layer runs within the retina between the inner nuclear layer (INL) and the

inner plexiform layer (IPL), with retinal ganglion cell bodies distributed in both the ganglion cell layer and the INL. Additionally, some retinal ganglion cells extend dendrites into the outer plexiform layer (OPL), suggesting that they may synapse directly with photoreceptors. These differences indicate that signal processing in the lamprey retina may diverge significantly from other vertebrates.

To explore this possibility, we made patch-clamp recordings from cells in the INL of lamprey retinal slices, using methods we have previously described [8]. We discovered clear examples of both OFF and ON bipolar cells (Figure 1A,B), with responses and morphology similar to those in the retina of other vertebrates [9]. Both kinds of cells had dendritic terminations in the OPL and axonal terminations in the IPL, and some had a process extending beyond the OPL up into the photoreceptor layer (not shown in Figure 1), similar to the Landolt club of lower vertebrates [10]. Light stimulation of the retina produced changes in current in both kinds of bipolar cell. The cell in Figure 1A is representative of 10 recordings for which full-field light produced an initial outward current response in voltage clamp and a hyperpolarization in current clamp; these were therefore OFF cells. The cell in Figure 1B is representative of 35 recordings for which light produced an initial inward current response in voltage clamp and a depolarization in current clamp; these were therefore ON cells. In many cells, the initial inward or outward current was followed by a delayed response producing a rapid inflection in the response waveform. This inflection may be produced in part by the different time courses of rod and cone inputs to the bipolar cell [5,6] and/or surround inhibition from horizontal cells.

To investigate the synaptic receptors underlying the ON bipolar-cell responses, we applied DL-AP4, a specific agonist of group III metabotropic glutamate receptors, including mGluR6. In vertebrates, DL-AP4 blocks the responses of ON bipolar cells by activating mGluR6, thereby driving TRPM1 channels further into the closed state and preventing a light-evoked response [2]. In Figure 1C–E, we show the responses of an ON bipolar cell to a series of flashes of increasing intensity. We then perfused the retina with 50 μM DL-AP4, which completely eliminated the light responses (Figure 1D). When DL-AP4 was washed off (Figure 1E), the responses returned. These recordings are representative of 16 similar experiments, 10 of which showed full recovery after washout (Figure 1F). While not every cell recovered, it is notable that the light-evoked response was suppressed in every ON bipolar cell we exposed to DL-AP4.

These experiments indicate that the lamprey retina establishes ON and OFF pathways at the level of the bipolar cells. Furthermore, the ON pathway is mediated by glutamate receptors sensitive to DL-AP4 similar to the ON bipolar cells of other vertebrates, suggesting that the lamprey glutamate receptor is also mGluR6. Because the mechanism of the ON bipolar-cell response is novel and unique to retina, we think it highly unlikely that the formation of this response could have emerged by parallel evolution in the retinas of lamprey and other vertebrates. The more likely explanation is that the fundamental division of retinal processing into ON and OFF pathways and the metabotropic mechanism producing the ON bipolar-cell response first appeared in the Cambrian and have remained relatively unchanged for 500 million years.

Our preliminary findings indicate that both ON and OFF bipolar cells can receive input from rods and cones. It remains to be seen whether separate classes of bipolar cells process distinct aspects of these photoreceptor signals. In addition, preliminary recordings from horizontal cells resemble those in other species. Thus, the OPL of lamprey retina seems to be organized much as in other vertebrates. We have occasionally encountered responses resembling those of vertebrate amacrine and ganglion cells but have not studied them in detail. It will be interesting to establish whether ganglion cells also come in ON and OFF varieties and to explore the organization of the IaPL, given the striking peculiarities of the anatomy of the lamprey inner retina [7]. We hope that continued investigation of the structure and function of lamprey retina will provide further insight into the evolution of vertebrate mechanisms of visual integration and contrast detection.

ACKNOWLEDGMENTS

This research was supported by a grant from the Great Lakes Fishery Commission, an unrestricted grant from Research to Prevent Blindness to the UCLA Department of Ophthalmology, the Stein Eye Institute Core Grant from the National Institutes of Health (EY00331), and the UCLA EyeSTAR program (to E.M.E.).

AUTHOR CONTRIBUTIONS

E.M.E., R.F., and A.M. conducted the experiments, obtained the data, and assisted in the design of experiments, and G.L.F. and A.P.S. assisted in the design of experiments and wrote the paper.

REFERENCES

1. Dowling, J.E. (2012). The Retina : An Approachable Part of the Brain (Cambridge, MA: Harvard University Press).
2. Martemyanov, K.A., and Sampath, A.P. (2017). The transduction cascade in retinal ON-bipolar cells: signal processing and disease. Annu. Rev. Vis. Sci. *3*, 25–51.
3. Kuraku, S. and Kuratani, S. (2006). Time scale for cyclostome evolution inferred with a phylogenetic diagnosis of hagfish and lamprey cDNA sequences. Zoolog. Sci. *23*, 1053–1064.
4. Lamb, T.D. (2019). Evolution of the genes mediating phototransduction in rod and cone photoreceptors. Prog. Retin. Eye Res. in press, 100823.
5. Morshedian, A. and Fain, G.L. (2015). Single-photon sensitivity of lamprey rods with cone-like outer segments. Curr. Biol. *25*, 484–487.
6. Asteriti, S., Grillner, S., and Cangiano, L. (2015). A Cambrian origin for vertebrate rods. eLife *4*, e07166.
7. Jones, M.R., Grillner, S., and Robertson, B. (2009). Selective projection patterns from subtypes of retinal ganglion cells to tectum and pretectum: distribution and relation to behavior. J. Comp. Neurol. *517*, 257–275.
8. Ingram, N.T., Sampath, A.P., and Fain, G.L. (2019). Voltage-clamp recordings of light responses from wild-type and mutant mouse cone photoreceptors. J. Gen. Physiol. *151*, 1287–1299.
9. Wu, S.M., Gao, F., and Maple, B.R. (2000). Functional architecture of synapses in the inner retina: segregation of visual signals by stratification of bipolar cell axon terminals. J. Neurosci. *20*, 4462–4470.
10. Landolt, E. (1871). Beitrag zur Anatomie der Retina vom Frosch, Salamander und Triton. Arch. Mikr. Anat. *7*, 81–100.

[1]Department of Ophthalmology and Jules Stein Eye Institute, University of California Los Angeles, Los Angeles, CA 90095, USA.
[2]Department of Integrative Biology and Physiology, University of California Los Angeles, Los Angeles, CA 90095, USA.
[3]These authors contributed equally to the work.
[4]Lead contact.
*E-mail: gfain@ucla.edu (G.L.F.), asampath@jsei.ucla.edu (A.P.S.)